ELUCIDATING THE ROLE OF SENATAXIN DURING HSV-1 INFECTION

ELUCIDATING THE ROLE OF SENATAXIN DURING HERPES SIMPLEX VIRUS TYPE-1 INFECTION

By BRAEDEN COWBROUGH, B.Sc.

A Thesis Submitted to the School of Graduate Studies in Partial Fulfilment of the Requirements for the Degree Master of Science

McMaster University MASTER OF SCIENCE (2018) Hamilton, Ontario (Biochemistry)

TITLE: Elucidating the Role of Senataxin During Herpes Simplex Virus Type-1 Infection

AUTHOR: Braeden Cowbrough, B.Sc. (Carleton University)

SUPERVISOR: Dr. Matthew S. Miller

NUMBER OF PAGES: xiii, 97

Lay Abstract

DNA viruses utilize host proteins in gene expression, therefore, associated factors play roles during DNA virus infections. Senataxin (SETX) is a RNA:DNA helicase associated with these proteins. *SETX* mutations are implicated in the neurodegenerative diseases Type 2 Ataxia with Oculomotor Apraxia (AOA2) and juvenile Amyotrophic Lateral Sclerosis (ALS4). Recently, our group demonstrated SETX antagonizes antiviral responses to RNA virus infections. Infections, including those caused by Herpes Simplex Virus type I (HSV-1), are identified as potential triggers of neurodegenerative diseases. We elected to study the role of SETX during DNA virus infections. Our data suggests that SETX is involved in the regulation of viral gene expression, facilitates HSV-1 DNA replication, attenuates the antiviral response, and in mouse models of infection, is protective against HSV-1 disease pathogenesis. These studies enhance understanding of the role of SETX during viral infection and may shed light on the mechanism(s) of SETX role in neurodegenerative disease.

ABSTRACT

Unlike RNA viruses, which typically encode their own RNA-dependent RNA polymerases, DNA viruses typically utilize host RNA Polymerase II (RNAPII) to transcribe their genes. Therefore, host factors that interact with RNAPII often maintain important regulatory roles during DNA virus infections. Senataxin (SETX) is a ubiquitously expressed 303 kDa RNA:DNA helicase that associates with RNAPII. It is involved in the resolution of R-loops and plays a role

during the DNA damage response. Mutations in *SETX* are implicated in the neurodegenerative diseases Type 2 Ataxia with Oculomotor Apraxia (AOA2) and juvenile Amyotrophic Lateral Sclerosis (ALS4). Recent work from our group has demonstrated that SETX also acts as an antagonist of the antiviral response during RNA virus infections. Infections, including those caused by Herpes Simplex Virus type I (HSV-1), have been identified as potential environmental triggers of neurodegenerative diseases. Therefore, we elected to study the role of SETX during DNA virus infections since, in addition to regulating host genes, it may also play a role in viral transcription and/or DNA replication. Our data suggests that SETX is involved in the regulation of viral gene expression, and that SETX facilitates DNA replication and contributes to viral biogenesis. SETX attenuates the antiviral response, and in mouse models of infection, is protective against HSV-1 disease pathogenesis. These studies have enhanced our understanding of the role played by SETX during viral infection and may shed light on the mechanism(s) through which SETX dysfunction results in neurodegenerative diseases.

ACKNOWLEDGEMENTS

There are too many people whom I am indebted to for their support, guidance and contributions throughout the completion of this work. I am truly surrounded by giants whose shoulders I stand on with those I mention below.

I am profoundly grateful and lucky to have worked under my supervisor, Dr. Matthew Miller. His guidance as a supervisor, a colleague, a teammate and friend has made my graduate career memorable beyond all means. Dr. Miller resides in my mind as a preeminent role model for all those interested in expanding our understanding of the world around us. I am privileged beyond explication to have been a member in the genesis of his laboratory, for which I know will reach prolific heights after my departure.

I cannot express the debt I owe to my fellow lab mates for all the time and effort they put into my work. None of this would have been possible without Mannie Lam, whose work in this project will resonate for all future researchers of Senataxin. Our lab manager, and friend, Jann Ang, helped make the lab my home away from the place I sleep. Without all the work you do, the lab would grind to a halt and I would have a head full of gray hairs. My fellow graduate student, Jonathan Mapletoft, who has made the hours spent flipping and spinning mice bearable. I know that a friendship has developed which will last through the years built out of mutual frustrations of simple things. Finally, to all those lab members I have not mentioned, you have all made our lab an enjoyable atmosphere to spend seemingly all our waking hours. I will never forget our constant arguments about the ***ubiquitous*** nature of words and the increasingly successful floorball hockey teams we produced. You have been unforgettable colleagues and friends, and I know Broken Down Golf Cart is in good hands without me.

Of course, I would be nowhere without my parents, Brian and Christine, and girlfriend, Emma. Your constant love and support has gotten me through arduous times and the sacrifices you made to get me to where I am will never be forgotten. You have been fundamental to all things I achieve.

TABLE OF CONTENTS

Chapter 1: Introduction

Chapter 2: Materials & Methods

LIST OF FIGURES

Chapter 1: Introduction

Chapter 2: Materials & Methods

Chapter 3: Results

Appendix 1: Supplementary and In-Progress Data

LIST OF TABLES

LIST OF APPENDICES

LIST OF ABBREVIATIONS

AD	Alzheimer’s Disease
AdV	Adenovirus
ALS4	Amyotrophic Lateral Sclerosis
AOA2	Ataxia with oculomotor apraxia type 2
ATCC	American Type Cell Culture
ATM	Ataxia-telangiectasia mutated serine/threonine kinase
ATR	Ataxia telangiectasia and Rad3-related protein

ATRIP	ATR interacting protein
BLAST	Basic Local Alignment Search Tool
bp	Base pair
BRCA1	Breast cancer type 1 susceptibility protein
cGAS	cyclic GMP-AMP synthase
CMV	Cytomegalovirus
CNS	Central Nervous System
CPE	Cytopathic effect
CPT	Camptothecin
CpG	5'Cytosine phosphate guanine 3'
CXCL10	CXC motif chemokine
DDR	DNA Damage Response
DNA	Deoxyribonucleic acid
DSB	Double strand DNA break
dsDNA	Double strand DNA
DMEM	Dulbecco's Modified Eagle's Medium
DMSO	Dimethyl sulfoxide
dNTP	Deoxy Nucleotide Triphosphate
DSB	Double Strand Break
dsDNA	Double stranded DNA
dSTING	Dead STING
E	Early
EDTA	Ethylenediaminetetraacetic acid
eIF4H	Eukaryotic translation initiation factor 4H
FBS	Fetal bovine serum
GAPDH	glyceraldehyde-3-phosphate dehydrogenase
GC	Guanine/cytosine
gDNA	Genomic DNA
GFP	Green fluorescent protein
G4	Guanine quadruplex
HCF1	Host cell factor C1
HEK	Human embryonic kidney cell
HET	Heterozygous
HERV	Human endogenous retrovirus
HFF	Human foreskin fibroblast
HIV	Human immunodeficiency virus
HSV-1	Herpes simplex virus type 1
Hpr1	Hyperrecombination protein 1 (or THO complex subunit HPR1)
HR	Homologous recombination
HRP	Horseradish peroxidase
hSTING	Hyper STING
H&E	Hematoxylin and eosin stain
IAV	Influenza A virus
ICP0	Infected cell polypeptide 0
IE	Immediate early
IFIT1	Interferon-induced protein with tetratricopeptide repeats 1

IFIT2	Interferon-induced protein with tetratricopeptide repeats 2
IFNβ	Interferon beta
IgG	Immunoglobulin G
IRE	IRF3 responsive elements
IRF3	Interferon regulatory factor 3
ISG	Interferon stimulated gene
ISGF3	Interferon stimulated gene factor 3
JAK	Janus kinase
kbp	kilobase pair
kDa	kilodalton
KO	Knockout
L	Late
MEF	Mouse embryonic fibroblast
MEM	Modified Eagle's Media
Mft1	Mitochondrial fusion target protein 1 (or THO complex subunit MFT1)
MOI	Multiplicity of Infection
MOPS	3-(N-morpholino) propanesulfonic acid
MRE11	Meiotic recombination 11 homolog 1
MRN	Mre11-Rad50-Nbs1
mRNA	Messenger RNA
NBS-1	Nibrin
ND	Neurodegenerative disease
OAS	2'-5'-oligoadenylate synthetase
OCT1	POU domain class 2 transcription factor 1
ORC	Origin recognition complex
PAMP	Pathogen associated molecular pattern
PBS	Phosphate buffered saline
PFU	Plaque forming units
PRR	Pathogen Recognition Receptor
PR8	Puerto Rico 1968
PVDF	Polyvinylidene fluoride
qRT-PCR	Quantitative reverse transcriptase polymerase chain reaction
RAD-50	DNA repair protein RAD-50
RNA	Ribonucleic acid
RNAi	RNA interference
RNAPII	RNA Polymerase 2
RNF8	E3 ubiquitin-protein ligase RNF8 (or RING finger protein 8)
RNF168	E3 ubiquitin-protein ligase RNF168 (or RING finger protein 168)
SETX	Senataxin
SDS-PAGE	sodium dodecyl sulfate polyacrylamide gel electrophoresis
siRNA	Short interfering RNA
S/G2	Synthesis phase/ Gap 2 phase
SOD1	Superoxide dismutase 1
SSB	Single strand DNA break
ssDNA	Single strand DNA
STAT	Signal Transducer and Activator

STING	Stimulator of interferon genes
TAE	Tris-Acetate EDTA
TAF4	TATA-box binding protein associated factor 4
TBK1	Tank binding kinase 1
Tg	Transgenic
THO	Tho2, Hpr1, Mft1, Thp2 complex
Tho2	THO complex subunit 2
Thp2	THO complex subunit THP2
TLR	Toll-like receptor
TSS	Transcriptional start site
TTS	Transcription termination site
U_L	Unique long
U_S	Unique short
VP16	Viral protein 16
WNV	West Nile virus
Xrn-2	5'-3' Exoribonuclease 2
γH2AX	Serine-139 phosphorylated histone 2A member x
53BP1	p53-binding protein 1

CONTRIBUTIONS

Dr. Karen Mossman - Provided the HSV-1 virus strains KOS and 17+.

Dr. Ali Ashkar - All HSV-1 mouse experiments were performed under the animal utilization protocol of, and Depo-Provera was provided by Dr. Ashkar

Dr. Joe Mymrk - Provided AdV-GFP virus used in fluorescence experiments.

Marianne Chew-	Aided in initial intravaginal infections of mice with HSV-1 in terms of procedures.
Susan Collins -	Aided in virus purification and titre methods
Mannie Lam -	Performed initial HSV-1 infections of HFF and corresponding qPCR, western blotting and 293T STING transfection
Peter Zeng-	Performed bioinformatical analysis of RNA sequencing data and developed *in-silico* prediction of R-loop figures.

Chapter 1

Introduction

1.1 Study of Host-pathogen Interactions

Viruses by their very nature are obligate parasites. They require viable cellular hosts to replicate and are therefore intrinsically intertwined with- and altered by- their cellular environments[1,2]. As a result, viruses are useful as tools in understanding cellular biology due to their innate ability to selectivity target cellular pathways in order to make the environment optimal for viral growth[3]. Understanding cellular factors that affect the viral life cycle has broad-sweeping applications relevant to both virology and cell biology, but also as an avenue for development the of novel antiviral therapeutics. With the advent of high-throughput sequencing methods and large-scale RNA interference (RNAi) and Clustered Regularly Interspaced Short Palindromic Repeats (CRISPR) libraries, cellular factors are being routinely identified as regulators of viral infection and new functions of previously cryptic proteins are being resolved[4,5].

The use of multiple short interfering RNA (siRNA) molecules now offers *in-vitro* systems where gene expression for a target can be depressed below pre-transfection levels for at least 7 days, depending on cellular division rates[6]. Combined with available gene knock-out (KO) models in which cellular environments are devoid of a gene product of interest, research into host dependent effects on viral gene infection and life cycle have become more focused and direct[4,7]. With these tools, research examining one can probe how viral infections influence disease outcome via interactions with specific genes/pathways.

1.2 The RNA:DNA Helicase Senataxin

Senataxin (SETX) is a ubiquitously expressed 303 kDa RNA:DNA helicase consisting of an N-terminal protein interaction domain and a C-terminal DEAD box helicase domain[8]. SETX

is found throughout mammalian species, but was first identified due to its association with two juvenile neurodegenerative diseases: Ataxia with Oculomotor Apraxia 2 (AOA2) and Amyotrophic Lateral Sclerosis 4 (ALS4)[9–11]. SETX mutations associated with AOA2 are autosomal recessive and are generally considered to be loss of function[12]. The disease is characterized by cerebral ataxia, peripheral neuropathy, oculomotor apraxia, elevated serum α-fetoprotein and defective DNA damage responses (DDR)[9,13–17]. By contrast, SETX mutations associated with ALS4 are autosomal dominant and considered to be gain of function mutations[12,18]. The disease manifests through upper and lower motor neuron degeneration which results in skeletal muscle atrophy[19]. Onset of disease typically occurs prior to age 25, and by contrast to more prevalent forms of ALS, is slower in progression with reduced bulbar and respiratory muscle involvement[10,20,21]. Numerous mutations of SETX have been identified for both AOA2 and ALS4[22–24]. A summary of the current knowledge of disease-associated mutations occurring in SETX can be found in *Figure 1.2.1* below. The potential neuroprotective effect conferred by functional SETX is poorly understood. However, a wide array of SETX functional roles and associations have been identified, including interactions with the cellular DDR[7,25–27], RNA:DNA helicase activity[9,11,18,28,29], RNA Polymerase II (RNAPII) interactions[14,18,25,30], and regulation of the antiviral response[30]

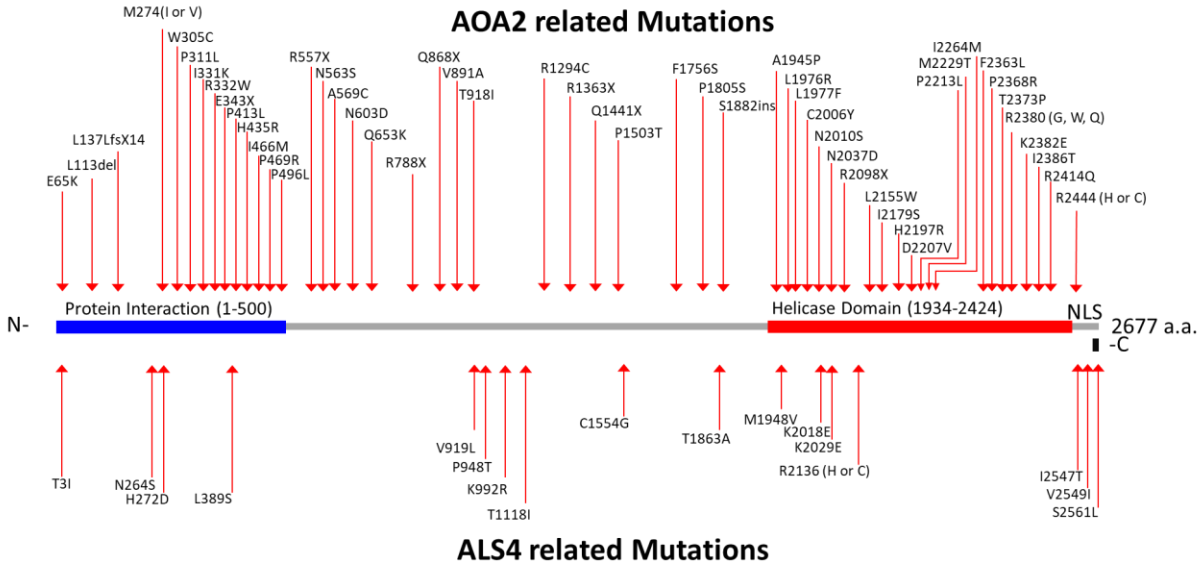

Figure 1.2.1 **Summary of SETX disease-associated mutations**. All currently known AOA2 and ALS4-associated mutations in SETX resulting in amino acid changes.

1.3 Senataxin and the Cellular DNA Damage Response

SETX has been repeatedly identified for involvement in the cellular response to DNA damage[7,25,26]. Initially, it was observed AOA2 patients had defective DDR. Specifically, patient cells were found to have increased sensitivity to DNA damage agents such as H_2O_2, camptothecin (CPT) and mitomycin C; this sensitivity did not apply to ionizing radiation[31]. This, combined with an intact single-strand DNA (ssDNA) break (SSB) repair response, suggested SETX role was specific to oxidative damage repair pathways and double-strand DNA (dsDNA) breaks (DSB)[31,32]. SETX was further implicated in the DDR through the finding that AOA2 patient cells have shortened telomeric DNA, and that in response to DNA damage agents such as CPT, the rate of shortening was increased[32]. SETX was found to co-localize to telomeric regions in a transcriptionally dependent manner suggesting its involvement in telomere homeostasis may be functionally related to the RNA:DNA helicase activity[32]. Additionally, SETX was found to form foci induced by replicative stress[28],with the most predominant foci appearing during S/G2 phase at peak DNA replication - corresponding to peak replication-induced damage[28]. Within these foci, SETX was found to be colocalized alongside DDR factors 53BP1, γH2AX, ATR interacting protein (ATRIP), and BRCA1. SETX foci were found to be resolved either through R-loop resolution or through transcription inhibition, but were increased with more RNA:DNA hybrid formation through the topoisomerase I inhibitor diospyrin D[28]. Recent work has identified a more direct role of SETX in DDR responses. SETX was found to resolve RNA:DNA hybrids which formed in transcriptional active loci where a DSB had occurred to allow access to repair proteins[27]. Furthermore, it was determined that SETX promoted RAD51 recruitment, reduced γH2AX accumulation without affecting DSB repair time, and reduced genomic translocation resulting in increased homologous recombination (HR)[27]. This novel function supports a role of

SETX in a form of transcription coupled DSB repair[27]. Overall, SETX role in the cell is heavily influenced by its RNA:DNA helicase activity and the associated role in R-loop homeostasis.

1.4 Senataxin, R-loops and Their Functions

The primary function of SETX, as it is currently understood, is as a RNA:DNA helicase involved in the resolution of R-loops[12]. R-loops are nucleic acid structures comprising the nascent RNA transcript hybridized to the template DNA and thus leaving the corresponding non-template strand exposed as ssDNA. The RNA:DNA hybrid formed prevents re-annealing between complimentary DNA and thus prevents transcription bubble closure *(Figure 1.4.1)*[33]. R-loop formation is associated with regions of high G/C content and a G/C skew towards the non-template strand, as it is more thermodynamically favorable for RNA:DNA hybridization, and due to the stabilizing effects caused by G quadruplex (G4) formation in the exposed non-template strand[34–36]. Although R-loops have important regulatory functions, prolonged R-loop formation can be deleterious to cells through exposure of the non-template strand to DNA damaging or modifying agents, and also due to the potential for collisions between the replication and transcriptional machinery which can result in DSB[37,38]. Numerous cellular mechanisms have evolved to prevent R-loop formation such as THO complex, comprising Tho2, Hpr1, Mft1 and Thp2 proteins, which binds the nascent mRNA to aid in packaging into ribonucleotide proteins or DNA topoisomerases which relax the negative supercoil formed behind an expanding transcription bubble which allows reannealing of complimentary DNA strands[39–41]. However, once R-loops have formed, resolution requires either destruction of the nascent transcript by enzymes such as RNase H, or preservation of the nascent transcript through unwinding of the RNA:DNA hybrid by SETX[37]. Interestingly, mutations in both SETX and RNaseH have been associated with neurodegenerative diseases; AOA2 and ALS4 in the case of SETX, and Aicardi-

Goutières Syndrome (AGS) in the case of RNaseH[10,31,42] - the latter of which resembles a congenital viral infection due to upregulation of type I interferon responses (IFN)[42]. R-loops homeostasis is therefore critical to cellular health, and mutations in factors that maintain R-loop homeostasis are implicated in several neurological diseases. [36].

R-loops and SETX may also play a role in DNA replication. The host DNA repliosome was found to act as an orientation-dependent R-loop regulator such that R-loops were promoted in head-on orientations and reduced in the co-directional orientation[43]. R-loop intermediates were demonstrated to act as primers in the replication of DNA by the T4 bacteriophages[44], and in yeast mitochondrial DNA replication, R-loops act as RNA primers for initiation[45]. Evidence is growing for a potential role of R-loops in eukaryotic nuclear DNA replication based on several observations. For example, the Origin Recognition Complex (ORC) is known to have high affinity for G4 formed on the non-template strand of R-loops, the highly conserved CpG island origins of replication have a propensity to form stable R-loops upon transcription[46]. Due to ORCs role as a platform for the assembly of the pre-replication complex, increased binding affinity to R-loop prone origins of replication likely plays some role in DNA replication initiation[46]. This was further supported through the observation that persistent R-loop formation in yeast cells was able to result in unlicensed origin-independent replication initiation; this effect being more pronounced in areas of high transcriptional activity such as rRNA genes[47]. R-loops clearly have some role in cellular DNA replication, but its role in gene regulation has not been more thoroughly studied[37].

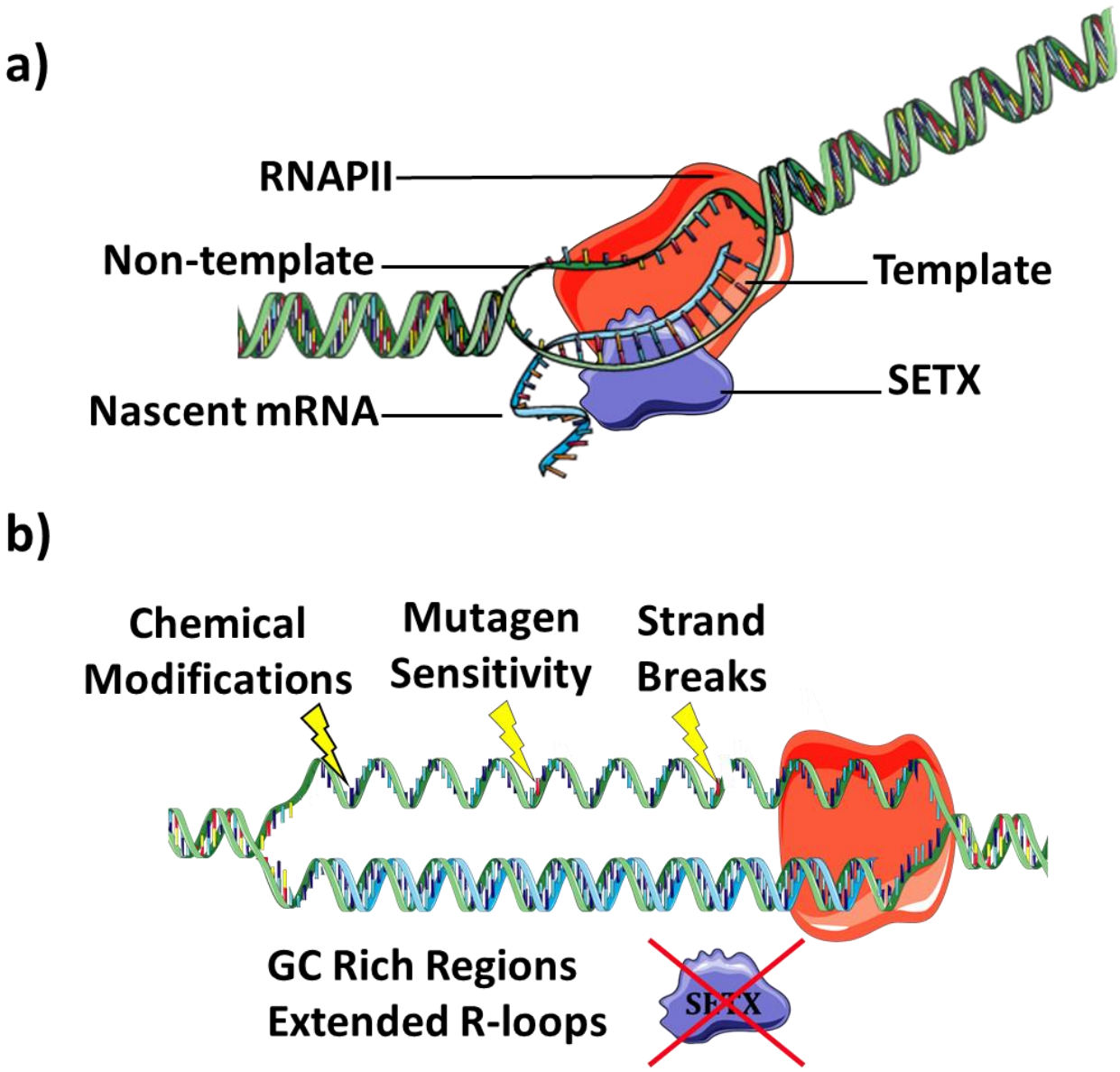

Figure 1.4.1. **R-loop structure and SETX function**. a) Diagram showing the formation of R-loop behind RNAPII comprising the template/non-template ssDNA and the corresponding mRNA hybridized to the template DNA. SETX associates with RNAPII and unwinds R-loops after formation. b) Diagram of extended R-loop formation in the absence of SETX forming in GC rich region contributing to genomic instability.

Across a prototypic gene, there is a skewing for R-loop formation at transcription start sites (TSS) and transcription termination sites (TTS)[37]. Depending on the location of R-loop formation across a gene body, different outcomes in gene regulation can occur. For example, R-loop enrichment at TSS is likely to increase gene expression[37]. It was hypothesized that this might occur as result of decreased DNA methylation of promoters, as R-loop formation negatively correlates with DNA methylation[48]. Indeed, this hypothesis was recently supported in a study using ALS4 patient cells, which have global decreases in R-loop persistence, resulting in decreased promoter methylation of over 1,200 genes[18]. DNA methyl-transferase 1 (DNMT1) has a greater affinity for dsDNA, and thus R-loop formation negatively regulates DNA methylation to promote transcription by blocking promoter methylation[18]. ALS4-associated mutations of SETX can thereby be considered to increase promoter methylation and decrease gene expression. Conversely, AOA2-associated mutations would be associated with increased gene expression of areas prone to R-loop driven promoter methylation[18]. Increased R-loop propensity at TTS is likely to promote transcriptional termination through RNAPII pausing, thereby decreasing gene expression[37]. This was demonstrated through the finding that SETX resolved R-loops at transcriptional pause sites allowing for Xrn-2 dependent 3' transcriptional termination[11]. This would mean that in genes with TTS prone to R-loop formation, ALS4 patients would likely experience greater transcriptional termination and AOA2 patients would show the reverse. Support is growing for the role of R-loops as potent differential regulators of cellular gene expression, specifically in response to exogenous stimuli, such as in the case of the antiviral response[30].

1.5 Senataxin and the Antiviral Response

The type I IFN response is the first line of defense against invading viral pathogens; the system directly interferes with viral biogenesis, hence the name "interferon"[49]. Nearly all cells can mount a type I IFN response. Fibroblasts, in particular, produce significant quantities of IFNβ upon viral infection, which can signal in an autocrine and paracrine manner[50,51]. The binding of IFN-β to the cognate IFNα receptor (IFNαR) ultimately results in the activation of IFN stimulated genes (ISG) via the signaling Janus Kinase (JAK)-Signal Transducer and Activator (STAT) (JAK-STAT) pathway, which results in the formation of the IFN Stimulated Gene Factor 3 (ISGF3) complex[51,52]. ISGF3 is responsible for transcription of numerous ISGs with a myriad of antiviral modalities[53]. These modalities include increasing pathogen sensing and response pathways through increasing pathogen recognition receptor (PRR) expression including Toll-like receptors (TLR), such as the endosomal RNA sensor TLR-3, and Interferon Regulatory Factor 1 or 7 (IRF1 and IRF7) expression, respectively[54–56]. Attacking viral nucleic acid and replication through the 2'-5'-oligoadenylate synthetase (OAS)/RNase L pathway and ISG15, a ubiquitin-like protein which inhibits viral replication[57,58]. Finally, by preventing viral egress to protect neighboring cells through the production of tetherin[59,60]. There are many ISGs expressed subsequent to sensing of viral infection and activation of the master regulator IRF3, which is the gatekeeper to the antiviral response[61]. Modifying the IRF3 response can therefore alter the course of the entire antiviral response[61].

Recently, our group determined a novel role of SETX in the context of infection by RNA viruses such as Influenza A Virus (IAV) and West Nile Virus (WNV)[30]. In the absence of SETX, infected cells increased expression of genes relevant to the antiviral response such as interferon β (IFNβ), IFN-induced protein with tetratricopeptide repeats 1 / 2 (IFIT1/2) and CXC motif

chemokine 10 (CXCL10)[30]. Importantly, this effect was dependent on RNA virus infection, as uninfected cells did not show this same elevation in antiviral gene expression[30]. It was determined that SETX caused premature transcription termination at IRF3 responsive elements (IRE) mediated through TATA-box binding protein associated factor 4 (TAF4) recruitment[30]. It is currently unknown whether ALS4 patients with gain of function mutations of SETX would display an inverse antiviral response phenotype such that cells have decreased response sensitivity[18]. There is significant support for involvement of the antiviral response in the context of neurodegenerative diseases based upon the consistent observation of chronic neuroinflammation as a signature of neurodegenerative diseases [62,63]. Therefore, viruses may serve to trigger and/or exacerbate these diseases.

1.6 Senataxin and Viruses

Thus far, the experimentally identified effect of SETX on viruses has been strictly indirect[30]. RNA viruses do not produce RNA:DNA hybrids through RNAPII, and additionally, encode their own RNA-dependent RNA polymerases[64]. Therefore, SETX has no (as we currently understand) opportunity for direct interactions with the virus genome. However, DNA viruses, such as Herpes Simplex Virus 1 (HSV-1), require host cell RNAPII for viral gene transcription[65,66]. Additionally, numerous cellular factors affect replication[3]. Examples of these type of factors include members of the DDR, of which aberrations in the DDR pathway have frequently been demonstrated to alter viral biogenesis[67,68]. Since SETX associates with RNAPII as a regulator of transcription, and SETX has various associations with the DDR, there is compelling rationale for investigating the potential impact of SETX on DNA viruses[9,11,12,14,25,28–32,69].

Choosing a well-characterized model such as HSV-1 to study the role of SETX on DNA viruses has multiple advantages. Fully annotated genomes exist for multiple strains of HSV-1 alongside a plethora of mutant viruses and other reagents[70–73]. HSV-1 replicates in the nucleus and uses RNAPII to transcribe its genes.[74] As a nuclear protein, SETX therefore has direct access to the viral genome. Additionally, HSV-1 is neurotropic and it has been associated with neurodegenerative diseases like Alzheimer's Disease (AD)[75]; therefore, it may be directly relevance to SETX-related neurodegenerative diseases [70,71,76].

1.7 Herpes Simplex Virus 1

HSV-1 belongs to the *Alphaherpesvirinae* subfamily[77]. It is an enveloped, neurotropic and neuroinvasive virus for which >80% of individuals test seropositive by adulthood[65]. HSV-1 is a human pathogen and is capable of infecting a plethora of cell types including neurons, epithelial cells and leukocytes during lytic infection, but is also able to establish lifelong latency in sensory neurons, and reactivate periodically under certain stimuli[65,78–81]. HSV-1 entry is mediated through initial interactions between viral glycoproteins gB and/or gC with heparan sulfate proteoglycans present on cellular surfaces to initially concentrate virus at the cell surface[82], but glycoproteins gD, gH-gL, and gB mediate fusion with the cellular plasma membrane, or vesicular membrane if HSV-1 is up-taken via endocytosis or phagocytosis[83,84]. This entry systems facilitates virus entry in a wide range of cell types *in vitro* and *in vivo.*[83].

Upon viral entry, HSV-1 deploys an elaborate arsenal to rapidly overwhelm the target cell and allow for viral growth[81,83,85]. Perhaps the most potent of these strategies is the virion host shutoff (VHS) protein which triggers rapid host protein synthesis shutdown[81]. VHS accomplishes this feat through binding of the mRNA 5' cap, via affinity towards the translation initiation factor eIF4H[81,86]. Subsequent uncapping and 5' to 3' RNase activity results in the degradation of the

targeted mRNA and a shutoff of corresponding protein synthesis[81,86]. Additionally, the viral E3-ubiquitin ligase Infected Cell Polypeptide-0 (ICP0) has strong anti-IFN activities by mechanisms such as the antagonism of IRF3 phosphorylation[87]. The immediate-early protein ICP27 interferes with the cellular pathways of sensing virus through the cyclic GMP-AMP synthase/Stimulated of IFN genes (cGAS/STING) system; downstream of Tank Binding Kinase-1 (TBK-1) prior to the activation of IRF3[86,88,89]. HSV-1 thus effectively targets the antiviral response at several stages, in order to prevent sensing while reconditioning the host cell to facilitate its own replication[87].

The virus carries a ~152 kbp dsDNA genome consisting of unique long (U_L) and unique short (U_S) genomic segments flanked by G/C-rich inverted repeat regions, with a potential for four possible genomic isomers[77,90]. The genome contains >80 viral genes which require host RNAPII to mediate transcription[81,91]. Upon viral entry into a target cell and transport of viral DNA to the nucleus, viral DNA circularizes and immediate early (IE) gene transcription begins[77]. IE transcription is regulated through formation of a transcriptional regulatory complex comprising viral protein 16 (VP16/*UL48*) and two host transcription factors: Host Cell Factor 1/VP16-accessory protein (HCF1) and POU homeodomain protein 1 (OCT1)[1,92]. VP16 is a viral late (L) protein delivered to the target cell via the viral tegument, and once in the cytoplasm, is imported into the nucleus where it binds HCF1 and subsequently OCT1[1]. The VP16 induced complex (VIC) binds "TAATGARAT" elements in the HSV-1 IE-gene promoter and activates transcription[1]. Upon IE protein synthesis, IE proteins activate early (E) gene transcription[1]. Many E proteins are involved in viral DNA replication, and following viral DNA synthesis, L genes are expressed[74]. L genes encode predominantly structural proteins and factors that facilitate viral egress, including VP16, the viral factor required for IE gene expression[77]. The temporal cascade of HSV-1 gene expression is illustrated below in *Figure 1.7.1.* With viral gene expression under

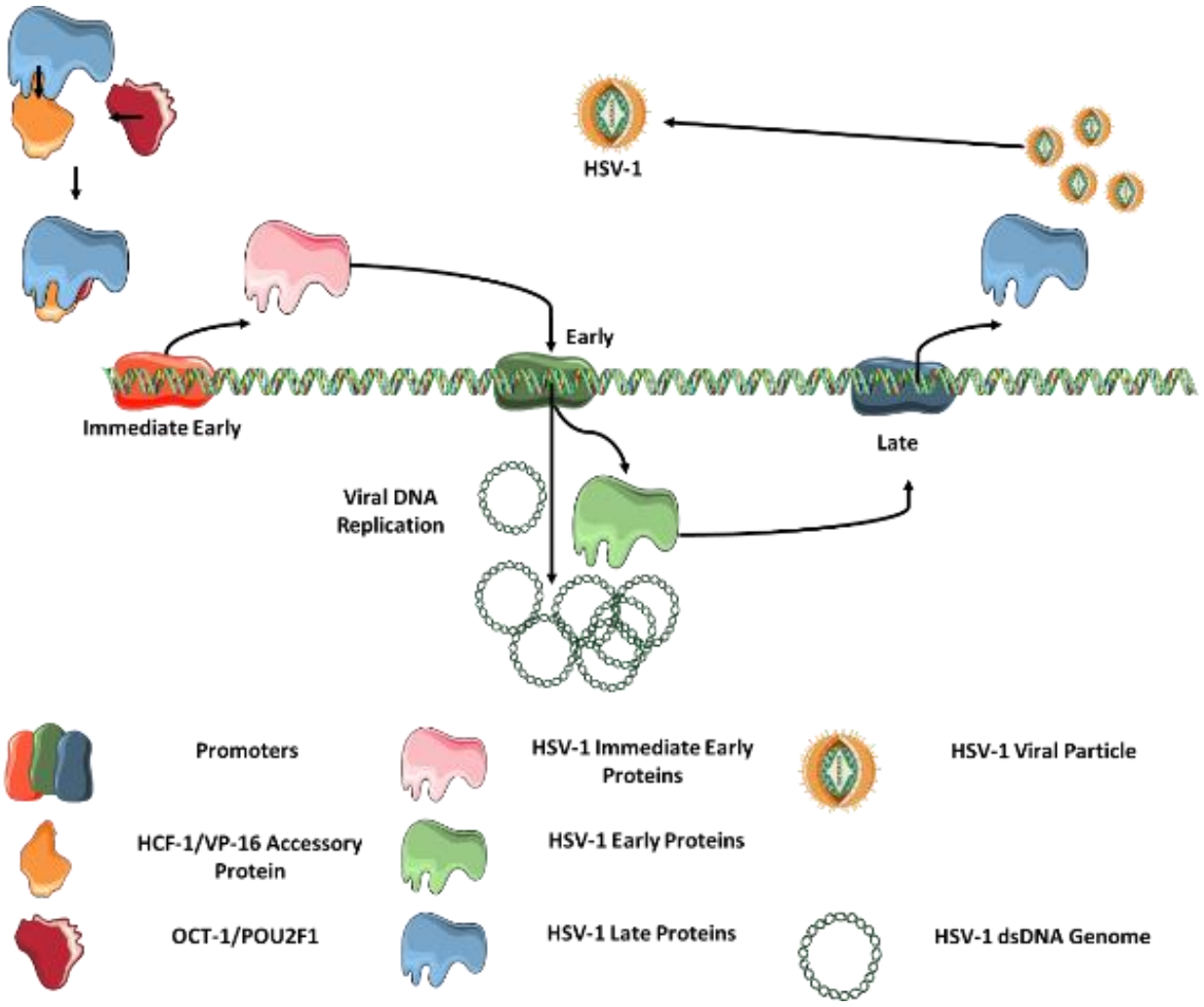

Figure 1.7.1. **HSV-1 temporal cascade of viral gene expression**. Initiation of immediate early (IE) gene transcription requires formation of the Viral initiation complex (VIC) comprising viral protein 16 (VP16) and cellular transcription factors HCF1 and OCT1. VIC binds the TAATGARAT box of the IE early promoter and viral transcription commences. Transcription of Early € genes requires IE proteins. E proteins are involved in replication of viral genome are required for transcription of Late (L) viral genes and subsequent viral capsid formation and viral particle packaging.

tight regulatory control, factors affecting any step in the pathway may ultimately alter viral biogenesis.

1.8 Herpes Simplex Virus 1 and the DNA Damage Response

Successful DNA replication is a complicated process for HSV-1, as DNA replication is tightly regulated in host cells [3,93]. Excessive DNA replication can result in increased DDR, ultimately triggering cellular apoptosis. Therefore, viral interplay with cellular DDR is unavoidable[94]. The HR DDR, a high fidelity/low error repair strategy,[95] is required to aid in viral DNA replication and recombination[3]. HR is responsible for genomic inversions between the U_L and U_S segments resulting in four potential viral genome isomers[96]. Viral replication is inhibited in cells lacking Ataxia Telangiectasia mutated (ATM) or the Mre-11, Rad-50, Nbs-1 (MRN) complex, and it has been demonstrated that HSV-1 infection induces ATM kinase activation resulting in γH2AX foci formation, a marker of DNA damage[3]. However, the HR repair factors BRCA1 and 53BP1 are not recruited to these foci, as the viral E3 ligase ICP0 targets their recruitment factors, RNF8 and RNF168, for degradation[97]. Therefore, HSV-1 inhibits the repair steps of HR, but requires initiation factors like ATM for productive infectious cycles[3,97].

Cells with an active ATM response can also be expected to activate the ATR response[98]. The ATR response becomes activated by long stretches of ssDNA, such as those formed by stable R-loops, or by substrates produced following ATM-mediated end resection[68]. Cells undergoing HSV-1 infection do not maintain proper ATR responses, as HSV-1 actively excludes both ATR and the corresponding recruitment factor ATRIP from viral replication compartments through ICP0[68]. This is likely to aid in viral recombination as exogenously induced ATR responses result in decreased viral recombination frequencies[3]. Fine tuning of the cellular DDR

pathways by HSV-1 may also be in response to the rolling circle mechanism HSV-1 employs in order to replicate viral DNA[3].

HSV-1 replicates via a rolling circle mechanism where the viral genome is contiguously produced by the viral DNA polymerase (UL30) in long, repeating genome concatemers arranged head-to-tail[99,100]. During viral genome packaging, unit-length genomes are cleaved off from the long concatemer into individual viral genomes; these cleavage events create structures analogous to DSBs[90]. Within the viral replication compartments the DSB are capable of being sensed through the sequestered DNA damage sensing MRN complex[101]. However, proper viral genomic processing requires the DSB and thus must inhibit repair factors of DDR as described above without triggering DNA damage triggered apoptosis[74,77,94]. This fine tuning of the DDR for viruses like HSV-1 is likely why various DDR factors are also associated with antiviral activities[2,3].

1.9 Viruses as they Relate to Neurodegeneration

There have long been associations between various viral infections and neurodegenerative diseases[75]. Poignantly, the example of poliomyelitis, caused by the enterovirus *Poliovirus,* is a hallmark reminder of the connection between viral infection and neurological damage[75,102]. Afflicted individuals suffer rapid loss of lower motor function resulting in asymmetrical lower limb paralysis. Interestingly, the sensory neurons are largely unaffected as is typical of motor neuron diseases such as ALS[75,102,103]. Even viruses often unassociated to the nervous system have neurological sequela[104]. Acute IAV infection has been shown to result in a short-term acute inflammation in infected tissues (typically respiratory), but also alteration of central nervous system (CNS) inflammatory profiles[104]. Specifically, neurotropic H7N7 IAV or non-neurotropic H3N2 IAV, results in impairment of spatial memory,

long term hippocampal functional/structural alterations and extended microglial inflammatory responses typical of chronic inflammation[104].

Recently, there has been evidence to support a potential link between human endogenous retrovirus (HERV) sequences and ALS[105]. ALS patients negative for exogenous retroviruses such as Human Immunodeficiency Virus (HIV) displayed unexpectedly high levels of reverse transcriptase activity in cerebrospinal fluid relative to healthy controls[106]. Post-mortem tissues of ALS patients also showed increased expression of HERV-K transcripts and envelope protein relative to controls[106]. Transgenic (Tg) mouse models expressing HERV-K envelope protein displayed ALS-like symptomology of upper and lower motor neuron degeneration[103]. It is not understood how HERV elements become activated, but the effect of exogenous retroviral infection causing reactivation has been ruled out as a likely possibility[103,105]. Developing applicable animal models of neurodegenerative disease are vital to study viral relationships with neurodegenerative diseases. This is especially important in the case of HSV-1, since a large portion of the population has been exposed to the virus [75].

To aid in the understanding of SETX and its role in neurodegenerative diseases, a SETX $^{(-/-)}$ KO mouse model was generated recently[7]. These mice were generated with the intention to be a model for AOA2 – since individuals with AOA2 generally fail to produce SETX protein[7]. However, under sterile housing conditions, these mice do not display any documented neurodegenerative diseases or related neurological phenomena and are not a demonstrated model of AOA2[7]. The only noted phenotype is that of SETX $^{(-/-)}$ male sterility due to the absence of SETX, which results in defects in spermatogenesis[7]. This lack of a neurodegenerative phenotype of the SETX mouse model will lend weight to the hypothesis that viruses may act as triggers of neurodegenerative disease onset and progression. A model

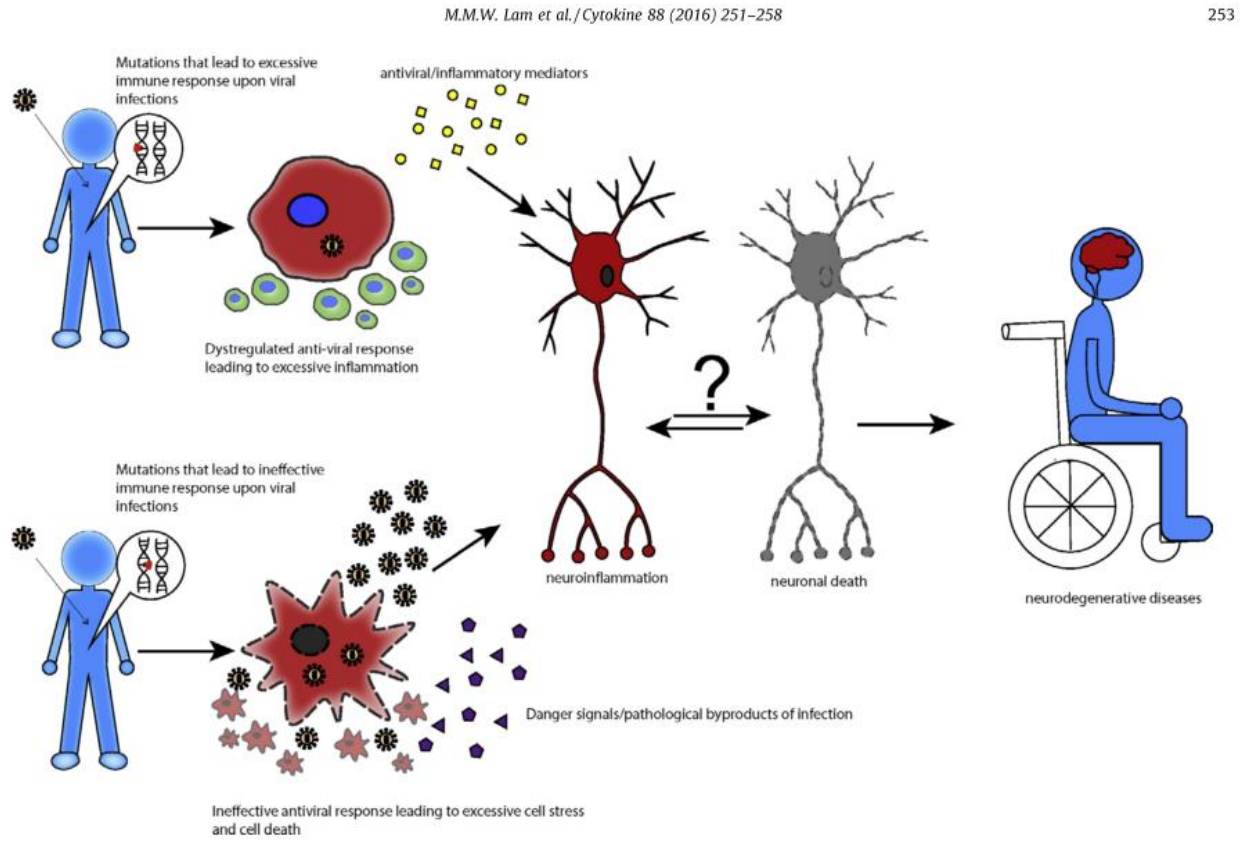

Figure 1.9.1. **Model of genetic/viral interactions that affect neurodegenerative disease.** Both gain-of-function and loss-of-function mutations in genes involved in antiviral response have been implicated in neurodegenerative diseases. Gain-of-function mutations in genes associated with the antiviral response might result in excessive inflammatory responses upon infection which promotes disease. In contrast, ineffective antiviral responses due to loss-of-function mutations would be predicted to delay viral clearance and promote cell stress pathways associated with disease etiology. **Taken from Lam *et al*., 2016 Fig 1.**

displaying genetic and viral interactions that will play roles in the development of neurodegenerative diseases can be found above (*Figure 1.9.1).*

1.10 Hypothesis

Currently, there have been no studies documenting affects cellular RNA:DNA helicases like SETX on a DNA virus replication. Our group has already demonstrated the novel role of SETX as a negative regulator of the antiviral response during exposure to RNA viruses [30]. The effects of SETX on RNA viruses were mediated via its regulation of the antiviral response[30]. However, based upon the known functions of SETX, there is a good rationale to infer SETX will not only have similar antagonism of host antiviral responses to HSV-1, but may also interact more directly with the virus by way of regulating viral transcription and viral DNA replication. Given the known functions of SETX, and their considerable overlap with pathways used during DNA virus transcription and replication, we proposed the hypothesis that ***SETX is involved in the regulation of viral DNA replication, viral gene transcription, and the innate immune response stimulated by viral DNA***. To investigate this, we developed the following three aims:

1. To determine whether SETX modulates viral DNA replication during infection.
2. To test whether SETX regulates viral gene expression during infection.
3. To confirm whether SETX antagonizes the antiviral response to DNA viruses.

Chapter 2

Materials & Methods

In-Vitro Experiments

2.1 Cell Lines

All cell lines were maintained at 37°C and 5% CO_2 in media supplemented with 100U/mL Penicillin, 100µg/mL streptomycin and 2mM L-glutamine unless otherwise stated. All incubation involving live cells were performed at 37°C and 5% CO_2 unless otherwise stated. Human Foreskin Fibroblasts (HFF), human embryonic kidney 293 (HEK-293), HEK-293-T, and Vero cells were originally obtained from the American Type Culture Collection (ATCC) and maintained in Dulbecco's Modified Eagle's Medium (DMEM) with 10% fetal bovine serum (FBS). IRF3/9 $^{-/-}$ mouse embryonic fibroblasts (MEF) were a kind gift from Dr. Karen Mossman (McMaster University) and were maintained in DMEM with 15% FBS. SETX$^{+/+}$ and SETX $^{-/-}$ MEF were isolated from pregnant SETX$^{+/-}$ mice bred with SETX$^{+/-}$ males at 13.5 days post-copulation and maintained in DMEM with 15% FBS.

2.2 Viruses

HSV-1 strain KOS and strain 17-syn^{+} (17+) were generous gifts from Dr. Karen Mossman (McMaster University). HSV-1 viruses were propagated on and titred on Vero Cells. E1-deleted Adenovirus-5 containing a green fluorescent protein (GFP) construct inserted under control of the human Cytomegalovirus (CMV) IE promoter (AdV-GFP) was a gift from Dr. Joe Mymryk (Western University) and was propagated in HEK-293 cells, and titred in HFF cells using immunofluorescence microscopy.

HSV-1 strains were sucrose cushion purified. Confluent Vero cell monolayers in T150 flasks were infected with HSV-1 at multiplicity of infection (MOI) of 0.01 plaque forming units (PFU), equivalent to $1.5x10^5$ PFU, in 4mL of serum-free DMEM for 1 hour at 37°C. Cells were washed with PBS and maintained in 5% FBS/DMEM. Cells were infected for 2-3 days until cells lifted from flask, after which cell-associated virus was separated from viral supernatant through centrifugation in an Allegra ® X-12R Centrifuge (Beckman Coulter) at 400 X g for 10 min. Viral Supernatant (1) was removed from associated Cell pellet (1), and pellet was resuspended in serum-free DMEM and frozen at -80°C and subsequently freeze/thawed three times, followed by homogenization with Dounce homogenizer and centrifugation in Allegra ® X-12R Centrifuge (Beckman Coulter) at 400 X g for 10 min to collect viral supernatant (2). Viral supernatant (1) virus was isolated by ultracentrifugation at 25,000 rpm for 2 hours at 4°C in SW32Ti (369694, Beckman Coulter) rotor in centrifuge tube (344058, Beckman Coulter) and the resultant viral pellet was suspended in viral supernatant (2). The combined virus was further purified through 36% sucrose cushion at 30,000 rpm for 2 hours at 4°C in SW41 rotor and tube (344059, Beckman Coulter). Supernatant was removed, and pellet was resuspended in serum-free DMEM, aliquoted and frozen at -80°C. Viral titres were determined following one freeze/thaw cycle and titre values were used for subsequent experiments.

AdV-GFP was purified using a CsCl gradient. HEK 293 cells were grown to 90% confluency in T150 flasks, washed with PBS and infected with MOI 5 AdV-GFP in 1X Modified Eagle's Medium (MEM)/F11 for 1 hour at 37°C. Inoculation media was removed and replaced with 10% FBS/DMEM and incubated for 48 hours until cytopathic effect (CPE) was noted. Flasks were agitated to remove cells and media was centrifuged at 1,500 RPM at room temperature in Allegra ® X-12R Centrifuge (Beckman Coulter) for 5 min. Cell pellet and

supernatant were separated and pellet was resuspended in 2 mL of PBS per flask used. Cell-associated fraction was freeze/thawed three times and vortexed with each thawing and then centrifuged at 3,000 RPM for 10 min in an Eppendorf 5424 centrifuge. Virus-containing supernatant was kept, and the cell pellet was discarded. A Beckman Coulter centrifuge tube (344058) was layered with 10 mL of 4M CsCl and level was marked. On top of this, 5 mL of 2.2M CsCl solution was added to generate the gradient. Supernatant of the cell-associated fraction was layered on top and additional volume was filled with the initial viral supernatant such that 0.5 cm of space was left at the top of the tube. The virus was ultra-centrifuged in SW32Ti (369694, Beckman Coulter) swing bucket rotor at 32,000 RPM at 15°C for 1 hour with no braking. Media was aspirated to above the hazy virus-containing band slightly above the marked line (~0.5 cm) and virus band was aliquoted and frozen at -80°C as purified AdV-GFP. Virus was then titred as described below in section 2.4.

2.3 Transfection

HFF and IRF3/9 MEF were transfected at 50% confluency with 50nM *SETX*-specific SMARTpool ON-Targetplus siRNA (siSETX), human cells (L-021420, Dharmacon) and mouse cells (L-066634, Dharmacon), or 50nM ON-Targetplus non-targeting pool (D-001810-10, Dharmacon) for control conditions. RNA was delivered in lipofectamine RNAiMAX (13778159, Invitrogen) in Opti-MEM ™ Reduced Serum Medium, GlutaMAX ™ Supplement (51985034, Gibco) for 24 hours and then removed and 10% or 15% FBS DMEM for HFF and MEF respectively. All cells in siRNA were depleted of SETX for 48 hours prior to experiments.

Hyper STING (hSTING) and dead STING (dSTING) plasmids were gifts from Dr. Brian Lichty (McMaster University) and were cloned into the pcDNA3.1+ vector. HEK293T cells

were transfected with hSTING or dSTING at a (1:10) ratio delivered in lipofectamine 2000 (11668019, Invitrogen) according to manufacturer's instructions. Cells were used for further assays following 24 hours of plasmid expression. STING experiments were performed by a previous lab member, Mannie Lam.

2.4 *In*-vitro Viral Infection

HSV-1 and AdV-GFP infections were performed with cells at 48 hours post transfection or 80-90% confluency for SETX MEF. Cells were washed with PBS and virus was diluted in serum-free DMEM to MOI = 5. Virus was added for 1 hour at 37°C and rotated every 10 min. Virus was removed, cells were washed with PBS and media was replaced with 10% FBS/DMEM for the extent of the experiment. Foscarnet (1283302 USP, Sigma-Aldrich) was added to a final concentration of 0.5 mg/mL from a 40 mg/mL stock following 1-hour infection in relevant experiments.

2.5 Nucleic Acid Isolation

RNA for RT-qPCR was isolated using TRIzol ® Reagent (15596026, Invitrogen). Cell supernatant was removed and 400 μL of TRIzol was added directly to cells and then homogenized. Samples were stored at -80°C until isolation where 80 μL (0.2 mL per 1 mL Trizol) of chloroform was added to RNA mixture. Tubes were inverted and incubated for 3 min at room temperature and centrifuged at 12,000 X g for 15 min at 4°C in an Eppendorf 5424 centrifuge. The upper clear aqueous phase was separated for RNA isolation. A carrier agent of 10 μg of RNase-free glycogen (R0551, Thermo Scientific) was added to each tube to aid in precipitation and 200 μL of isopropanol (0.5 mL / 1 mL Trizol) was added for 10 min incubation

at 4°C. Samples were centrifuged at 12,000 X g for 10 min at 4°C and supernatant was removed from RNA pellet. RNA pellet was resuspended in 400 µL of 75 % ethanol, vortexed briefly, and centrifuged at 7,500 X g for 5 min at 4°C. Supernatant was discarded and pellet was air dried for 5-10 min and then resuspended in 30 µL of nuclease-free water. RNA concentration was analyzed using a DeNovix Ds-11 spectrophotometer and samples were stored at -80°C until usage.

Cell-associated DNA for qPCR was isolated from 12-well plates by removing supernatant, rinsing gently with PBS, and then adding 160 µL of 2X Trypsin/EDTA (15400054, Gibco) for 5 min at 37°C to release cells. Trypsin was neutralized with 1mL of 10% FBS/DMEM and suspension cells were centrifuged at 500 X g for 5 min in Eppendorf 5424 centrifuge at room temperature. Supernatant was removed and cells were washed with 1 mL of PBS and pelleted again at 500 X g for 5 min. Cells were resuspended in 250 µL of nuclease-free water and an equal volume of phenol: chloroform: isoamyl alcohol (25:24:1 v/v) (15593031, Invitrogen) was added with suspended cells and mixed by inversion for 20 seconds (s) to ensure layer mixing. Mixture was centrifuged at 16,000 X g for 5 min at room temperature and top aqueous layer was separated into RNase/DNase free tube and stored at -80°C until purification.

DNA was purified through addition of 20 µg RNase-free glycogen (R0551, Thermo Scientific), 0.5X sample volume NH_4OAC (125 µL), and 2.5X total volume 100% ethanol (937.5 µL). Tubes were mixed through inversion and stored at -20°C for 12 hours to precipitate DNA, and then centrifuged at 16,000 g in Eppendorf 5424 centrifuge for 30 min at 4°C to pellet the gDNA. Supernatant was removed and 150 µL of 70% ethanol was added to wash pellet and sample was centrifuged at 16,000g for 2 min at 4°C. Wash step was repeated, ethanol was removed, and pellet was air dried for 5-10 min. Pelleted gDNA was resuspended in 30 µL of

nuclease-free water. DNA concentration was analyzed using a DeNovix Ds-11 spectrophotometer and samples were stored at -80°C until usage.

RNA for RNA-Sequencing was isolated using RNeasy ® Mini Kit (74104, Qiagen) according to manufacturer specifications. All steps of centrifugation were performed at room temperature in an Eppendorf 5424 centrifuge. To each well, 350 µL of buffer RLT was added and incubated at room temperature until complete cell lysis was observed under microscope. Lysate was then centrifuged at maximum speed for 3 min and supernatant was removed and mixed with 350 µL 70% molecular grade ethanol (676829, Sigma-Aldrich) and then applied to RNeasy Mini spin column. Column was spun at 10,000 X g for 15 s and 350 µL of buffer RW1 from RNase-free DNase set (79254, Qiagen) was added directly onto column and then centrifuged for 15 s at 10,000 X g. A volume of 10 µL of the DNase I stock solution was added to buffer RDD, mixed by inversion, and then 80µL of the mixture was applied directly to spin column membrane for 15 min. Buffer RW1 was then applied to column and centrifuged for 15 s at 10,000 X g. A volume of 500 µL of buffer RPE was then added to the RNeasy spin column and centrifuged for 15 s at 10,000 X g, and then once more with 500 µL of buffer RPE but for 2 min at 10,000 X g to wash membrane. Spin column was then placed in a RNase free 1.5mL collection tube and 35 µL of RNase-free water was added directly to the membrane and centrifuged for 1 min at 10,000 X g to elute RNA. Flow-through was collected and reapplied to membrane to concentrate RNA and centrifuged again as above. RNA concentration was analyzed using a DeNovix Ds-11 spectrophotometer and samples were stored at -80°C until usage.

2.6 Quantitative PCR

RNA for RT-PCR was transcribed into cDNA using the Maxima First Strand cDNA Synthesis Kit for RT-qPCR (K1641, Thermo Scientific) according to manufacturer specifications. RNA was aliquoted to 500-1000 ng per reaction mixture. To each 20 µL reaction mixture, 4 µL of 5X Reaction Mix and 2 µL of Maxima Enzyme Mix were added. The remaining volume was filled with nuclease-free water. Additional negative controls containing no RNA template (NTC) and no reverse transcriptase (-ve) were made where the additional volume was filled by water. Reaction was mixed through inversion and then incubated in Veriti ™ 96-Well Thermal Cycler (4375786, Applied Biosystems) for 10 min at 25°C, 15 min at 65°C and then reaction as terminated at 85°C for 5 min. Synthesized cDNA was stored at -80°C until usage.

All quantitative PCR was performed in triplicate using SensiFast SYBR Hi-ROX kit (BIO-82005, FroggaBio) as described by manufacturer guidelines in a MicroAmp® Fast 96-Well reaction plate (4346907, ThermoFisher). All qPCR amplification was performed using the QuantStudio 6 Flex (4485697, Applied Biosystems). cDNA or gDNA samples were diluted to standard concentration across all samples. All reagents were kept on ice and the Fast 96-Well reaction plate was kept on 96-well plate ice block. Master mix solutions were prepared for a given number of samples in triplicate based on the mixture of 10 µL 2X SensiFAST SYBR Hi-ROX mix, 0.16 uL forward and 0.16 µL reverse primer, and 4.68 µL nuclease-free water per sample (e.g. 5 DNA samples, 15 reactions, 150 µL reaction mix, 2.4 µL of each primer, 70.2 µL water). For each triplicate reaction, 45 µL of master mix was aliquoted onto parafilm, and 15 µL of template DNA was mixed in droplet and 19 µL of mixture was added to individual reaction wells for three wells of 19 µL of reaction mixture. This was repeated for all samples. Additional

non-template controls were made where 15 µL of water was used in place of DNA template for gDNA samples.

PCR reactions were performed using standard reaction conditions optimized to primer design based on manufacturer recommendations of 1 cycle polymerase activation (95°C X 2 min) and 40 cycles denaturation and annealing/extension (95°C X 5 s, 65°C X 30 s) with melt-profile generated at end of reaction. All RT-PCR data output was analyzed through a ΔΔ cycle threshold (Ct) method. Gene expression was normalized to either GAPDH or 18s RNA and expressed as fold changed relative to the control or WT condition at 0 hours for host genes, or earliest timepoint for viral genes.

Quantification of viral gDNA of *UL54* and *UL44* was normalized to the amount of cellular GAPDH gDNA. Ct value was converted to numerical value of $2^{\wedge-CT}$, and converted into a relative amount of viral to host gDNA. Ratio values between *UL54* and *UL44* were compared and found to be within one standard deviation of the mean and averaged to determined relative viral to host gDNA content per cell.

2.7 Viral Titration and Plaque Assays

All HSV-1 viral titration plaque assays were performed using Vero cells. Virus titred was 10-fold serially diluted in serum-free DMEM. Vero cells were plated in 6-well plates at 5 X 10^5 cells/well and infected at 90-95% confluency. Wells were washed with PBS and infected with 400 µL of virus dilutions for 1 hour at 37°C, rotating plates every 10 min. Viral media was removed, and wells were washed three times with PBS and then suspended in 5% FBS/1% Human Serum (H4522, SIGMA) DMEM. Cells were maintained for 48 hours at 37°C and 5% CO_2 and then fixed with 3.7% paraformaldehyde in PBS for 1 hour and then stained with Crystal

Violet (C3886, SIGMA) for 20 min. Plaques were counted and viral titre was determined. Viral titres of samples below the limit of detection were defined as the limit of detection divided $\sqrt{(2)}$ (~1.414)[107]. For example, if the limit of detection was 250 PFU/mL, a sample containing no positive plaques would be assigned a value of ~177 PFU/mL.

AdV-GFP was titred using HFF cells. Virus was serially diluted 10-fold in serum-free DMEM. HFF cells were plated in 24-well plates and infected at 90-95% confluency. Wells were washed with PBS and infected with 100 µL of virus dilutions for 1 hour at 37°C, rotating plates every 10 min. Viral media was removed, wells were washed with PBS, and media was replaced with 5% FBS/DMEM. Infected cells were maintained at 37°C for 48 hours and then imaged using an EVOS ™ FL Imaging System (AMF4300, ThermoFisher) with GFP (AMEP4651, ThermoFisher) light cube. GFP positive cells were counted to determine viral titre at specified dilutions.

2.8 Protein Extraction and Western Blot Analysis

Cells were lysed in Pierce Protease and Phosphatase Inhibitor (88668, ThermoScientific) diluted in NP-40 lysis buffer and quantified using a BCA Assay Kit (23225, ThermoScientific) and quantifying via a SpectraMax®i3 (Molecular Devices) relative to a Bovine Serum Albumin (BSA) protein standard.

All sodium dodecyl sulfate polyacrylamide gel electrophoresis (SDS-PAGE) and Western blotting was performed using Bolt ™ Mini Gel Tank (A25977, ThermoFisher) at room temperature. Protein samples were diluted to constant concentrations across all samples. Lysates were incubated for 5 min at 95°C in 4X NuPAGE ™ LDS Sample Buffer (NP0007, Invitrogen) and then loaded onto to 1.0 mm NuPAGE ™ 4-12% Bis-Tris Protein Gels (NP0321BOX,

Invitrogen™) along with 5 µL of BLUelf prestained protein ladder (PM008-0500, Gene Direx) and electrophoresed at 100 V for 90 min in 1X Bolt ™ 3-(N-morpholino) propanesulfonic acid (MOPS) SDS Running Buffer (B000102, Invitrogen™).

Proteins were wet transferred from gel using Bolt ™ Mini Bolt Module (B1000, ThermoFisher). A 0.2 µm Polyvinylidene fluoride (PVDF) membrane (10600021, GE Healthcare) was activated with 100 % methanol for 5 s, washed in distilled water for 2 min, and then incubated in transfer buffer (25mM Tris, 192 mM Glycine, 3% Methanol v/v, 0.5% SDS w/v, 0.1% Bolt ™ antioxidant [BT0005, Invitrogen]) for 5 min. Sponge pad and filter paper were soaked in transfer buffer and mini blot was prepared layering from the bottom of the cassette to the top, in order of: sponge pad, filter paper, gel, PVDF membrane, filter paper, sponge pad. Module was closed and transferred for 90 min at 125mA. Membrane was removed and blocked for 1 hour in blocking buffer made with 5 % skim milk powder in TBS-T (50mM Tris-Cl pH 7.5, 150mM NaCl, 0.05 % Tween20) and was agitated at room temperature. Primary antibody was diluted in blocking buffer to a minimum of 10 mL volume, concentrations are reported in *Table 2.10.2*, and incubated with membrane under agitation overnight at 4°C. Membrane was washed four times for 15 min at room temperature in TBS-T under agitation and horse radish peroxidase (HRP)-bound secondary antibody, corresponding to species of primary antibody, was diluted in blocking buffer and added to membrane for 1 hour at room temperature under agitation. Membrane was then washed 3 X for 15 min with TBS-T and then for 15 min with TBS (50mM Tris-Cl pH 7.5, 150mM NaCl). Protein bands were visualized with Pierce ECL Western Blotting Substrate (32106, Invitrogen) and Blu-Lite Autoradiography film (DIAFILM810-LITE, Diamed). Substrate was applied to membranes in plastic sheet for 1 min to ensure even absorption onto membrane. Films were exposed for a range of times depending on protein.

2.9 Immunofluorescence Microscopy

HFF cells infected with AdV-GFP were washed with PBS and imaged using EVOS ™ FL Imaging System (AMF4300, ThermoFisher) using GFP (AMEP4651, ThermoFisher) light cube under lowest exposure periods to reduce background fluorescence and saturation. AdV-GFP expression of GFP was quantified using ImageJ software. [108,109] Images were converted to 8-bit color, binary colors, and threshold set to 3-255 pixels. Measurement was set to percent area and integrated density and particle size was set to 30-infinity in size. Measurement of integrated density was taken for all images. Uninfected cells were used as negative control for each time point and background fluorescence was subtracted for each infected cell timepoint.

2.10 DNA Primers and Antibodies

All DNA primers and antibodies used throughout the course of this thesis are found below in *Table 2.10.1* and *Table 2.10.2,* respectively. All DNA primers, except for those derived from published sources, such as SETX-1,2,3, were designed using the National Center for Biotechnology Information (NCBI) primer-BLAST tool[110]. Primers for cDNA were designed using exon-exon spanning sequences, where possible. Melting temperatures were all set to ~60°C and between primer binding sites were selected to contain 50-60% GC content, where possible. All primers were ordered from Invitrogen™ and diluted in nuclease-free water upon delivery to a standard concentration of 50 μM and stored at -20°C. All antibodies were stored as prescribed by manufacturer. Dilutions for assays used are described in *Table 2.10.2*.

Table 2.10.1. **Summary of primers used throughout all experiments oriented 5' to 3'.**

Gene Target	Forward Primer	Reverse Primer
Human GAPDH cDNA	GCAAATTCCATGGCACCGT	GCCCCACTTGATTTTGGAGG
Human 18S rRNA cDNA	GTAACCCGTTGAACCCCATT	CCATCCAATCGGTAGTAGCG
Human SETX cDNA	CAGGGTCGGCAGAAGGATT	TCCAATGCTGGTTTTCCATCAG
Human IFNβ cDNA	AGCACTGGCTGGAATGAGAC	TCCTTGGCCTTCAGGTAATG
Human IFIT1 cDNA	AAAAGCCCACATTTGAGGTG	GAAATTCCTGAAACCGACCA
Human IFIT2 cDNA	AGGCTTTGCATGTCTTGG	GAGTCTTCATCTGGTTGTTG
Human OCT-1 cDNA	GGTCCAACTCGCTGGAACAA	GCGTCAAAGTAAGCCCAGTT
Human HCF-1 cDNA	AAGTGGCCAATGGCATCGAG	GGTGCCCAAATCATCGTCTG
Human STING cDNA	GGGATTAAGAACCGCGTGTA	TCCTGAGACATTGCGAACAG
Human CXCL10 cDNA	CCTTATCTTTCTGACTCTAAGTGGC	ACGTGGACAAAATTGGCTTG
Human GAPDH gDNA	CTTAAAAAGTGCAGGGTCTGGCG	GAGGGTCTCTCTCTTCCTCTTGT
Mouse 18S rRNA cDNA	GTAACCCGTTGAACCCCATT	CCATCCAATCGGTAGTAGCG
Mouse SETX cDNA	GATAAGAAAGGACCTGCAGAAGTG	ACTTGGCTCGTGTAATGGTGA
Mouse GAPDH gDNA	TGAAATGTGCACGCACCAAG	GGGAAGCAGCATTCAGGTCT
HSV-1 *UL54* cDNA	AAGATGTGCATCCACCACAA	ACGAAGGATGCAATGTCCTT
HSV-1 *UL29* cDNA	TAGTGCGATGGCGTCAGTTT	TCGAGCTTCTGGCGTTACTG
HSV-1 *UL44* cDNA	AGGTCCTGACGAACATCACC	GCCCGGTGACAGAATACAAC
HSV-1 *UL54* gDNA	CAGAGGCCATATCCGACACC	CTGCTGTCCGATTCCAGGTC
HSV-1 *UL44* gDNA	AAGATCCTCGGGCTACTGGT	CAAACTGAACAAAGCCCCCG
SETX-1-LoxPR		CGAAGTTATATTAAGGT
SETX-2-Ln3F	TTTAAGGAACAGTGCTGC	
SETX-3-Ln3R		ATGAAGCAGGTAGGATT

Table 2.10.2. **Summary of antibodies used throughout all experiments with assay relevant dilutions.**

Target	Manufacturer	Immunoblot	Immunofluorescence
Mouse anti-HSV1 ICP0	H1A027, Virusys	1:3000	
Mouse anti-HSV1 gC	H1A022, Virusys	1:4000	1:1000
Goat anti-mouse IgG HRP	2907, Santa Cruz	1:3000	
1° GAPDH (G-9) mAb IgG1 mouse	365062, Santa Cruz	1:3000	

2.11 RNA-Sequencing

RNA sequencing was performed by the MOBIX Lab at McMaster University. RNA was Polyadenylated transcript-enriched and sequenced using HiSeq 2500 System (Illumina). Samples were loaded at equimolar ratios and run on 2 lanes with read length of 1X50bp. Sequence reads were aligned to HSV-1 KOS genome, GenBank ID: JQ673480.1 [70] via HISAT2, and then transcripts were aligned using Stringtie[111,112]. DESeq2 was used to test for differential expression against a Log(0) fold change null hypothesis and assigning a p-value via Wald test, adjusting for multiple testing through Benjamini and Hochberg procedure[113]. Prediction of R-loop bias was determined using the QmRLFS-finder *in-silico* prediction tool[114]. HSV-1 KOS genome JQ673480.1 was analyzed for R-loop bias across the total genome.

In-Vivo Experiments

2.12 Genotyping and Isolation of SETX MEF

All animal work was performed in full compliance with the Canadian Council on Animal Care (CCAC) and approved by the Animal Research Ethics Board (AREB) of McMaster University.

All SETX mice and embryos were genotyped prior to usage based upon methods developed by Becherel *et al.* [7]. For genotyping of either tail clippings or embryonic tissue, 300µL of DirectPCR (Tail) (102-T, Viagen Biotech) lysis reagent was used in conjunction with 120 µg of proteinase K solution (25530049, Invitrogen). Samples were incubated at 56°C overnight, centrifuged at room temperature in Eppendorf 5424 centrifuge at 14,000 RPM for 10 min to remove undigested material, and then proteinase K was inactivated at 85°C for 30 min. DNA was stored at -20°C until usage.

All SETX genotyping was performed using a primer mix of SETX-1, SETX-2, and SETX-3 primers (*Table 2.10.1*), specific to the $SETX^{-/-}$ knock-out (KO) and $SETX^{+/+}$ wild-type (WT) alleles. The master mix for each genotype sample was comprised of AmpliTaq Gold ® 360 DNA polymerase kit (43988976, Applied Biosystems) and a dNTP mixture (10297018, Invitrogen) made to 10mM of each nucleotide. Master mix contained 5 μL buffer, 4 μL $MgCl_2$, 4 μL dNTP, 1 μL GC enhancer, 1 μL (0.5 nmole) of SETX-1, SETX-2, SETX-3 primers and 27.75 μL nuclease-free water per sample. Mix was added with 5 μL DNA sample and 0.25 μL per reaction of AmpliTaq Gold ® 360 DNA polymerase directly prior to thermocycling. Thermocycling protocol was performed in Veriti ™ 96-Well Thermal Cycler (4375786, Applied Biosystems) with conditions as followed: 1x (15 min at 95°C), 40x (30 s at 95°C, 30 s at 49°C, 60 s at 72°C), 1x (7 min at 72°C), hold at 4°C. Samples were stored at -20°C until usage.

Genotyping was performed using 1% agarose in TAE (0.04M tris-acetate, 0.001M Ethylenediaminetetraacetic acid (EDTA)) gel with 1x RedSafe Nucleic acid stain (221141, FroggaBio). Samples were loaded using 1:5 volume of 30% v/v glycerol and a 100bp ladder (DM001-R500, FroggaBio). Gel was run at 120 V for 60 min at room temperature and imaged under UV using an AlphaInnotech Cabinet Imager. WT allele produced a product of 600 bp and 339 bp for the KO allele, heterozygous (HET) animals display both bands[7]. An example genotyping is shown below in *Figure 2.3.1*.

SETX mice were kept under clean housing conditions at the McMaster Central Animal Facility. $SETX^{+/-}$ parents were housed separately and then combined for 12 hours for copulation. Males were then removed, and females were weighed and examined for vaginal plugs. Female mice were monitored for weight gain >1.5 g and euthanized through cervical dislocation at day 13.5 in pregnancy. Individual embryos were removed, rinsed in phosphate buffered saline (PBS),

and separated into 100 mm dishes with 10 mL of PBS. The head and fetal liver were removed, and the remaining embryo was transferred to new 100 mm dish containing 4 mL of 2X Trypsin/ EDTA (15400054, Gibco) in PBS and segmented using scalpel blades into smaller pieces. Contents of dish were transferred to a 15 mL tube and incubated in a water bath for 20 minutes (min) at 37°C. An additional 4mL of 2x Trypsin/EDTA was added and tube was returned for further 20 min incubation. Tubes were removed from water bath and 6 mL of 15%FBS/DMEM was added prior to centrifuging embryos at 400 X g in an Allegra ® X-12R Centrifuge (Beckman Coulter) for 5 min. Supernatant was removed and cells were resuspended in 10mL of 15% FBS/DMEM and filtered through a 70 μm sterile filter (10199-656, VWR) to remove larger undigested tissue. Cells were counted using 0.4% Trypan Blue (50-751-7527, Fisherscientific) on a Bright-Line™ hemacytometer (Z359629, SIGMA) and $3x10^6$ cells were added to individual T-150 flasks (08-772-47, Fisherscientific) for expansion. Cells were frozen in 10% Dimethyl sulfoxide (DMSO)/FBS for longer term storage in liquid nitrogen.

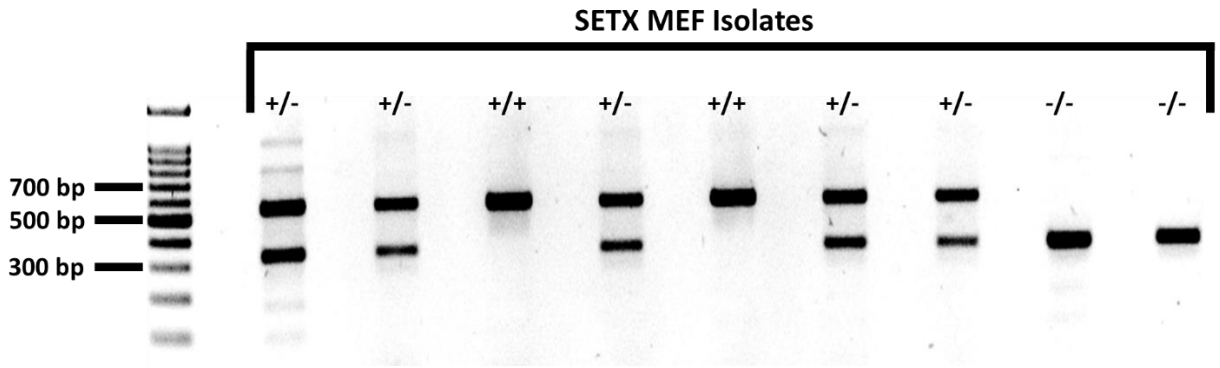

Figure 2.2.12 **SETX MEF genotyping.** SETX MEF isolates were genotyped based upon protocol developed by Becherel *et al.*[7]. Cells were digested in DirectPCR reagent and 120 µg of proteinase K solution. PCR was performed as described in methods and genotype was assigned based upon 600 bp WT (+) SETX allele and or 339 bp KO (-) SETX allele. DNA was separated using 1% agarose gel and bands were visualized using 1X RedSafe Nucleic acid stain.

2.13 Intravaginal Infection and Vaginal Lavage

SETX mice were weaned from mothers at 21 days and injected with 2.5 mg (50μL) of Depo-Provera (medroxyprogesterone acetate) subcutaneously, provided by Dr. Ali Ashkar (McMaster University), four days prior to infection at day 42 of age. Animals were anaesthetized using a ketamine (Narketan 10, Vetoquinol)/xylazine (Rompun 20mg/mL, Bayer) mixture (3:1) diluted in sterile PBS (1:4). Animals were injected intraperitoneally with 150 μL of anesthetic, equivalent to 112.5 mg/kg ketamine and 7.5 mg/kg xylazine. Vaginal tracts were washed with 30 μL of PBS and wash was collected for confirmation of diestrus, where leukocytes are the predominate population in vaginal wash fluid[115]. Mice were weighed and then infected with 10 μL of 10^5 PFU HSV-1 17+ for 1 hour. Weight change, genital pathology and ALS-like symptom onset was monitored daily for at least 14 days post infection. Mice were euthanized upon reaching defined endpoints, as outlined in *Table 2.13.1* Vaginal tracts were washed with two volumes of 30 μL of PBS on days 1, 3, 5 and 7 post infection. Vaginal wash was vortexed briefly and centrifuged in Eppendorf 5424 centrifuge at 500 X g for 10 min to pellet cells and mucous. Aliquots of 50 μL of wash were taken and diluted in 100 μL of PBS (3X dilution) and separated for viral titres and cytokine analysis.

Table 2.13.1 **Endpoint monitoring system used during HSV-1 infection of SETX mice.** Animals who reached stage 4 were euthanized humanely with isoflurane anesthetic followed by cervical dislocation.

Genital Pathology Scoring	Mouse ALS Clinical Scoring
0 – No apparent infection	0 – Full extension of legs when suspended by tail
1 – Slight redness of external vagina	1 – Collapse of leg extension or trembling of legs when suspended by tail
2 – Redness and swelling of external vagina	2 – Toes curl under when walking or foot drags
3 – Severe redness and swelling of external vagina and surrounding tissue	3 – Rigid paralysis of legs; foot not used for forward motion
4 – Genital ulceration with severe redness and hair loss of genital and surrounding tissue	**4 – Unable to right within 30 s**

2.14 Cytokine Analysis

Vaginal wash cytokine analysis was performed by Eve Technologies (Calgary, AB, Canada) using their Mouse Cytokine Array/ Chemokine Array 31-Plex (MD31).

2.15 Vaginal Histology

Mice were infected with HSV-1 17+ as previously described and monitored until day 5 post infection, at which animals were euthanized through cervical dislocation. Vaginal tracts, including cervix and uterus, were removed and immediately placed in 3.7% paraformaldehyde in PBS for 72 hours. Samples were rinsed with ethanol and histology was performed by the Histology Department at the John Mayberry Histology facility at McMaster University, Ontario, Canada. Vaginal tracts were embedded in paraffin, and 3 μm sections were cut along the transverse plane inferior to the cervix. Three sections were taken at 100 μm increments from central slice and stained in Hematoxylin and eosin stain (H & E stain) and imaged via Leica microscope (Leica Microsystems).

2.16 Infection of SOD-1^{G93A} Mice

WT and transgenic (SOD-1^{G93A}**)** mice (B6SJL.SOD1-G93A, The Jackson Laboratory) were raised to 60 days of age and infected intranasally with Influenza A Virus Puerto Rico 1968 (PR8). Animals were anaesthetized with isoflurane and were inoculated with 20 μL per nostril of PR8 virus diluted in PBS according to dosage (1 LD50/ 3000 PFU, 0.1 LD50/ 300 PFU). Animals were monitored for 14 days following infection with daily weighing and were euthanized if weight fell below 75 % pre-infection values.

2.17 SOD-1 G93A Mice ALS-like Development

SOD-1 transgenic animals were monitored weekly for weight change and ALS-like symptom development until day 90, at which point biweekly monitoring was enacted, and at 120 days of age daily monitoring was performed. Mice were euthanized via cervical dislocation when unable to right after 30 s, (see Mouse ALS clinical scoring *Table 2.13.1*).

Mice were measured for hind limb coordination weekly following infection via a Rotarod test (LE8205, Panlab, Harvard Apparatus). Mice were placed on rotor at 4 RPM prior to initiating timing. Speed was incrementally increased from 4 RPM to 15 RPM over 60 s and then held constant until animal fell or 180 s of rotation had occurred. Trials were repeated six times, or 3 full trials of 180 s rotation without falling. If animal was unable to be placed on at 4 RPM, a value of 0 s was given, and if all 6 trials returned a value of 0 s the mouse was considered failed out of measurements and was no longer tested.

Mice were measured for hind limb strength weekly following infection recovery via inverted wire-mesh grip test. Animals were inverted while clinging to metal mesh and measured for fall time up to 180 s. Tests were repeated for 3 trials. If mouse was unable to grip from initial inversion it was assigned a value of 0 s. Three trials of 0 s was considered failed and the mouse was no longer tested.

2.18 Neurological Tissue Homogenates

Mice were anaesthetized with isoflurane and euthanized through cervical dislocation. Immediately following dislocation, mouse brain was removed, rinsed in PBS, and sectioned into three equal segments along frontal plane (frontal, medial, hind brain segments). Mouse spines were removed from tail to cervical vertebrae. Spinal cords were washed with PBS. Tissues (brain

or spine) were weighed and added to screw-cap RINO® (Next Advance) tubes along with stainless steel beads and a 2:1 volume (V/W) of PBS and homogenized in Bullet Blender Homogenizer (BB24-AU, Next Advance) at 4°C for Time 3 and Speed 8. Homogenates were removed from beads and centrifuged for 5 min at 500 X g in Eppendorf 5424 centrifuge. Supernatant was aliquoted and frozen. Samples were titred on Vero cells as described above in section 2.4 .

2.19 Statistical Analyses

All data sets are presented as the mean with standard error of the mean (SEM) indicated and analyzed using GraphPad Prism 7.04 (GraphPad Software). Statistical significance was determined through 1-way or 2-way analysis of variance (ANOVA). Analysis of survival curve data was performed through Log-rank test.

Chapter 3

Results

3.1 A Role for SETX in HSV-1 DNA Replication and Viral Biogenesis

There is strong evidence to suggest that SETX is involved in the cellular DDR[7,25–27]. However, to date, no study has examined potential influences of SETX on the replication and processing of viral DNA during infection, and by association, what affect this might have on viral biogenesis. Viruses such as HSV-1 actively modulate cellular DDR to achieve ideal environments for viral replication [3], and thus SETX deficiency may alter viral biogenesis over the course of infection via the DDR. Given the breadth of known associations between viral DNA replication and components of the DDR, we sought to understand if/how SETX might influence HSV-1 DNA replication.

siRNA was employed to deplete SETX in HFF cells prior to infection by HSV-1. HFF were treated with siCtrl or siSETX RNA for 48 hours prior to infection with HSV-1 KOS at high MOI (= 5). HSV-1 genomes were quantified relative to the number of cellular genomes in a given sample. The relative quantification method was based upon the principle that for a given cellular gene target (i.e. GAPDH)[116], two alleles are present per cell, but for a given viral gene (i.e. *UL54* and *UL44*) only one copy existed per genome, with notable exceptions[70]. Cell-associated DNA was extracted from HSV-1 infected HFF cells and was quantified using qPCR (*Figure 3.1.1a)*. GAPDH-specific primers were used to measure HFF gDNA, while to quantify viral gDNA, primers specific for two individual genes: the IE gene *UL44* and the L gene *UL54* were used. The use of two viral genes served as an internal control to confirm successful amplification and quantification of targets (since both should be present in the same relative quantity). Read-outs of CT *UL44*:*UL54* were within one standard deviation of the mean, confirming efficacy of both primer sets. Viral gDNA was quantified relative to host gDNA, and

Foscarnet-treated samples were initially included as negative controls. Viral genome replication can be restricted through the use of Foscarnet, a HSV-1 DNA polymerase processivity factor (*UL42*) inhibitor which significantly impacts viral DNA replication[91]. Efficient antagonism of viral DNA replication occurred in foscarnet-treated samples, as expected (*Figure 3.1.1a).* Uninfected samples at 0 hours were included as a non-template control for viral gDNA, and indeed no viral DNA was detected. Viral gDNA quantities remained stable throughout the course of infection up to 24 hours in foscarnet treated cells. No significant differences across times or siRNA treatments were found within foscarnet-treated samples (*Figure 3.1.1a).*

HSV-1-infected cells that did not receive foscarnet treatment showed enrichment of viral gDNA over the course of infection, as would be expected for a productive replication cycle[73,74] (*Figure 3.1.1a).* Significant differences were not found between 4 and 12 hours post infection (*Figure 3.1.1a).* At 24 hours post infection there was a significant decrease (~2-fold) in viral gDNA in SETX-depleted cells relative to control conditions (*Figure 3.1.1a).* This would suggest that SETX facilitates viral gDNA replication in SETX depleted conditions in HFF.

Further corroboration of this phenotype was demonstrated using SETX$^{-/-}$ MEFs (*Figure 3.1.1b)* [7,30]. The phenotype was accentuated (~3-fold) in the SETX $^{(-/-)}$ MEF such that at both 12h and 24h a significant difference was observed between SETX $^{(+/+)}$ sufficient and $^{(-/-)}$ deficient cells (*Figure 3.1.1b).*

Modest differences in viral gDNA replication efficiency may not directly correlate with differences in viral titre, and thus examining viral titres in the supernatant of infected cells was relevant to understanding the ramifications of alterations in viral DNA replication[117]. Significant differences between HSV-1 titres was not observed for either HFF treated with siRNA or SETX MEFs (*Figure 3.1.1c-d).* Interestingly, both infected HFF and MEF titres display a 2-fold

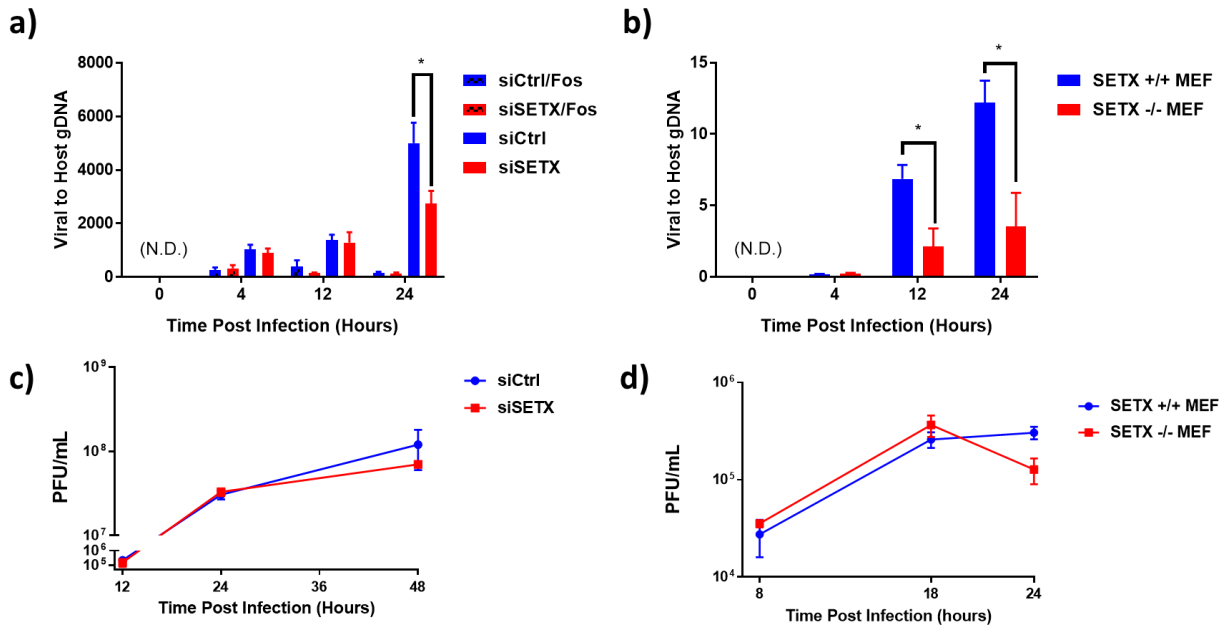

Figure 3.1.1. **SETX facilitates HSV-1 viral biogenesis.** (a) Human foreskin fibroblasts (HFF) were treated with 50nM siCtrl or siSETX for 48 hours prior to infection. (a-b) HFF and SETX MEF cells were infected at high MOI (= 5) with HSV-1 KOS in the presence or absence of foscarnet (Fos). Whole cells were collected at indicated times and DNA was isolated and quantified through qPCR relative to GAPDH DNA. Data represents the mean and standard error of n=3 individual experiments. (c-d) Viral supernatants were collected at identified times from (a-b) and titred on Vero Cells via a 10-fold dilution method. Data represents the mean and standard error of n = 3 individual experiments. * $p < 0.05$ as found by 2-way ANOVA.

difference in viral titres at 48 or 24 hours post-infection between the SETX sufficient and deficient conditions, respectively. Viral gDNA was ~5000-fold higher relative to host GAPDH in HFF compared to that of viral gDNA relative to GADPH in SETX MEF (*Figure 3.1.1a-b),* as were corresponding viral titres (*Figure 3.1.1c-d).* This is consistent with the fact that HSV-1 is a human pathogen, and the murine cells are generally less permissive to infection[83,118,119].

Given the known function of SETX as a regulator of the antiviral response[30], we evaluated HSV-1 gDNA replication efficiency in a system deficient of the antiviral response. MEFs from mice deficient of IRF3 and IRF9 (IRF3/9$^{(-/-)}$) were produced alongside congenic WT MEFs (IRF3/9$^{(+/+)}$). Over the course of culturing, IRF3/9$^{(-/-)}$ reached confluency in less time than the corresponding IRF3/9$^{(+/+)}$ MEF despite equivalent seeding densities. Additionally, the IRF3/9$^{(-/-)}$ were noted for abundant dead cells present in the media during culturing. These cells were infected as described above (HSV-1 KOS at MOI = 5) and viral gDNA replication and viral titres were quantified as previously discussed above (*Figure 3.1.2a-b).* In contrast to previous results, there were no significant differences between viral gDNA replication efficiencies after siRNA treatments for either the IRF3/9$^{(+/+)}$ or IRF3/9$^{(-/-)}$ MEF (*Figure 3.1.1, Figure 3.1.2).* Surprisingly, viral replication in IRF3/9$^{(-/-)}$ was roughly 0.5-1 log-fold lower than the corresponding IRF3/9$^{(+/+)}$ cells (*Figure 3.1.2b).* These results suggest that an intact antiviral response is conducive to HSV-1 titres in MEFs.

In summary, SETX facilitated viral DNA replication in HFF depleted of SETX with siRNA and SETX$^{-/-}$ MEF and slight elevations in viral titres were observed at 24 hours *in vitro* in the absence of SETX (*Figure 3.1.1*). HSV-1 replicated with increased efficiency in human versus mouse derived cells (*Figure 3.1.1).*

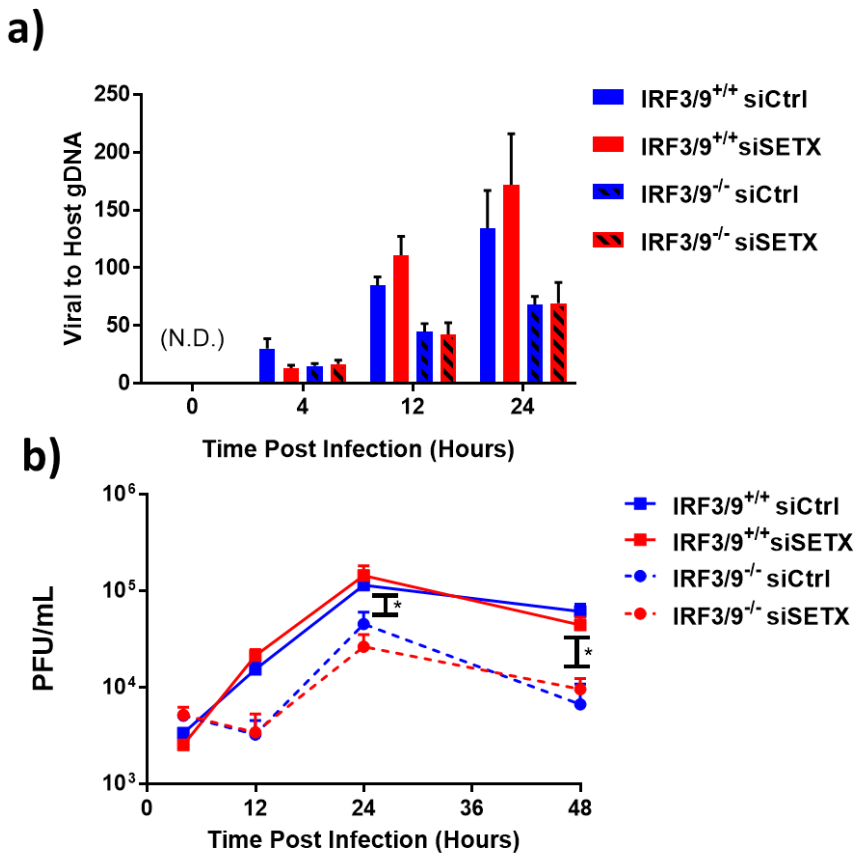

***Figure 3.1.2* siRNA depletion of SETX does not affect viral biogenesis in IRF3/9 MEFs.** (a) IRF3/9 $^{(+/+)}$ or IRF3/9 $^{(-/-)}$ MEFs were treated with 50nM siCtrl or siSETX for 48 hours prior to infection. Cells were infected at high MOI (= 5) with HSV-1 KOS and whole cells or viral supernatants (b) were collected at identified times. DNA was isolated and quantified through qPCR relative to GAPDH DNA. (b)Viral supernatants were titred on Vero Cells via a 10-fold dilution method. Data represents the mean and standard error of n = 3 individual experiments. * $p < 0.05$ as found by statistical 2-way ANOVA performed for significance.

3.2 SETX Regulation of HSV-1 Gene Expression

HSV-1 utilizes host RNAPII and contains a GC rich genome (68% GC) which has a significant potential to form R-loops; these factors provide a strong rationale for studying the role of SETX on HSV-1 gene expression [114,120–122]. To accomplish this, SETX was depleted in HFF cells for 48 hours prior to HSV-1 KOS (MOI = 5.0) infection. Three prototypic HSV-1 genes were chosen as representatives of viral gene expression. Each gene corresponded to a different class of HSV-1 temporally-controlled genes (IE, E, L). RNA was extracted over a time course of infection and viral gene expression of *UL54* (IE gene), *UL29* (E gene), *UL44* (L gene) and host *SETX* and *GAPDH* mRNA were analyzed by RT-qPCR. SETX mRNA was reduced by >80% relative to control conditions across all timepoints (*Figure 3.2.1a),* confirming successful suppression of SETX gene expression in HFF cells up to 96 hours post initial transfection. Expression of the IE gene *UL54* was significantly elevated at 48 hours post infection in cells treated with siSETX (*Figure 3.2.1. b).* There were no significant differences in transcription for *UL29* and *UL44* genes across all timepoints and siRNA treatments (*Figure 3.2.1 c, d).*
Due to differences observed in gene expression, we examined whether HSV-1 protein expression was also affected. Protein lysates corresponding to 0, 8 and 24 hours post-infection with HSV-1 KOS (MOI = 5) of siRNA treated HFF were used to examine HSV-1 protein expression over the course of infection. Immunoblotting for IE protein ICP0 and L protein gC, corresponding to viral genes *RL2/IE110* and *UL44,* showed enhanced expression of viral proteins in SETX-depleted conditions (*Figure 3.2.1 e).* These observations suggest that SETX antagonizes UL54 RNA expression at 48 hours and antagonizes protein expression of gC and ICP0 at 8 and 24 hours post infection. Because SETX appears to also affect viral DNA replication as demonstrated above (*Figure 3.1.1),* it was necessary to eliminate indirect effects

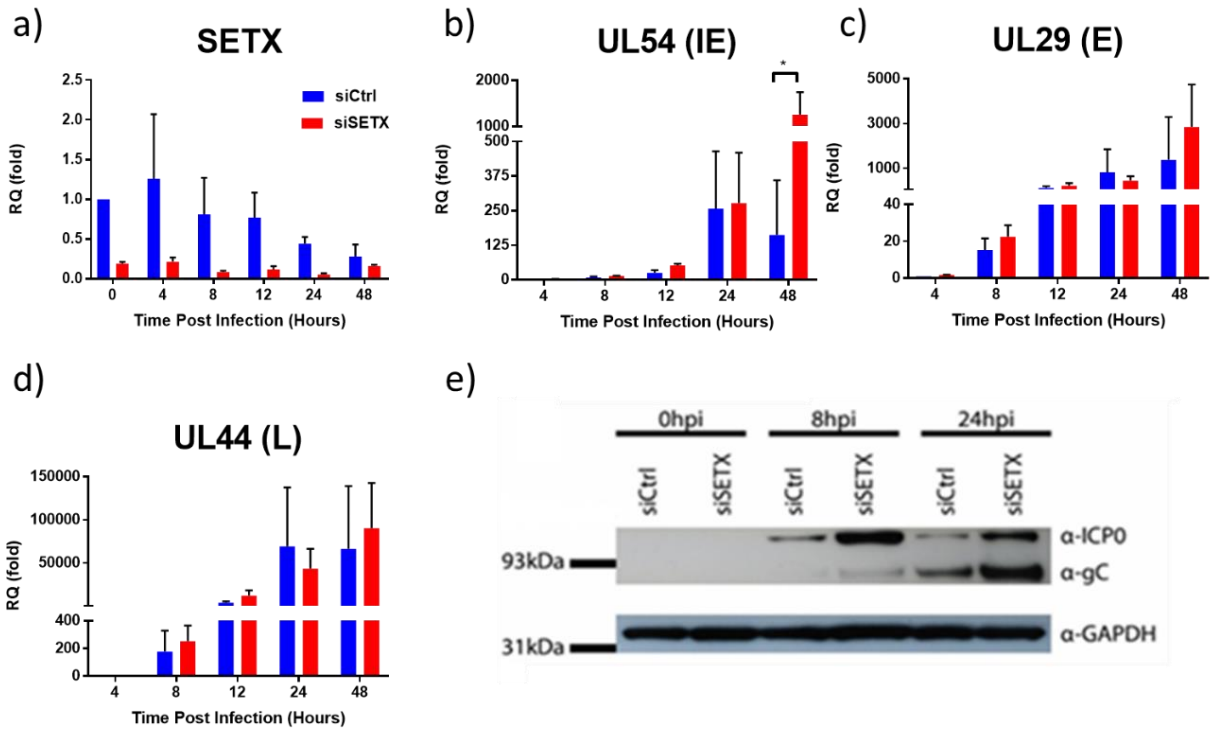

Figure 3.2.1 **SETX antagonizes HSV-1 gene expression**. (a-e) HFF were treated with siSETX or siCtrl for 48h prior to infection with HSV-1 strain KOS at an MOI of 5. Cells were collected at the indicated times and (a-d) qRT-PCR was performed to quantify expression of (a) SETX, (b) *UL54*, (c) *UL29* and (d) *UL44* relative to GAPDH. Data represents the mean and standard error of 3 independent experiments. *$p<0.05$ as determined by 2-way ANOVA. (e) Expression of ICP0, gC and GAPDH was evaluated by immunoblot at 0, 8 and 24 hours post infection. Experiments were performed by a previous lab member, Mannie Lam and further analyzed.

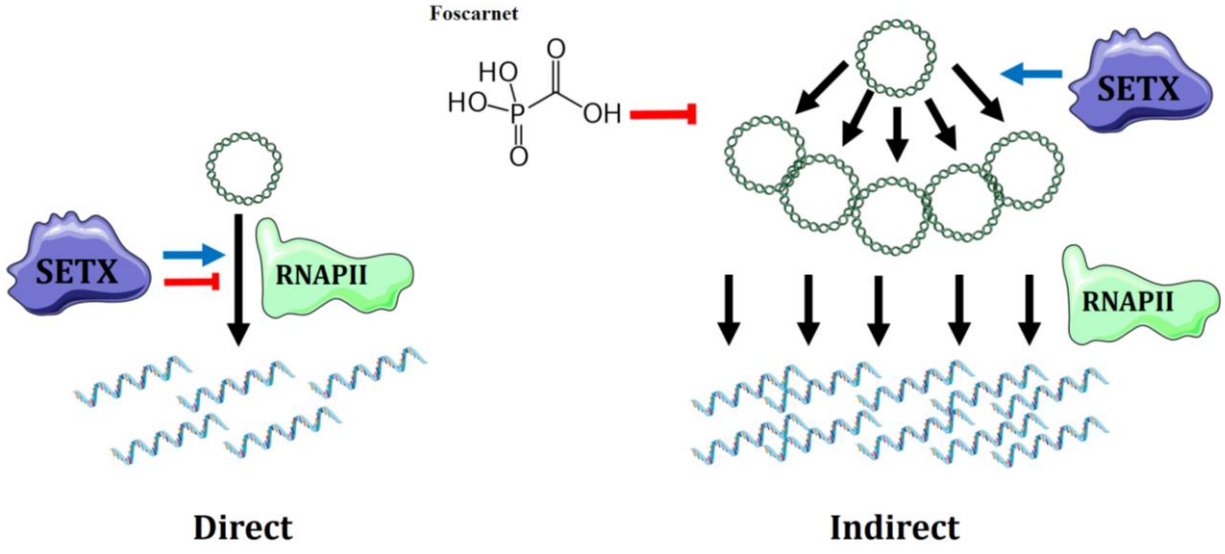

Figure 3.2.2. **Model of potential direct and indirect effects of SETX on viral gene transcription**. SETX has the potential to affect viral gene transcription directly through regulation of viral gene transcriptional. SETX could also indirectly affect viral gene transcription include altering viral DNA replication, and thereby affecting transcription. Foscarnet inhibits viral DNA replication and can thus help to distinguish between direct and indirect effects.

of viral DNA replication on viral gene expression as outlined in *Figure 3.2.2.* This was done using foscarnet, a viral polymerase processivity factor inhibitor[73,91].

Viral genome replication can be restricted through the use of Foscarnet as demonstrated previously (*Figure 3.1.1)*[91]. Using foscarnet, an *in-vitro* system was developed whereby viral genome copy number was held constant between throughout HSV-1 infection to determine whether SETX might directly viral gene transcription. The effectiveness of this treatment was demonstrated previously in the viral DNA replication studies (*Figure 3.1.1a).* In conditions of foscarnet inhibition and SETX depletion with siRNA, upregulation of viral gene expression became more prevalent in genes analyzed (*UL54, UL29*, *UL44*) (*Figure 3.2.3a-d),* although differences were still not statistically significant. The expected temporal regulation of viral gene expression was clear in these studies (*Figure 3.2.3 b-d).* The results of this experiment support a model whereby SETX-mediated antagonism of viral gene expression was independent of viral genome replication. Experiments were repeated in IRF3/9 $^{+/+,\ -/-}$ MEF to confirm the inability of the cell type to recapitulate results seen previously in other cell models (*Figure 3.2.1*, *Figure 3.1.2),* IRF3/9 $^{+/+,\ -/-}$ MEF were not an appropriate model for examining SETX impact on HSV-1 gene expression and was therefore included in supplementary information (*Figure S1.1).*

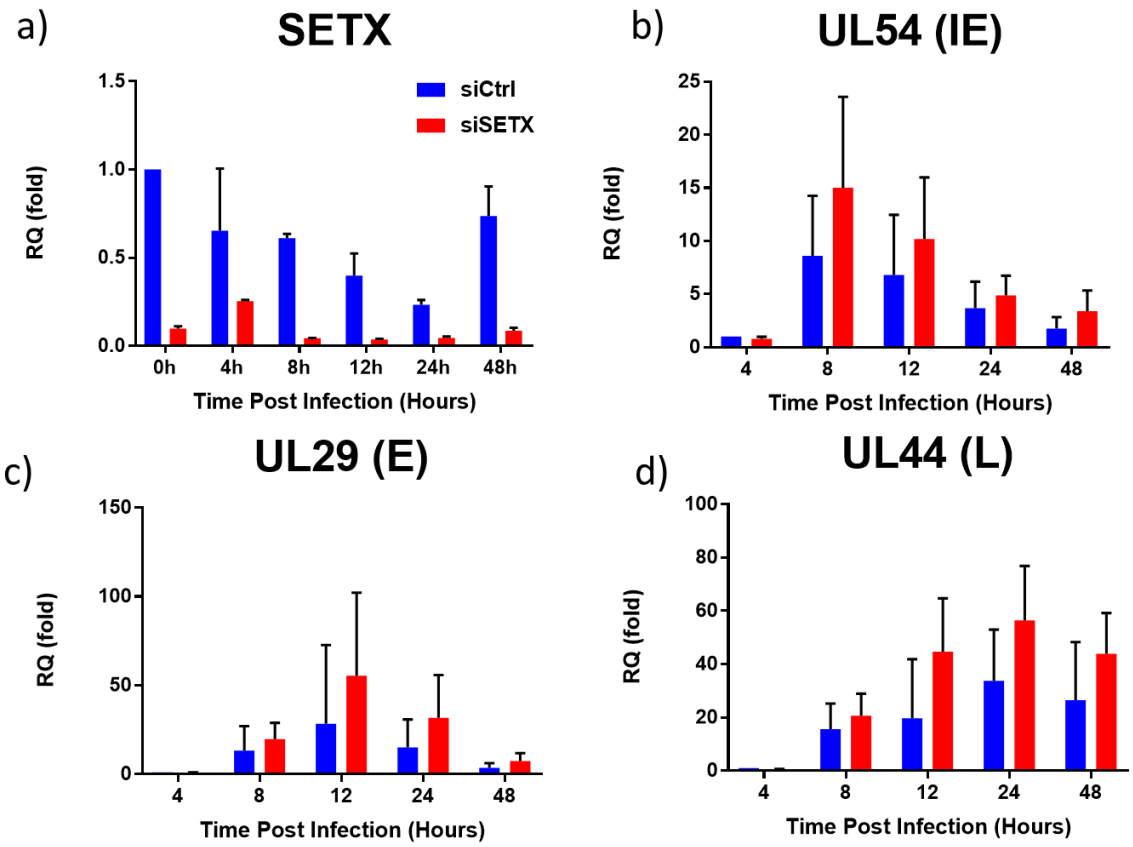

Figure 3.2.3. **SETX mediated antagonism of HSV-1 gene expression independent of viral DNA replication.** (a-d) HFF were treated with siSETX or siCtrl prior to foscarnet treatment and infection with HSV-1 KOS at MOI = 5. Cells were collected at the indicated times and expression of (a) SETX, (b) *UL54*, (c) *UL29* and (d) *UL44* were quantified by qRT-PCR relative to GAPDH. Data represents the mean and standard error of 3 independent experiments. Statistical significant was assessed by 2-way ANOVA. A sampling of experiments were performed by a previous lab member, Mannie Lam, and further analyzed.

3.3 SETX Regulation of Host Factors Required for HSV-1 Gene Expression

HSV-1 IE expression is unique in its requirement for host cellular factors to commence transcription[1,123]. The cellular factors HCF1 and OCT1 are required for initial transcription after being bound by VP16 delivered from viral particles [1,123]. Since SETX had been documented to alter host expression patterns[30], it could potentially indirectly affect viral IE expression through the host cellular factors HCF1 and OCT1[92,124]. Through qRT-PCR of siRNA treated, SETX-depleted HFFs infected with HSV-1 KOS (MOI = 5) as described previously, it was found that although host transcript levels of OCT1 and HCF1 were both initially greater in SETX depleted samples prior to infection; after 8 hours there was little variation between siSETX and siCtrl samples and significant reduction in expression, presumably due to viral host shutoff (*Figure 3.3.1a-b).* At 4 hours post infection expression of the gene targets were elevated in siCtrl-treated samples, but a significant difference was found in the siSETX group where induction of the transcription factors expression did not occur (*Figure 3.3.1a-b).* This result demonstrated that in the presence of SETX, HSV-1 induced increased transcription of genes like HCF1 and OCT1. In the absence of SETX, the basal expression level of the transcription factors was greater (~2-fold) than control conditions.

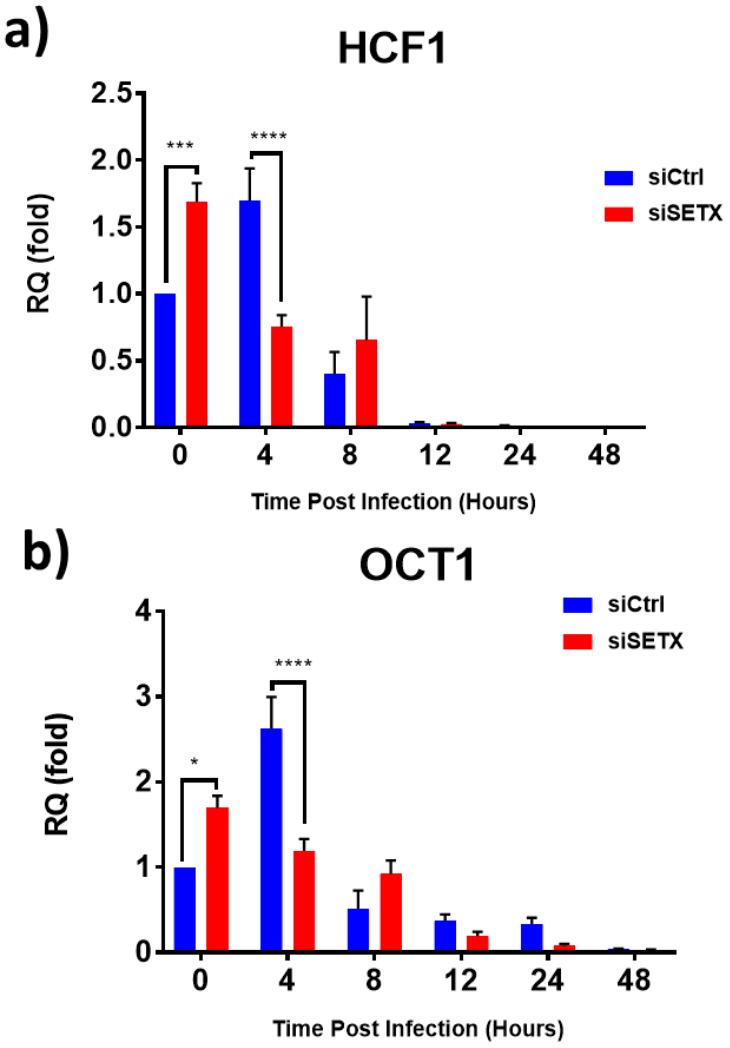

Figure 3.3.1. **SETX upregulates cellular factors required in HSV-1 immediate early transcription.** (a-b) HFF were treated with siSETX or siCtrl prior to infection with HSV-1 KOS at MOI = 5. Cells were collected at the indicated times and expression of (a) HCF1 and (b) OCT1 were quantified by qRT-PCR relative to 18sRNA. Data represents the mean and standard error of n=3 individual experiments. *p<0.05, ***p< 0.001, **** p<0.0001 as performed by statistical 2-way ANOVA.

3.4 Specificity of SETX Regulation of HSV-1 Gene Expression

It was demonstrated that SETX antagonized expression of the viral IE gene *UL54* (*Figure 3.2.1)* and that this effect was maintained in foscarnet-treated cells where viral DNA replication was inhibited (*Figure 3.2.3).* Antagonism was thus independent of viral DNA replication. Additionally, whilst not significant at the RNA level, at the protein expression level viral gene products were enhanced in the absence of SETX (*Figure 3.2.1e).* It was also demonstrated that SETX depletion altered expression of the host transcription factors HCF1 and OCT1 pertinent to viral immediate early gene expression (*Figure 3.3.1)*[1,123]. This led us to investigate the effect of SETX on viral gene expression more generally. Was the effect specific to a viral gene? Viral gene class? Was it specific to HSV-1 or all DNA viruses? Additionally, could any transcriptional effect be detected at the protein level?

To ascertain whether SETX antagonism of viral gene expression could be generalized to IE gene of other viruses, a new *in-vitro* system was designed. HFF were depleted of SETX with siRNA and infected with AdV-GFP, an E1-deleted, replication-incompetent DNA virus in which GFP expression was driven by the human CMV IE promoter (a beta herpesvirus). Thus, GFP fluorescence was used as a metric of IE promoter-driven viral gene expression. Since HFF cells were used, viral DNA replication would not be possible for AdV-GFP (IE gene expression is required for replication) and the effect of SETX on viral IE expression could be examined independent of viral DNA replication. GFP fluorescence was quantified through integrated density, a measure of both intensity and area fluorescence, over the course of 120h and background fluorescence was subtracted using mock infected cells (*Figure 3.4.1)*[108,109]. No significant differences between SETX-depleted conditions and controls as measured by integrated density were noted for all times measured (*Figure 3.4.1b).* Therefore, SETX did not

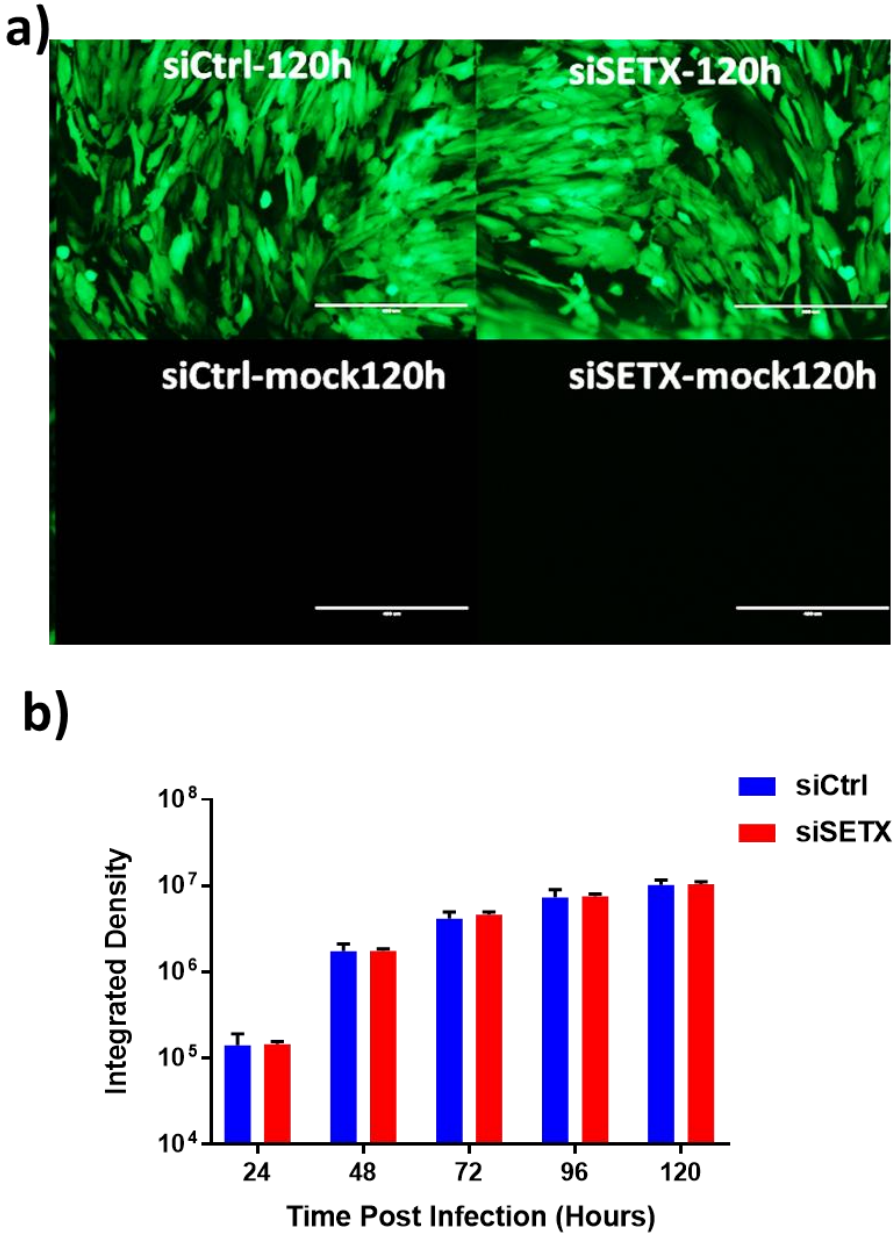

Figure 3.4.1 **SETX does affect general IE-driven virus gene expression** (a-b) HFF cells were infected with a replication-deficient AdV-GFP (MOI = 5) following 48h siRNA depletion of SETX. (a) GFP fluorescence was measured using EVOS FL cell imaging system over 120h of infection, intensity was held constant between timepoints and mock infected controls were used to normalize background fluorescence. (b) Three image fields were used to quantify integrated density through ImageJ of fluorescence after normalization to mock infection for each time point. Data represents the mean and standard error of 3 independent experiments. No significant differences were found by 2-way ANOVA for comparisons between siCtrl and siSETX conditions.

affect GFP expression under the control of human CMV IE promoter in HFF infected with AdV-GFP to any detectable amount as measured by fluorescence integrated density.

Experiments previously performed looked at either specific HSV-1 genes such as *UL54*, *UL29*, or *UL44*, (*Figure 3.2.1, Figure 3.2.3)* or looked at a GFP gene expression under control of a viral IE promoter by means of GFP fluorescence (*Figure 3.4.1)*. These experiments were designed to test whether SETX affected a given gene/gene class (IE, E or L), or had potential for more general effects across DNA viruses. However, since the effects of SETX would be predicated to be most pronounced for genes wherein R loops are likely to occur, we analyzed the genome of HSV-1 KOS (GenBankID: JQ673480.1) for R-loops *in-silico* using QmRLFS finder software[114]. The data is depicted as a heat map showing regions of the genome where R loop bias occurred (*Figure 3.4.2a-b)*. The high G/C content terminal repeat regions displayed strong R-loop bias predictions, as would be expected[70,114]. Candidate HSV-1 genes that were previously analyzed by qPCR did not fall within regions displaying strong R-loop bias (*Figure 3.4.2a-b*). Additionally, the human CMV IE promoter was analyzed for R-loop bias and none was detected (not shown). Three genes noted in regions of strong R-loop bias were the neurovirulence factor ICP34.5/*RL1*, the viral transcription factor ICP4/*RS1* which is found on both strands of genome[70,77], and the viral E3 ubiquitin ligase ICP0/*RS2 (Figure 3.4.2a-b)*[70,87].

To examine the impact of SETX on global viral gene transcription of HSV-1 in an unbiased manner, $SETX^{-/-}$ MEF were infected with HSV-1 and RNA was collected at various times throughout the infection. Genes showing the most pronounced differential regulation occurred within regions of high R-loop bias, with *RS1, RS2* and *RL1* among genes most differentially regulated (*Figure 3.4.2a-b).* A more detailed representation of the values of HSV-1 differential gene expression can be found in the supplementary information (*Figure S1.2*).

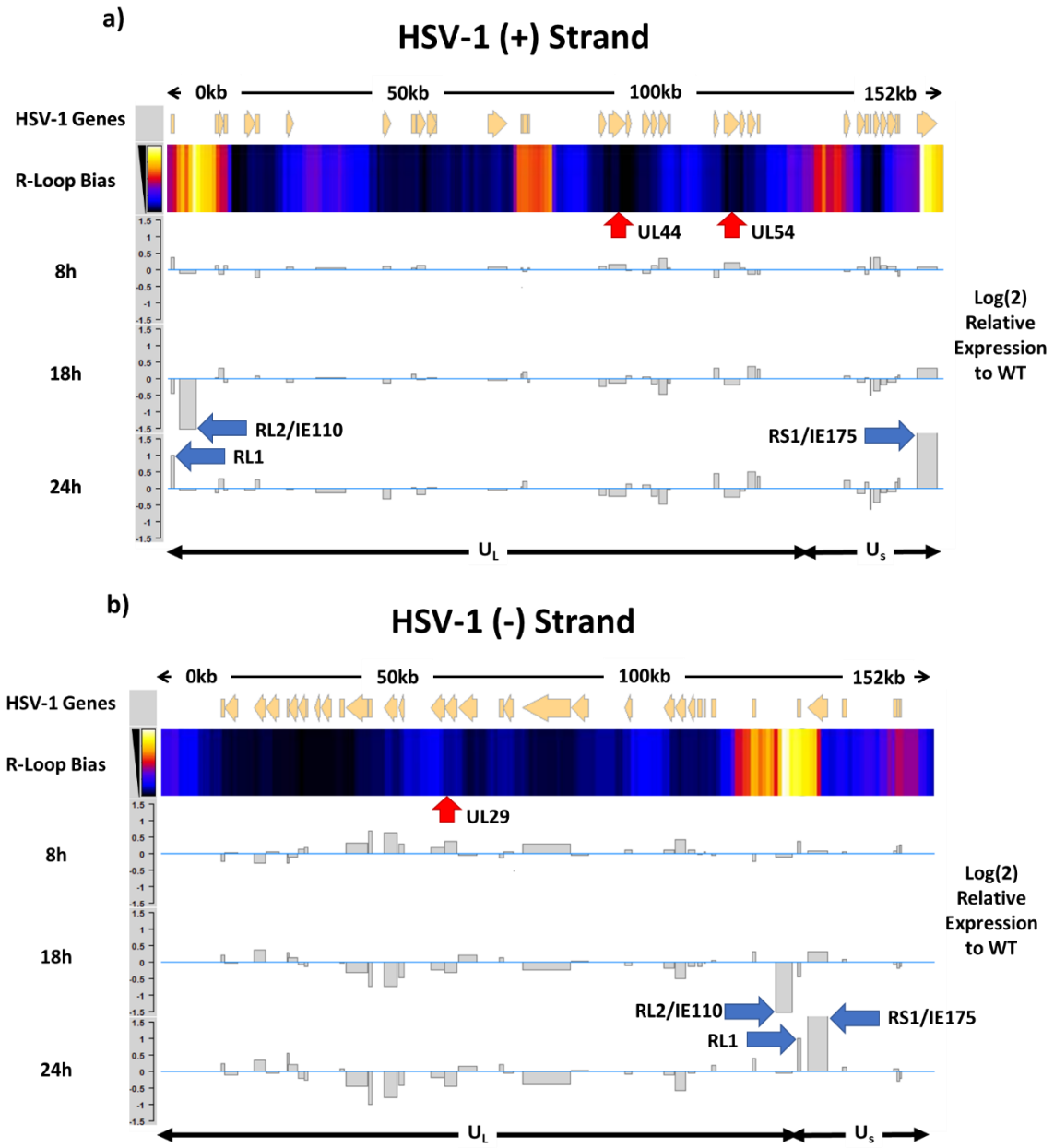

Figure 3.4.2. **R-loop bias as predictor of differential SETX-mediated HSV-1 gene expression.** Heat map of in-silico R-loop predictions generated through QmRLFS finder over (+) (a) and (-) (b) strands of whole genome HSV-1 (GenBank ID: JQ673480.1). Yellow denotes areas with high predicted likelihood for R-loop formation. Select differentially regulated genes are denoted with blue arrows and previously examined genes are denoted with red arrows. Differential expression of viral genes from RNA sequencing SETX$^{+/+}$ and SETX $^{-/-}$ MEF infected with HSV-1 KOS (MOI = 5.0) across select timepoints. RNA was sequenced using Illumina HiSeq single read (50bp), via HISAT2, and then transcripts were aligned using Stringtie[108,109]. DESeq2 was used to test for differential expression against a Log (0) fold change null hypothesis and assigning a p-value via Wald test, adjusting for multiple testing through Benjamini and Hochberg procedure[110]

In summary on the effects of SETX on gene expression, SETX was found to modestly antagonize specific viral gene expression in HFF cells depleted of SETX through siRNA treatment (*Figure 3.2.1).* This effect could be detected at the protein level for both ICP0 (*RL1*) and gC (*UL44*) (*Figure 3.2.1).* SETX was found to alter expression of cellular transcription factors HCF1 and OCT1 which were required for viral IE gene expression (*Figure 3.3.1*). *In-silico* prediction of R-loop bias was an indicator for increased differential HSV-1 gene expression in $SETX^{-/-}$ MEF relative to $SETX^{+/+}$MEF (*Figure 3.4.2a-b).* Regions displaying high R-loop bias showed enrichment in differentially regulated genes, especially on the anti-sense strand (*Figure 3.4.2a-b).*

3.5 Impact of SETX on the Antiviral Response to DNA Viruses

To determine if SETX suppressed the antiviral response to DNA viruses as was found previously for RNA viruses, a reductionist system was employed. Cellular DNA sensors such as cGAS are responsible for initial detection of HSV-1 DNA, and result in STING activation[125–127]. STING activation ultimately results in IRF3 activation leading to transcription of IRF3 responsive elements, ultimately producing antiviral mediators and type I IFN[49,125,128]. SETX has previously been shown to attenuate the antiviral response downstream of IRF3[30], thus we proposed it would also act downstream of STING as STING ultimately activates IRF3. HEK-293T cells lack the viral DNA sensor cGAS and thus, do not efficiently respond to viral DNA[129]. Using FLAG-tagged constitutively active (hyper) or inactive (dead) STING constructs expressed in HEK-293T cells, we assessed the impact of SETX on STING-mediated antiviral signaling. Cells were treated with control or SETX siRNA and were then transfected with dead STING, hyper STING or empty vector controls. RNA was collected 24 hours post transfection and ISG

expression (IFIT1, IFIT2, CXCL10 and IFNβ) was analyzed through RT-qPCR (*Figure 3.5.1a-d).* ISG expression was not detected for vector or dead STING samples as predicted (*Figure 3.5.1a-d).* SETX depleted samples showed a 2-4 fold increased in ISG expression relative to the control in hyper STING samples (*Figure 3.5.1a-d).* Dead and hyper STING protein expression at 24 hours was confirmed through immunoblotting (*Figure 3.5.1e).* Overall this result supported the hypothesis that cells infected with a DNA virus would also experience enhanced antiviral responses downstream of cellular DNA sensors in the absence of SETX. In summary, SETX was shown to negatively regulate the antiviral response to DNA sensing pathways downstream of STING (*Figure 3.5.1).*

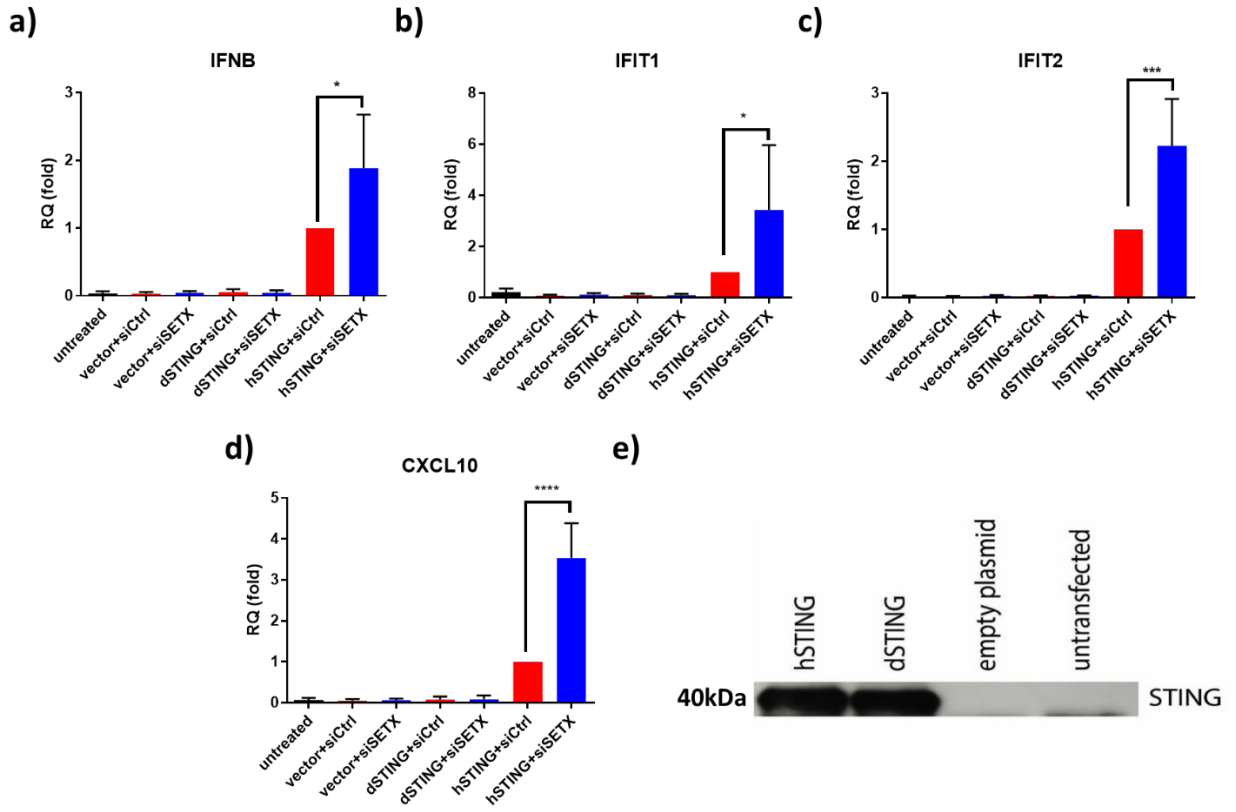

Figure 3.5.1. **SETX antagonizes the antiviral response downstream of DNA sensor STING**. (a-e) 293T cells were treated with siSETX or siCtrl 24h prior to transfection with constitutively inactive STING (dSTING) or constitutively active STING (hSTING). 24h post-transfection, cells were collected and the expression of (a) IFNβ, (b) CXCL10, (c) IFIT1 and (d) IFIT2 were quantified by qRT-PCR. Data represent the mean and standard error of 3 independent experiments. *p<0.05, **p<0.01, ***p<0.001, ****p<0.0001 as determined by one-way ANOVA. (e) Expression of STING was quantified by immunoblot from protein extracts of 293T cells harvested 24 hours post-infection. STING experiments were performed by a previous lab member, Mannie Lam.

3.6 SETX Prevents HSV-1 Disease Pathogenesis in Mice

Given the vast number of pathways through which SETX might influence HSV-1 replication, using an *in vivo* infection model was essential to determine what ultimate outcome SETX might have on viral pathogenesis. Becherel *et al*. generated a line of C57BL6/129Sv mice expressing a copy of the *SETX* gene where exon 4 was excised resulting in a non-functional allele with Mendelian inheritance patterns[7]. The outcome of murine models of HSV-1 infections vary based on route of entry, initial inoculum, and viral strain[130–132]. Due to this, HSV-1 17+ was selected for mouse infections and a vaginal infection route was chosen, as HSV-1 strain KOS (used in *in vitro* experiments) is not very pathogenic in mice[132]. A dosage of 10^5 PFU of HSV-1 17+ was administered intravaginally. Mice were given the hormonal contraceptive Depo-Provera prior to infection which synchronized their estrus cycles and also renders mice more susceptible to infection[131]. Diestrus was confirmed by performing vaginal smears at day 0 of infection (42 days of age), which contain predominantly leukocyte populations during diestrus [115].

A total of 33 female mice were infected with HSV-1 17+ intravaginally, representing the three potential genotypes of $SETX^{+/+}$ (WT), $SETX^{+/-}$ (HET), $SETX^{-/-}$ (KO) at frequencies of n = 8, 14, and 11, respectively. Overall, no significant difference in weight loss among genotypes is observed over the course of infection (*Figure 3.6.1a-d).* Animal survival from infection showed significant differences in the $SETX^{-/-}$ group, with only two mice (18% of total) surviving to 14 days (*Figure 3.6.1e/ Table 3.6.1*). Among the $SETX^{+/+}$ and $SETX^{-/-}$ animals, a reduction in weight occurred in individual animals between 4-9 days post infection (*Figure 3.6.1a,c).* The animals which displayed a reduction in weight suffered hind-limb paralysis *(Figure 3.6.1/Table 3.6.1).*

Over the course of infection, three distinct endpoints appeared relating to the HSV-1 infection of SETX mice as highlighted in *Table 2.13.1* and *Table 3.6.1*.Mouse survival occurred when animals reached 14 days post infection without reaching predetermined endpoints (*Table 2.13.1).* Animals which developed genital pathology did not experience noticeable weight change (*Figure 3.6.1a-c)*. $SETX^{+/-}$ animals displayed no decreases in weight between 4-14 days following infection and no animals experienced hind limb paralysis in this group (*Figure 3.6.1*b / *Table 3.6.1*). 13 % of $SETX^{+/+}$ and 45 % of $SETX^{-/-}$ animals experienced hind limb paralysis (*Table 3.6.1),* which was associated with significant loss of animal weight between 6-9 days following infection (*Figure 3.6.1a, c).* Importantly, the primary endpoint in $SETX^{-/-}$ mice was hind limb paralysis, suggesting an increase in neurological involvement. A small percentage of animals (n =1) experienced an unexplained endpoint, where the animal was found dead in the cage without experiencing significant genital pathology development, weight loss or observed hind limb paralysis (*Table 3.6.1).*

In addition to monitoring mouse survival over the course of infection, vaginal washes were performed at days 1, 3, 5 and 7 post infection. Vaginal washes were used to evaluate viral shedding. Virus was titred on Vero cells (*Figure 3.6.2).* Virus was generally detectable up to day 7 post infection (*Figure 3.6.2*). Vaginal washes were also initially taken at day 14 following infection; however, no titre was detectable among all animal groups and thus titres were ceased at this time point (data not shown). No significant differences were determined between genotypes across all timepoints (*Figure 3.6.2).* A trend toward elevated viral titres was detectable among $SETX^{-/-}$ animals at days 5 and 7 relative to the $SETX^{+/+}$ and $SETX^{+/-}$ animals (*Figure 3.6.2).*

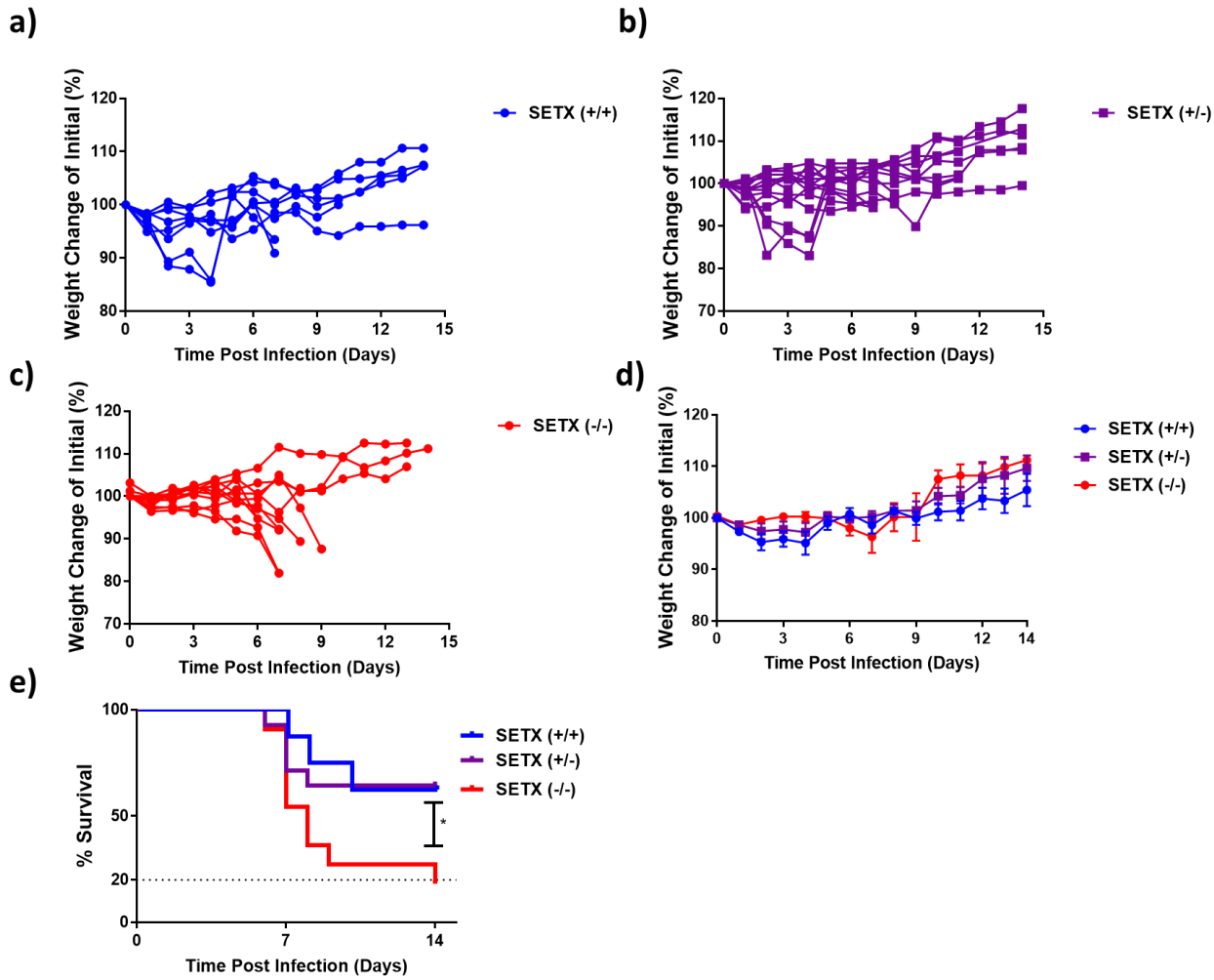

***Figure 3.6.1* SETX is protective against HSV-1 disease pathogenesis in mice.** (a-e) SETX $^{(+/+,\ +/-,\ -/-)}$ were infected intravaginally for one hour with 10^5 PFU of HSV-1 17+ four days following treatment with 2.5 mg of Depo-Provera. (a-c) Mice were weighed daily and percent change from pre-infection weight was calculated up to 14 days post-infection. (d)Weight change as represented by mean and standard error. (e) Mice were monitored and euthanized according to the humane endpoints of severe genital pathology or hind limb paralysis to measure HSV-1 disease pathogenesis. Experiment consists of n = 8, 14, 11 individual mice of the corresponding genotypes of SETX $^{(+/+,\ +/-,\ -/-)}$, respectively. $p < 0.05$, * was determined with a Log-rank test using GraphPad Prism 7.

***Table 3.6.1* Endpoints of HSV-1 infected mice.**

SETX (+/+)	SETX (+/-)	SETX (-/-)
Genital Pathology (25%)	Genital Pathology (36%)	Genital Pathology (28%)
Hind Limb Paralysis (13%)	Hind Limb Paralysis (0%)	**Hind Limb Paralysis (45%)**
Unexplained (0%)	Unexplained (0%)	Unexplained (9%)
Survival (62%)	**Survival (64%)**	Survival (18%)

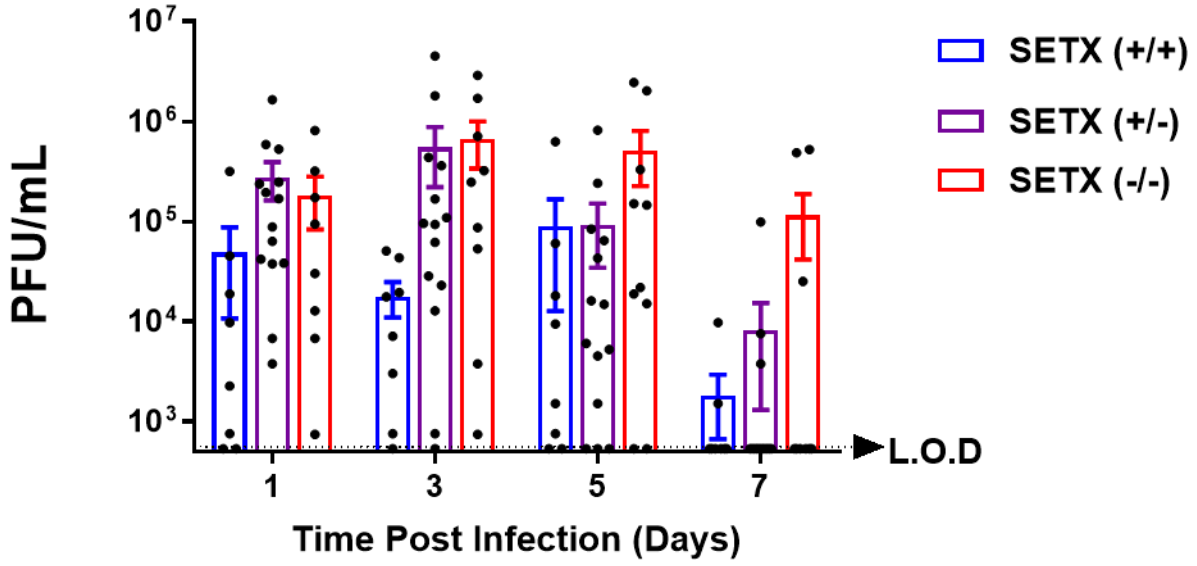

Figure 3.6.2 **SETX aids in clearance of HSV-1 from vaginal lumen**. SETX $^{(+/+,\ +/-,\ -/-)}$ were infected intravaginally for one hour with 10^5 PFU of HSV-1 17+ four days following treatment with 2.5mg of Depo-Provera. Vaginal washes were performed on days 1, 3, 5, and 7 and viral yields were evaluated by titration on Vero cells to a limit of detection of 750 PFU/mL. Experiment consists of n = 8, 14, 11 individual mice of the corresponding genotypes of SETX $^{(+/+,\ +/-,\ -/-)}$, respectively. All data sets were determined non-significant by 2-way ANOVA.

Throughout the course of the HSV-1 infection of SETX mice, vaginal washes were performed. During a vaginal infection, various cytokines, chemokines and immune cells are secreted or migrate into the vaginal lumen and can be collected through vaginal washes[133,134]. Cytokine and chemokine profiles were quantified using Eve Technologies MD-31 discovery assay. A select panel of cytokine and chemokines, specifically IFNγ, IL-6, TNFα as prototypic inflammatory response cytokines and interferons[135,136] , CXCL1, CXL10, CCL5 as CXL10 was previously examined transcriptionally and CXCL1 and CCL5 for their roles in inflammatory diseases[136], and IL-4 and IL-13 for their roles as anti-inflammatory cytokines and as an example that some analytes weren't detected[135,136], were collated (*Figure 3.6.3*). A general phenotype of increased inflammatory cytokines/chemokines between days 3 and 5 in the $SETX^{-/-}$ animals was observed (*Figure 3.6.3a-f),* and overall minimal typical anti-inflammatory cytokines were detected in all animals (*Figure 3.6,3g-h)*[135]. Analyte concentrations of $SETX^{-/-}$ animals tended to remain relatively stable over the course of infection, but cytokine/chemokine levels in $SETX^{+/+}$ animals consistently decreased from day 1 onward during infection (*Figure 3.6.3a-f).* Additional vaginal wash analytes from the MD-31 discovery assay are displayed in *Appendix 1, Figure S1.3.* No other measured cytokine/chemokines were found to be significant by two-way ANOVA.

In Summary, HSV-1 infections of $SETX^{+/+,+/-,-/-}$ mice demonstrated that SETX protected against HSV-1 disease pathogenesis with respect to both overall survival, and development of hind-limb paralysis (*Figure 3.6.1, Table 3.6.1).* SETX was found to promote clearance of virus from the vaginal lumen at later stages of infection (*Figure 3.6.2).* $SETX^{-/-}$ mice displayed an overall increase in inflammatory markers in the vaginal lumen later during infection, though these were not statistically significant. Additionally, it appeared that $SETX^{-/-}$ mice displayed

more long-lasting elevations in cytokine profiles whereas $SETX^{+/+}$ animals generally had declining cytokine/chemokine concentrations over time (*Figure 3.6.3*).

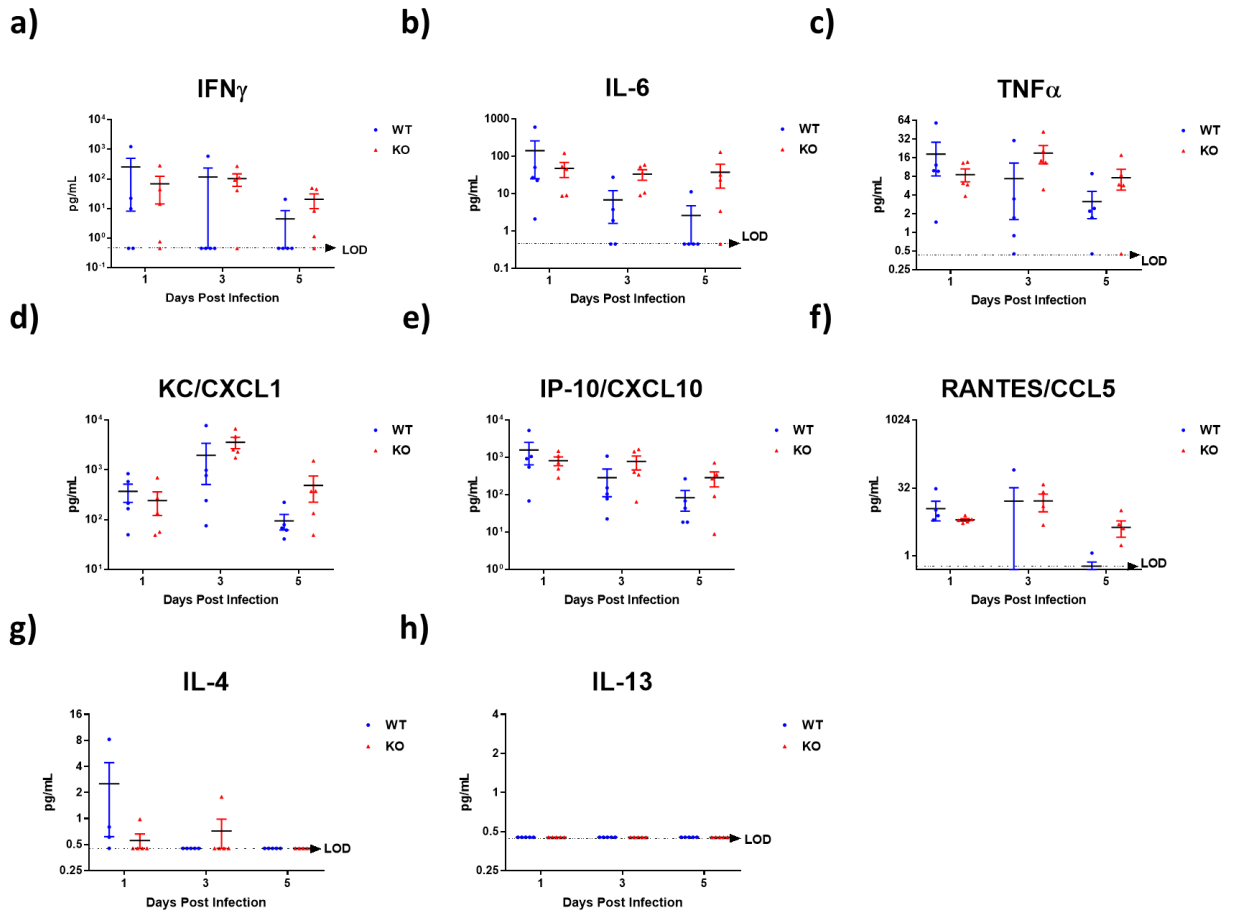

Figure 3.6.3. **SETX promotes reduced inflammatory vaginal environment during vaginal HSV-1 infection in mice.** (a-h) SETX $^{(+/+,\ -/-)}$ were infected intravaginally with 10^5 PFU of HSV-1 17+ four days following treatment with 2.5mg of Depo-Provera. Vaginal washes were performed on days 1, 3, 5 and Eve Technologies MD-31 discovery assay was performed to quantify cytokine and chemokine profiles. (a-i) Concentrations of cytokine/chemokines detected for n = 5 mice per group. (a-f) Representative inflammatory cytokine and chemokines. (g-h) Representative anti-inflammatory cytokines. All data was analyzed with two-way ANOVA and shown to be non-significant.

Chapter 4

Discussion & Conclusions

4.1 SETX Facilitation of Viral DNA Replication

The role of SETX during HSV-1 infection is multifaceted due to its ability to act on both the virus and the host through direct and indirect means[7,18,27,30,69]. SETX has been considered a 'genome guardian' through its' role in R-loop homeostasis[137]. SETX protection of cellular DNA against R-loop would potentially also apply to HSV-1 DNA[137]. The potential to form R-loops is also present within the HSV-1 genome (*Figure 3.4.2)*[114], and thus, the deleterious effects of R-loops occurring during HSV-1 DNA replication could inhibit replication in a similar manner to cellular R-loop formation (*Figure 1.4.1*)[137]. The resolution of R-loops by SETX would, by this reasoning, be protective to HSV-1 DNA replication. Although SETX-mediated enhancement of viral DNA replication was modest (~2-fold), it was a significant and consistent across both human and mouse derived cells and was replicated using either an siRNA knockdown (KD) system (transient model) in human tissues, or a mouse gene knockout (*Figure 3.1.1*). This body of work was the first demonstration of SETX affecting viral DNA replication.

Various potential mechanisms exist which may explain this difference in viral gDNA replication efficiency (*Figure 3.1.1).* The first, and most likely explanation, lies with the well-described function of SETX as an R-loop unwinding RNA:DNA helicase[11,32,37,137]. During cellular DNA replication R-loops accumulate in the head-on orientation; the direction in which deleterious collisions can occur [38,43]. These occur due to positive and negative supercoiling which forms as result of DNA replication[40,43], and are intrinsic to the process of DNA replication. HSV-1 DNA replication is also thought to result in supercoiling; especially given the observation HSV-1 recruits, and requires, cellular topoisomerase (supercoiling resolution

enzyme) for DNA replication[74,138]. Interestingly, the three HSV-1 origins of replication align with three (~70 kbp into U_L fragment, both bias regions of U_S) areas of high R-loop bias shown through the R-loop prediction (*Figure 3.4.2)*[70]. This is important as supercoiling has been suggested to facilitate unwinding of origins of replication in HSV-1 DNA, as this may be involved in replication initiation[74]. With an increased prevalence of R-loops in and around replication origins, initial stages of replication would be altered as the incidence of replication/transcription machinery collisions increases[38,43]. Due to the generation of viral DNA replication supercoiling, the association of R-loop bias regions with HSV-1 replication origins and the increased incidence of R-loop generation as result[43], it is likely that a global increase in R-loop prevalence would also result in increases of R-loop dependent DNA damage on the viral genome[31,139]. R-loop formation in IE, E and leaky L HSV-1 genes, which do not require DNA replication for expression, would be likely to produce transcription machinery stalling[140,141]. This poses a potential threat, as the co-occurrence of stalled transcriptional machinery and active replication bubbles generates potential for DSB[38]. Increased DNA damage to the HSV-1 viral genome would thereby decrease replication efficiency. The HSV-1 polymerase is known to have modest RNaseH activity within the 3'-5' exonuclease activity of the complex[142]. It may be that this RNaseH activity has roles in preventing R-loop dependent damage. Indeed, RNaseH plays a role in degrading R-loops when they cannot be resolved in cellular DNA[36]. Confirming that the effects of SETX on HSV-1 DNA replication are R-loop- mediated could be accomplished through overexpression of RNaseH[139]. Over expression of RNaseH should nullify any R-loop mediated effects caused by SETX depletion or $SETX^{-/-}$ KO [143]. Alternatively, use of SETX mutants lacking the helicase or RNA binding activity could also be employed in $SETX^{-/-}$ models to ascertain if the R-loop remediation functionality is important in viral DNA replication[30].

Another potential mechanism by which SETX may facilitate HSV-1 viral DNA replication is through its involvement in the cellular DDR [3,74]. During HSV-1 rolling circle DNA replication, which is believed to be initiated through recombination, structures analogous to DSB must occur between head-to-tail unit length genomes along the concatemer[99,100,144]. There is potential for SETX to regulate the recruitment of DDR factors to the sites of DSB in a form of transcriptional coupled repair[27]. DSB occurring in sites of active transcription result in R-loop formation across the break[27]. SETX inhibits translocation of the break to non-homologous sequences and may thus prevent DNA repair prior to processing[27]. This would be predicted to reduce packaging of DNA into viral particles and replication may also stall.

To test whether SETX alters processing of viral genome concatemers, a modified Southern Blotting method using Pulse Field Gel Electrophoresis (PFGE) to separate out the large viral concatemers (>150 kbp) could be employed. Processing efficiency could be analyzed by looking for DNA laddering of concatemers into n=1,2,3, etc. lengths of ~150kbp genomes. Altered processing dynamics would result in shifts in laddering patterns and/or banding intensity.

A final potential mechanism by which SETX may have facilitated HSV-1 viral DNA replication is through negative regulation of the antiviral response[30]. ISGs such as protein kinase R (PKR) are capable of blocking protein translation, and suppressing viral protein synthesis, ultimately reducing viral replication[145]. Despite the exacerbated antiviral response in SETX deficient systems[30], HSV-1 may not be affected. HSV-1 antagonism of IFN pathways by VHS, ICP0, ICP27, ICP34.5 and numerous others viral proteins, effectively make HSV-1 IFN resistant in *in-vitro* systems[86,87,146,147]. Additionally, if this exacerbation of the antiviral response resulted in decreases in viral DNA replication efficiency, it would be probable to see improved infection outcomes and reduced viral titres in the vaginal washes of HSV-1 infected mice (*Figure 3.6.2),*

however the opposite was true. Testing the intersection of the antiviral response with HSV-1 DNA replication could be accomplished by combining the siRNA KD model with human telomerase reverse transcriptase (hTERT) immortalized fibroblasts deficient in IRF3 which are currently available[148]. Typical immortalization strategies perturb type I IFN signaling, and it has been shown that hTERT immortalization leaves antiviral signaling mostly intact [148].

The lack of appreciable effect of SETX on HSV-1 DNA replication in IRF3/9 MEF experiments was not necessarily surprising (*Figure 3.1.2).* Transient KD with siRNA do not precisely recapitulate SETX$^{-/-}$ cellular environments[149]. SETX KD models may be more indicative of an exaggerated heterozygous mutation in which a depleted amount of SETX is present. Complete loss of functional SETX may be required for apparent disease phenotypes. HSV-1 is primarily a human pathogen[83]. Both in IRF3/9 and SETX MEF, viral gDNA and titres were an order of magnitude lower than the comparative HFF cells (*Figure 3.1.1, Figure 3.1.2).* The effect of SETX may have been accentuated in SETX MEF (*Figure 3.1.1b),* but since it is a modest effect, it likely requires either greater replication efficiencies such as those that are present in human cell lines (*Figure 3.1.1c),* or more effective systems devoid of SETX, as in the case of SETX$^{-/-}$ MEF (*Figure 3.1.1b, d).* If this is the appropriate explanation, AOA2 patient-derived fibroblasts would show the greatest effect on HSV-1 in terms of viral DNA replication efficiency. The other side of this would be using either a more susceptible mouse background than C57BL6 used, such as BALB/c[150], or using a more mouse virulent strain of HSV-1 such as HSV-1 17+ or HSV-1 strain McKrae, in a MEF siSETX KD system to see a recapitulation of this effect[132,151].

4.2 SETX Regulation of R-loops as a Modifier of Gene Expression

SETX had been shown to regulate a variety of host cellular genes to-date, and this effect was dependent on its RNA:DNA helicase activity[11,18,30]. Deleterious effects associated with failure to resolve R-loops are thought to be coupled to DNA replication. However, recent studies have shown altered transcription profiles in SETX deficient systems for a variety of host genes[18,30]. Currently, no study has examined the influences of SETX on viral transcriptional systems.

SETX had a modest effect on viral gene expression, but this effect seemed gene specific, and not global based upon later observations. Examination of initial candidate genes showed that SETX modestly antagonized specific HSV-1 genes (*Figure 3.2.1, Figure 3.2.3),* but this effect was not recapitulated in the system using the AdV-GFP (*Figure 3.4.1)*. RNA-Seq of HSV-1 infected SETX MEF and comparison to *in-silico* R-loop predictions showed results consistent with the known function of SETX at cellular genes (*Figure 3.4.2)*. Areas showing the greatest differential gene regulation were found in predominantly R-loop rich regions. Conversely, the CMV IE promoter was not predicted as a region prone to R-loop formation[114]. Genes identified from the RNA-Seq should be confirmed through qPCR.

Confirmation that the differential regulation of genes by SETX was specific to R-loops could be ascertained through a form of chromatin immunoprecipitation (ChIP) called bisulfite DNA-RNA immunoprecipitation (bisDRIP)[152]. The technique employs an R-loop specific antibody called S9.6 and a bisulfite treatment to convert ssDNA cytosine to uracil to increase resolution of the process to the nucleotide level[152]. Pulling out sequences specific to genes such as *RL1* (which is found in a region predicted to be rich in R-loops) would substantiate the presence of R-loops on the viral genome. ChIP may also be possible with SETX, however, SETX antibodies do not consistently detect through immunoblot (data not shown) and therefore

a successful SETX ChIP may prove difficult. The potential indirect effects of SETX in regulating viral gene expression because of its role in regulating viral genome replication must also be acknowledged. Decreases of viral DNA template in the absence of SETX would likely result in decreases in viral gene expression, especially in true late genes requiring HSV-1 DNA replication[122].

R-loop mediated differential regulation of gene expression can cause either increases or decreases in gene expression, dependent on the location of the R-loop[37]. R-loop formation in promoter regions has been demonstrated to reduce methylation and there by increase gene expression[18], and conversely, R-loops can result in premature transcription termination in the transcriptional termination region in a SETX-dependent manner[11,30]. DNA viruses like HSV-1 are generally undermethylated (as methylation is associated with reduced replication and transcription[153], so therefore it would be unlikely methylation based effects play a significant role in gene expression. On the other hand, the absence of SETX is likely to result in reduced premature transcription termination caused by R-loops forming in termination regions, similar as to what was observed for IRF3-responsive loci[30]. Both positive and negative regulation of HSV-1 gene expression was evident from the RNA-Seq data (*Figure 3.4.2*) analysis. If bis-DRIP analysis is performed, the sites of R-loops with respect to promoter regions and termination regions should be compared to the change in gene expression observed.

The initial increase in host pools of OCT1/HCF1 may offer a potential avenue to explain the increases of viral IE *UL54* gene expression during SETX depletion in HFF cells (*Figure 3.3.1).* A multiprotein complex comprising OCT-1, HCF-1 and VP16 are required for IE gene expression[1]. Previously, HSV-1 has been demonstrated to induce expression of OCT-1 during infection of mouse trigeminal ganglia and human foreskin fibroblasts[154,155]. However, the

induction of gene expression of HCF-1 has not yet been documented. Thus, directly from onset of infection, HSV-1 IE gene expression has a larger pool of cofactors necessary for expression in SETX depleted cells. This may facilitate an increase viral transcription prior to activation of the antiviral response. Indeed, HSV-1 could utilize SETX initially to upregulate HCF1 and OCT1 during early stages of infection to make the cellular environment more conducive to viral growth.

4.3 SETX Antagonism of Antiviral Response

A reductionist system was used to examine SETX antagonism of the antiviral response downstream of the DNA sensor STING. Ultimately, all viral nucleic acid sensing pathways, for both RNA and DNA , converge at the level of IRF3 activation [156,157]. SETX was previously found to antagonize IRF3 responsive loci in response to RNA viruses[30], and therefore we expected to see the same antagonism of transcription in response to DNA virus sensing (*Figure 3.5.1).* It is likely that the same mechanism of premature transcription termination caused by TAF4 recruitment of SETX to IRF3 responsive loci would resulted in the negative regulation of DNA sensing responses[30].

The antagonism of the antiviral response downstream of DNA sensor STING should be confirmed using DNA virus infections, like HSV-1. Standard HSV-1 strains may be unlikely to show an distinct phenotype because of their proficient antagonism of the antiviral response [83,87,158]. UV-inactivation of HSV-1 which allows viral particle entry and delivery of viral PAMPs are one potential approach to overcome this issue[159]. Alternatively, attenuated mutant strains could be employed, such as the HSV-1 0ΔNLS, which lacks both the ICP0 gene and a nuclear localization signal (NLS), and is extremely susceptible to type I IFN responses *in-vitro.*[160]

4.4 SETX Prevention of HSV-1 Disease Pathogenesis in Mice

The 2-fold difference in HSV-1 viral DNA replication was not detected in viral titres using *in-vivo* infections models of HSV-1 in SETX $^{-/-}$ mice titre. In fact, it appeared that HSV-1 replication was enhanced/prolonged in the SETX$^{-/-}$ animals. The explanation for increased detectable virus in SETX$^{-/-}$ animals is likely multifactorial. There is possibility that SETX-mediated effects on gene expression of factors such as ICP34.5 and ICP0 cause increased virulence of HSV-1. ICP0 null viruses are heavily susceptible to type I IFN responses, and ICP34.5 is a known HSV-1 virulence factor[160,161]. It may be that the role of SETX in supporting viral DNA replication are being overwhelmed by increased expression of viral virulence factors in the absence of SETX, which leave HSV-1 less susceptible to host immune responses[162]. Altered expression of these virulence factors like ICP34.5 is part of the rationale behind the increased neurovirulence of HSV-1 strain McKrae, which is among the most virulent HSV-1 strains in mice [132]. Use of ICP34.5 deficient strains could be useful to determine the impacts of virulence factors on viral replication in SETX$^{-/-}$ mice[85].

Perhaps the most striking observation reported here was the survival differences observed in SETX$^{+/+}$ and SETX$^{-/-}$ mice after HSV-1 infection. SETX$^{-/-}$ mice were significantly more susceptible to HSV-1 pathogenesis (*Figure 3.6.1).* The elevated rates of neurological sequelae observed in HSV-1 infected SETX$^{-/-}$ mice may be a result of SETX affecting the antiviral response. Treatments with adjuvants to mice infected with HSV-1 resulted in increased hind-limb paralysis incidence in response to HSV-1 infection[163]. Additionally, susceptibility of mice to HSV-1 encephalitis (HSE) correlates with elevations in inflammatory markers upon corneal infection[164]. Depletion of inflammatory macrophages and neutrophils resulted in improved disease outcome in animals, demonstrating that gross indicators of tissue inflammation do not

necessarily correlate with disease outcome [164]. Examinations of immune cell activation and function in SETX$^{-/-}$ animals infected with HSV-1 infection may help to clarify the basis for the neuropathology phenotype that we have observed.

There is also the potential that SETX altered the expression of ICP34.5, an HSV-1 neurovirulence factor[85], based upon the discovery that R-loop bias was a predictor of differential gene expression and *RL1/*ICP34.5 lies in distinct R-loop bias regions *(Figure 3.4.2).* HSV-1 mutants lacking ICP34.5 are significantly neuroattentuated[85], and thus altered expression of ICP34.5 as a result of SETX deficiency could explain the increasing incidence of hind limb paralysis in HSV-1 infected SETX mice. Further infections of HSV-1 in SETX$^{-/-}$mice could include ICP34.5 null mutants.

The previous examinations of SETX antagonism of the antiviral response were all strictly *in-vitro* models[30]. The current study using intravaginal infection of SETX$^{-/-}$ mice provides the first observation of altered immune responses in SETX-deficient animals. SETX fine tuning of the antiviral response has been typically undetectable at later stages during *in-vitro* infection[30]. Increased inflammatory responses as result of HSV-1 infection may be indicative of expanding viral infection[165]. This would be in line with the decreases in mouse survival observed earlier in SETX$^{-/-}$ animals, who had greater virus titres late after infection (*Figure 3.6.1)*. Examining mouse cytokine profiles in response to attenuated or inactivated HSV-1 would reveal if the inflammatory profile is entirely due to the host response, or in response to prolonged viral infection. Cytokine profiles of neural tissues such as brain and spinal cord could provide insights into whether SETX$^{-/-}$ produces a systemic inflammatory response and provide further insight into the increased neuropathology seen previously. Additionally, SETX$^{-/-}$ animals who survived infection should be examined for phenotypes of neuroinflammation within neural tissues[78].

4.5 Overall Implications and Conclusions

This work provides a novel role for SETX with respect to HSV-1 DNA replication and gene expression. Further work is required to demonstrate the specific mechanisms by which SETX is affecting HSV-1 and whether it is a direct interaction with the virus or mediated through specific host responses. The role of SETX during viral infection has important implications in the context of neuroinflammation and neurodegenerative disease. Viruses may act as triggers of disease in susceptible individuals and our mouse experiments would lend support to this[75]. SETX mice infected with HSV-1 show increased neurological disease symptomology, likely as result of increase immunopathology, and the ALS model SOD1 mice show faster progression of ALS-like symptoms following recovery from IAV infection (*Figure S.2.1)*[163]. A hallmark of neurodegenerative diseases is uncontrolled inflammation in neurological tissues. The initial cause of onset of this inflammation is unknown, but progresses over the course of the disease[62]. Our results would support a role of viral infections in the etiology of neurodegenerative disease as potential triggers or contributors of inflammation leading to disease development.

References

1. Wysocka, J. & Herr, W. The herpes simplex virus VP16-induced complex: The makings of a regulatory switch. *Trends Biochem. Sci.* **28,** 294–304 (2003).
2. Turnell, A. S. & Grand, R. J. DNA viruses and the cellular DNA-damage response. *J. Gen. Virol.* **93,** 2076–2097 (2012).
3. Smith, S., Weller, S. K. HSV-1 and the cellular DNA damage response. *Futur. Virol* **10,** 383–397 (2015).
4. Hsu, T.-H. & Spindler, K. R. Identifying Host Factors That Regulate Viral Infection The Host Side of Viral Infection. *PLoS Pathog.* **8,** 1–3 (2012).
5. Sander, J. D. & Joung, J. K. CRISPR-Cas systems for genome editing, regulation and targeting. *Nat. Biotechnol.* **32,** 347–355 (2014).
6. Bartlett, D. W. & Davis, M. E. Insights into the kinetics of siRNA-mediated gene silencing from live-cell and live-animal bioluminescent imaging. *Nucleic Acids Res.* **34,** 322–333 (2006).
7. Becherel, O. J. *et al.* Senataxin Plays an Essential Role with DNA Damage Response Proteins in Meiotic Recombination and Gene Silencing. *PLoS Genet.* **9,** (2013).
8. Chen, Y.-Z. *et al.* Senataxin, the yeast Sen1p orthologue: Characterization of a unique protein in which recessive mutations cause ataxia and dominant mutations cause motor neuron disease. *Neurobiol. Dis.* **23,** 97–108 (2006).
9. Moreira, M.-C. *et al.* Senataxin, the ortholog of a yeast RNA helicase, is mutant in ataxia-ocular apraxia 2. *Nat. Genet.* **36,** 225–227 (2004).
10. Chen, Y.-Z. *et al.* DNA/RNA helicase gene mutations in a form of juvenile amyotrophic lateral sclerosis (ALS4). *Am. J. Hum. Genet.* **74,** 1128–35 (2004).
11. Skourti-Stathaki, K., Proudfoot, N. J. & Gromak, N. Human Senataxin Resolves RNA/DNA Hybrids Formed at Transcriptional Pause Sites to Promote Xrn2-Dependent Termination. *Mol. Cell* **42,** 794–805 (2011).
12. Lavin, M. F., Yeo, A. J. & Becherel, O. J. Senataxin protects the genome: Implications for neurodegeneration and other abnormalities. *Rare Dis.* **1,** e25230 (2013).
13. Asaka, T., Yokoji, H., Ito, J., Yamaguchi, K. & Matsushima, A. Autosomal recessive ataxia with peripheral neuropathy and elevated AFP: Novel mutations in SETX. *Neurology* **66,** 1580–1581 (2006).
14. Suraweera, A. *et al.* Functional role for senataxin, defective in ataxia oculomotor apraxia type 2, in transcriptional regulation. *Hum. Mol. Genet.* **18,** 3384–3396 (2009).
15. Szpisjak, L., Obal, I., Engelhardt, J. I., Vecsei, L. & Klivenyi, P. A novel SETX gene mutation producing ataxia with oculomotor apraxia type 2. *Acta Neurol. Belg.* **116,** 405–407 (2016).
16. Tazir, M. *et al.* Ataxia with oculomotor apraxia type 2: A clinical and genetic study of 19

patients. *J. Neurol. Sci.* **278,** 77–81 (2009).

17. Lu, C., Zheng, Y.-C., Dong, Y. & Li, H.-F. Identification of novel senataxin mutations in Chinese patients with autosomal recessive cerebellar ataxias by targeted next-generation sequencing. *BMC Neurol.* **16,** 179 (2016).

18. Grunseich, C. *et al.* Senataxin Mutation Reveals How R-Loops Promote Transcription by Blocking DNA Methylation at Gene Promoters. *Mol. Cell* **69,** 426–437 (2018).

19. Rabin, B. a *et al.* Autosomal dominant juvenile amyotrophic lateral sclerosis. *Brain* **122 (Pt 8,** 1539–50 (1999).

20. Chance, P. F. *et al.* Linkage of the gene for an autosomal dominant form of juvenile amyotrophic lateral sclerosis to chromosome 9q34. *Am. J. Hum. Genet.* **62,** 633–640 (1998).

21. Arning, L. *et al.* The SETX missense variation spectrum as evaluated in patients with ALS4-like motor neuron diseases. *Neurogenetics* **14,** 53–61 (2013).

22. Airoldi, G. *et al.* Characterization of two novel SETX mutations in AOA2 patients reveals aspects of the pathophysiological role of senataxin. *Neurogenetics* **11,** 91–100 (2010).

23. Hirano, M. *et al.* Senataxin mutations and amyotrophic lateral sclerosis. *Amyotroph. lateral Scler.* **12,** 223–7 (2011).

24. Anheim, M. *et al.* Ataxia with oculomotor apraxia type 2: Clinical, biological and genotype/phenotype correlation study of a cohort of 90 patients. *Brain* **132,** 2688–2698 (2009).

25. Alzu, A. *et al.* Senataxin associates with replication forks to protect fork integrity across RNA-polymerase-II-transcribed genes. *Cell* **151,** 835–846 (2012).

26. Yeo, A. J. *et al.* Senataxin controls meiotic silencing through ATR activation and chromatin remodeling. *Cell Discov.* **1,** 15025 (2015).

27. Cohen, S. *et al.* Senataxin resolves RNA:DNA hybrids forming at DNA double-strand breaks to prevent translocations. *Nat. Commun.* **9,** 533 (2018).

28. Yüce, Ö. & West, S. C. Senataxin, defective in the neurodegenerative disorder ataxia with oculomotor apraxia 2, lies at the interface of transcription and the DNA damage response. *Mol. Cell. Biol.* **33,** 406–17 (2013).

29. Mischo, H. E. *et al.* Yeast Sen1 helicase protects the genome from transcription-associated instability. *Mol. Cell* **41,** 21–32 (2011).

30. Miller, M. S. *et al.* Senataxin suppresses the antiviral transcriptional response and controls viral biogenesis. *Nat. Immunol.* **16,** 485–94 (2015).

31. Suraweera, A. *et al.* Senataxin, defective in ataxia oculomotor apraxia type 2, is involved in the defense against oxidative DNA damage. *J. Cell Biol.* **177,** 969–979 (2007).

32. De Amicis, A. *et al.* Role of senataxin in DNA damage and telomeric stability. *DNA Repair (Amst).* **10,** 199–209 (2011).

33. Yeo, A. J. *et al.* R-Loops in proliferating cells but not in the brain: Implications for AOA2 and other autosomal recessive ataxias. *PLoS One* **9,** (2014).

34. Duquette, M. L., Handa, P., Vincent, J. A., Taylor, A. F. & Maizels, N. Intracellular transcription of G-rich DNAs induces formation of G-loops, novel structures containing G4 DNA. *Genes Dev.* **18,** 1618–1629 (2004).

35. Groh, M. & Gromak, N. Out of Balance: R-loops in Human Disease. *PLoS Genet.* **10,** 1–9 (2014).

36. Richard, P. & Manley, J. L. R Loops and Links to Human Disease. *J. Mol. Biol.* **429,** 3168–3180 (2017).

37. Skourti-Stathaki, K. & Proudfoot, N. J. A double-edged sword: R loops as threats to genome integrity and powerful regulators of gene expression. *Genes Dev.* **28,** 1384–1396 (2014).

38. Pomerantz, R. T. & O'Donnell, M. What happens when replication and transcription complexes collide? *Cell Cycle* **9,** 2537–2543 (2010).

39. Pfeiffer, V., Rô Me Crittin, J., Grolimund, L. & Lingner, J. The THO complex component Thp2 counteracts telomeric R-loops and telomere shortening. *EMBO J.* **32,** 2861–2871 (2013).

40. Marinello, J. *et al.* Dynamic Effects of Topoisomerase I Inhibition on R-Loops and Short Transcripts at Active Promoters. *PLoS One* **11,** 1–18 (2016).

41. Salas-Armenteros, I. *et al.* Human THO-Sin3A interaction reveals new mechanisms to prevent R-loops that cause genome instability. *EMBO J.* **36,** 3532–3547 (2017).

42. Crow, Y. J. *et al.* Mutations in genes encoding ribonuclease H2 subunits cause Aicardi-Goutières syndrome and mimic congenital viral brain infection. *Nat. Genet.* **38,** 910–916 (2006).

43. Hamperl, S. *et al.* Transcription-Replication Conflict Orientation Modulates R-Loop Levels and Activates Distinct DNA Damage Responses. *Cell* **170,** 774–774.e19 (2017).

44. Nossal, N. G., Dudas, K. C. & Kreuzer, K. N. No TitBacteriophage T4 Proteins Replicate Plasmids with a Preformed R Loop at the T4 ori(uvsY) Replication Origin In Vitrole. *Mol. Cell* **7,** 31–41 (2001).

45. Xu1, B. & Clayton2, D. A. RNA-DNA hybrid formation at the human mitochondrial heavy-strand origin ceases at replication start sites: an implication for RNA-DNA hybrids serving as primers. *EMBO J.* **15,** 3135–3143 (1996).

46. Biamonti, G. *et al.* R-loops and initiation of DNA replication in human cells: a missing link? *Front. Genet.* **6,** 1–7 (2015).

47. Stuckey, R., García-Rodríguez, N., Aguilera, A. & Wellinger, R. E. Role for RNA:DNA hybrids in origin-independent replication priming in a eukaryotic system. *Proc. Natl. Acad. Sci.* **112,** 5779–5784 (2015).

48. Al-Hadid, Q. & Yang, Y. R-loop: an emerging regulator of chromatin dynamics. *Acta*

Biochim Biophys Sin **48,** 623–631 (2016).

49. Ivashkiv, L. B. & Donlin, L. T. Regulation of type I interferon responses. *Nat. Rev. Immunol.* **14,** 36–49 (2013).

50. Marozin, S. *et al.* Inhibition of the IFN-beta response in hepatocellular carcinoma by alternative spliced isoform of IFN regulatory factor-3. *Mol. Ther.* **16,** 1789–1797 (2008).

51. Sheikh, F., Dickensheets, H., Gamero, A. M., Vogel, S. N. & Donnelly, R. P. An essential role for IFN-β in the induction of IFN-stimulated gene expression by LPS in macrophages. *J. Leukoc. Biol.* **96,** 591–600 (2014).

52. Darnell, J. E., Kerr, I. M. & Stark, G. R. Jak-STAT pathways and transcriptional activation in response to IFNs and other extracellular signaling proteins. *Science (80-.).* **264,** 1415–1421 (1994).

53. Wong, M.-T. & Chen, S. S.-L. Emerging roles of interferon-stimulated genes in the innate immune response to hepatitis C virus infection. *Cell. Mol. Immunol.* **13,** 11–35 (2016).

54. Ning, S., Pagano, J. S. & Barber, G. N. IRF7: activation, regulation, modification and function. *Genes Immun.* **12,** 399–414 (2011).

55. Thompson, M. R., Kaminski, J. J., Kurt-Jones, E. A. & Fitzgerald, K. A. Pattern recognition receptors and the innate immune response to viral infection. *Viruses* **3,** 920–940 (2011).

56. Schneider, William M., Chevillotte, Meike D., Rice, C. M. Interferon-Stimulated Genes: A Complex Web of Host Defenses. *Annu Rev Immunol* **32,** 513–545 (2014).

57. Chakrabarti, A., Jha, B. K. & Silverman, R. H. New insights into the role of RNase L in innate immunity. *J. Interferon Cytokine Res.* **31,** 49–57 (2011).

58. Zhang, D. & Zhang, D.-E. Interferon-stimulated gene 15 and the protein ISGylation system. *J. Interferon Cytokine Res.* **31,** 119–30 (2011).

59. Perez-Caballero, D. *et al.* Tetherin inhibits HIV-1 release by directly tethering virions to cells. *Cell* **139,** 499–511 (2009).

60. Blondeau, C. *et al.* Tetherin Restricts Herpes Simplex Virus 1 and Is Antagonized by Glycoprotein M. *J. Virol.* **87,** 13124–13133 (2013).

61. Hiscott, J. Triggering the innate antiviral response through IRF-3 activation. *J. Biol. Chem.* **282,** 15325–15329 (2007).

62. Hooten, K. G., Beers, D. R., Zhao, W. & Appel, S. H. Protective and Toxic Neuroinflammation in Amyotrophic Lateral Sclerosis. *Neurotherapeutics* 364–375 (2015). doi:10.1007/s13311-014-0329-3

63. Streit, W. J., Mrak, R. E. & Griffin, W. S. T. Microglia and neuroinflammation: a pathological perspective. *J. Neuroinflammation* **1,** 4 pages (2004).

64. Harwig, A., Landick, R. & Berkhout, B. The Battle of RNA Synthesis: Virus versus Host. *Viruses* **9,** 1–18 (2017).

65. Steiner, I., Kennedy, P. G. & Pachner, A. R. The neurotropic herpes viruses: herpes simplex and varicella-zoster. *Lancet Neurol.* **6,** 1015–1028 (2007).

66. Costanzo, F., Campadelli-Fiume, G., Foa-Tomasi, L. & Cassai, E. Evidence that herpes simplex virus DNA is transcribed by cellular RNA polymerase B. *J. Virol.* **21,** 996–1001 (1977).

67. Alekseev, O., Donovan, K. & Azizkhan-Clifford, J. Inhibition of ataxia telangiectasia mutated (ATM) kinase suppresses herpes simplex virus type 1 (HSV-1) keratitis. *Investig. Ophthalmol. Vis. Sci.* **55,** 706–715 (2013).

68. Wilkinson, D. E. & Weller, S. K. Herpes simplex virus type I disrupts the ATR-dependent DNA-damage response during lytic infection. *J. Cell Sci.* **119,** 2695–703 (2006).

69. Richard, P., Feng, S. & Manley, J. L. A SUMO-dependent interaction between Senataxin and the exosome, disrupted in the neurodegenerative disease AOA2, targets the exosome to sites of transcription-induced DNA damage. *Genes Dev.* **27,** 2227–2232 (2013).

70. Macdonald, S. J., Mostafa, H. H., Morrison, L. A. & Davido, D. J. Genome sequence of herpes simplex virus 1 strain KOS. *J. Virol.* **86,** 9540–9541 (2012).

71. Macdonald, S. J., Mostafa, H. H., Morrison, L. A. & Davido, D. J. Genome Sequence of Herpes Simplex Virus 1 Strain McKrae. *J. Virol.* **86,** 9540–9541 (2012).

72. Taylor, K. E., Chew, M. V, Ashkar, A. A. & Mossman, K. L. Novel Roles of Cytoplasmic ICP0: Proteasome-Independent Functions of the RING Finger Are Required To Block Interferon-Stimulated Gene Production but Not To Promote Viral Replication. *J. Virol.* **88,** 8091–8101 (2014).

73. Chilukuri, S. & Rosen, T. Management of acyclovir-resistant herpes simplex virus. *Dermatologic Clinics* **21,** 311–320 (2003).

74. Weller, S. K. & Coen, D. M. Herpes Simplex Viruses: Mechanisms of DNA Replication. *Cold Spring Harb. Perspect. Biol.* **4,** a013011–a013011 (2012).

75. Zhou, L., Miranda-Saksena, M. & Saksena, N. K. Viruses and neurodegeneration. *Virol. J.* **10,** 1 (2013).

76. Lam, M. M. W., Mapletoft, J. P. & Miller, M. S. Abnormal regulation of the antiviral response in neurological/neurodegenerative diseases. *Cytokine* **88,** 251–258 (2016).

77. Knipe, D.M., Howley, P. M. *Fields Virology*. (2013).

78. Martin, C. *et al.* Inflammatory and neurodegeneration markers during asymptomatic HSV-1 reactivation. *J. Alzheimer's Dis.* **39,** 849–859 (2014).

79. Perry, A. K., Chen, G., Zheng, D., Tang, H. & Cheng, G. The host type I interferon response to viral and bacterial infections. *Cell Res* **15,** 407–422 (2005).

80. Limongi, D. & Baldelli, S. Redox Imbalance and Viral Infections in Neurodegenerative Diseases. *Oxid. Med. Cell. Longev.* **2016,** 1–13 (2016).

81. Smiley, J. R. Herpes simplex virus virion host shutoff protein: immune evasion mediated

by a viral RNase? *J. Virol.* **78,** 1063–1068 (2004).

82. Connolly, S. A., Jackson, J. O., Jardetzky, T. S. & Longnecker, R. Fusing structure and function: a structural view of the herpesvirus entry machinery. *Nat. Rev. Microbiol.* **9,** 369–381 (2011).

83. Karasneh, G. A. *et al.* Herpes simplex virus infects most cell types in vitro: clues to its success. *Virol. J.* **8,** 481 (2011).

84. Agelidis, A. M. & Shukla, D. Cell entry mechanisms of HSV: what we have learned in recent years. *Future Virol.* **10,** 1145–1154 (2015).

85. Orvedahl, A. *et al.* HSV-1 ICP34.5 Confers Neurovirulence by Targeting the Beclin 1 Autophagy Protein. *Cell Host Microbe* (2007). doi:10.1016/j.chom.2006.12.001

86. Shu, M., Taddeo, B., Zhang, W. & Roizman, B. Selective degradation of mRNAs by the HSV host shutoff RNase is regulated by the UL47 tegument protein. *Proc. Natl. Acad. Sci. U. S. A.* **110,** E1669-75 (2013).

87. Smith, M. C., Boutell, C. & Davido, D. J. HSV-1 ICP0: paving the way for viral replication. *Future Virol.* **6,** 421–429 (2011).

88. Tang, S., Patel, A. & Krause, P. R. Herpes simplex virus ICP27 regulates alternative pre-mRNA polyadenylation and splicing in a sequence-dependent manner. *Proc. Natl. Acad. Sci.* **113,** 12256–12261 (2016).

89. Christensen, M. H. *et al.* HSV-1 ICP27 targets the TBK1-activated STING signalsome to inhibit virus-induced type I IFN expression. *EMBO J.* **35,** 1385–1399 (2016).

90. Simmons, A. Herpes Simplex Virus Genome Isomerization : Origins of Adjacent Long Segments in Concatemeric Viral DNA. *J. Virol.* **73,** 810–813 (1999).

91. Trego, K. S., Zhu, Y. & Parris, D. S. The herpes simplex virus type 1 DNA polymerase processivity factor, UL42, does not alter the catalytic activity of the UL9 origin-binding protein but facilitates its loading onto DNA. *Nucleic Acids Res.* **33,** 536–545 (2005).

92. Nogueira, M. L., Wang, V. E. H., Tantin, D., Sharp, P. a & Kristie, T. M. Herpes simplex virus infections are arrested in Oct-1-deficient cells. *Proc. Natl. Acad. Sci. U. S. A.* **101,** 1473–1478 (2004).

93. Rass, U., Ahel, I. & West, S. C. Defective DNA Repair and Neurodegenerative Disease. *Cell* **130,** 991–1004 (2007).

94. Weller, S. K. Herpes simplex virus reorganizes the cellular DNA repair and protein quality control machinery. *PLoS Pathog.* **6,** 1–3 (2010).

95. Li, X. & Heyer, W.-D. Homologous recombination in DNA repair and DNA damage tolerance. *Cell Res.* **18,** 99–113 (2008).

96. Muylaert, I., Tang, K.-W. & Elias, P. Replication and Recombination of Herpes Simplex Virus DNA. *J. Biol. Chem.* **286,** 15619–15624 (2011).

97. Lilley, C. E. *et al.* A viral E3 ligase targets RNF8 and RNF168 to control histone

ubiquitination and DNA damage responses. *EMBO J.* **29,** 943–955 (2010).

98. Shirata, N. *et al.* Activation of ataxia telangiectasia-mutated DNA damage checkpoint signal transduction elicited by herpes simplex virus infection. *J. Biol. Chem.* **280,** 30336–30341 (2005).

99. Deiss, L. P. & Frenkel, N. Herpes simplex virus amplicon: cleavage of concatemeric DNA is linked to packaging and involves amplification of the terminally reiterated a sequence. *J. Virol.* **57,** 933–41 (1986).

100. McVoy, M. a, Nixon, D. E., Hur, J. K. & Adler, S. P. The ends on herpesvirus DNA replicative concatemers contain pac2 cis cleavage/packaging elements and their formation is controlled by terminal cis sequences. *J. Virol.* **74,** 1587–1592 (2000).

101. Chaurushiya, M. S. & Weitzman, M. D. Virus manipulation of DNA repair and cell cycle checkpoints. *DNA Repair (Amst).* **8,** 1166–1176 (2009).

102. Mehndiratta, M. M., Mehndiratta, P. & Pande, R. Poliomyelitis : Historical Facts , Epidemiology , and Current Challenges in Eradication. *The Neurohospitalist* **4,** 223–229 (2014).

103. Li, W. *et al.* Human endogenous retrovirus-K contributes to motor neuron disease. *Sci. Transl. Med.* **7,** 1–12 (2015).

104. Hosseini, S. *et al.* Long-term neuroinflammation induced by influenza A virus infection and the impact on hippocampal neuron morphology and function. *J. Neurosci.* 1740–17 (2018). doi:10.1523/JNEUROSCI.1740-17.2018

105. Alfahad, T. & Nath, A. Retroviruses and amyotrophic lateral sclerosis. *Antiviral Res.* **99,** 180–187 (2013).

106. Douville, R. N. & Nath, A. Human Endogenous Retrovirus-K and TDP-43 Expression Bridges ALS and HIV Neuropathology. *Front. Microbiol.* **8,** 1–8 (2017).

107. Succop, P. A., Clark, S., Chen, M. & Galke, W. Imputation of data values that are less than a detection limit. *J. Occup. Environ. Hyg.* **1,** 436–441 (2004).

108. Rueden, C. T. *et al.* ImageJ2: ImageJ for the next generation of scientific image data. *BMC Bioinformatics* **18,** 529 (2017).

109. Schneider, C. A., Rasband, W. S. & Eliceiri, K. W. NIH Image to ImageJ: 25 years of image analysis. *Nat. Methods* **9,** 671–675 (2012).

110. Ye, J. *et al.* Primer-BLAST: a tool to design target-specific primers for polymerase chain reaction. *BMC Bioinformatics* **13,** 134 (2012).

111. Sirén, J., Välimäki, N. & Mäkinen, V. Indexing graphs for path queries with applications in genome research. *IEEE/ACM Trans. Comput. Biol. Bioinforma.* **11,** 375–388 (2014).

112. Pertea, M., Kim, D., Pertea, G. M., Leek, J. T. & Salzberg, S. L. Transcript-level expression analysis of RNA-seq experiments with HISAT, StringTie and Ballgown. *Nat. Protoc.* **11,** 1650–1667 (2016).

113. Love, M. I., Huber, W. & Anders, S. Moderated estimation of fold change and dispersion for RNA-seq data with DESeq2. *Genome Biol.* **15,** 1–21 (2014).

114. Jenjaroenpun, P., Wongsurawat, T., Yenamandra, S. P. & Kuznetsov, V. A. QmRLFS-finder: A model, web server and stand-alone tool for prediction and analysis of R-loop forming sequences. *Nucleic Acids Res.* **43,** W527–W534 (2015).

115. Byers, S. L., Wiles, M. V, Dunn, S. L. & Taft, R. A. Mouse Estrous Cycle Identification Tool and Images. *PLoS One* **7,** (2012).

116. Ercolani, L., Florence, B., Denaro, M. & Alexander, M. Isolation and complete sequence of a functional human glyceraldehyde-3-phosphate dehydrogenase gene. *J. Biol. Chem.* **263,** 15335–15341 (1988).

117. Kim, E. T., White, T. E., Brandariz-Núñez, A., Diaz-Griffero, F. & Weitzman, M. D. SAMHD1 Restricts Herpes Simplex Virus 1 in Macrophages by Limiting DNA Replication. *J. Virol.* **87,** 12949–12956 (2013).

118. Berges, B. K. & Tanner, A. Modelling of human herpesvirus infections in humanized mice. *Journal of General Virology* **95,** 2106–2117 (2014).

119. Boettcher, M. & McManus, M. T. Choosing the Right Tool for the Job: RNAi, TALEN, or CRISPR. *Molecular Cell* **58,** 575–585 (2015).

120. Brown, J. C. High G+C Content of Herpes Simplex Virus DNA: Proposed Role in Protection Against Retrotransposon Insertion. *Open Biochem. J.* **1,** 33–42 (2007).

121. Boehmer, P. E. RNA binding and R-loop formation by the herpes simplex virus type-1 single-stranded DNA-binding protein (ICP8). *Nucleic Acids Res.* **32,** 4576–4584 (2004).

122. Harkness, J. M., Kader, M. & Deluca, N. A. Transcription of the Herpes Simplex Virus 1 Genome during Productive and Quiescent Infection of Neuronal and Nonneuronal Cells. *J. Virol.* **88,** 6847–6861 (2014).

123. Johnson, K. M., Mahajan, S. S. & Wilson, a C. Herpes simplex virus transactivator VP16 discriminates between HCF-1 and a novel family member, HCF-2. *J. Virol.* **73,** 3930–40 (1999).

124. Fogel, B. L. *et al.* Mutation of senataxin alters disease-specific transcriptional networks in patients with ataxia with oculomotor apraxia type 2. *Hum. Mol. Genet.* **23,** 4758–4769 (2014).

125. Burdette, D. L. *et al.* STING is a direct innate immune sensor of cyclic di-GMP. *Nature* **478,** 515–518 (2011).

126. Ishikawa, H., Ma, Z., Barber, G. N. STING regulates intracellular DNA-mediated, type I interferon-dependent innate immunity. *Nature* **461,** 788–792 (2009).

127. Ablasser, A. *et al.* cGAS produces a 2'-5'-linked cyclic dinucleotide second messenger that activates STING. *Nature* **498,** 380–384 (2013).

128. Tanaka, Y., Chen, Z. J. STING Specifies IRF3 phosphorylation by TBK1 in the Cytosolic DNA Signaling Pathway. *Sci Signal* **5,** ra20 (2012).

129. Diner, Elie J., Burdette, Dara L., Wilson, Stephen C., Monroe, Kathryn M., Kellenberger, Colleen A., Hyodo, Mamoru, Hayakawa, Yoshihiro, Hammond, Ming C., Vance, R. E. *et al.* The innate immune DNA sensor cGAS produces a non-canonical cyclic-di-nucleotide that activates human STING. *Cell Rep.* **3,** 1355–1361 (2013).

130. Zheng, M., Conrady, C. D., Ward, J. M., Bryant-Hudson, K. M. & Carr, D. J. J. Comparison of the host immune response to herpes simplex virus 1 (HSV-1) and HSV-2 at two different mucosal sites. *J. Virol.* **86,** 7454–8 (2012).

131. Kaushic, C., Ashkar, A. a, Reid, L. a & Rosenthal, K. L. Progesterone Increases Susceptibility and Decreases Immune Responses to Genital Herpes Infection. *J. Virol.* **77,** 4558–4565 (2003).

132. Wang, H., DAvido, D.J., Morrison, L. A. HSV-1 strain McKrae is more neuroinvasive than HSV-1 KOS after corneal or vaginal inoculation in mice. *Virus Res.* **173,** 436–440 (2014).

133. Milligan, G. N. Neutrophils Aid in Protection of the Vaginal Mucosae of Immune Mice against Challenge with Herpes Simplex Virus Type 2. *J. Virol.* **73,** 6380–6386 (1999).

134. Kumamoto, Y. & Iwasaki, A. Unique features of antiviral immune system of the vaginal mucosa. *Current Opinion in Immunology* **24,** 411–416 (2012).

135. Cavaillon, J. M. Pro- versus anti-inflammatory cytokines: myth or reality. *Cell. Mol. Biol. (Noisy-le-grand).* **47,** 695–702 (2001).

136. Ramesh, G., MacLean, A. G. & Philip, M. T. Cytokines and Chemokines at the Crossroads of Neuroinflammation, Neurdegeneration and Neuropathic Pain. *Mediators Inflamm.* **2013,** 1–20 (2013).

137. Groh, M., Albulescu, L. O., Cristini, A. & Gromak, N. Senataxin: Genome guardian at the interface of transcription and neurodegeneration. *J. Mol. Biol.* **In Press A,** 1–15 (2016).

138. Advani, S. J., Weichselbaum, R. R. & Roizman, B. Herpes simplex virus 1 activates cdc2 to recruit topoisomerase II alpha for post-DNA synthesis expression of late genes. *Proc Natl Acad Sci U S A* **100,** 4825–4830 (2003).

139. Amon, J. D. & Koshland, D. RNase H enables efficient repair of R-loop induced DNA damage. *Elife* **5,** (2016).

140. Dembowski, J. A., Dremel, S. E. & DeLuca, N. A. Replication-Coupled Recruitment of Viral and Cellular Factors to Herpes Simplex Virus Type 1 Replication Forks for the Maintenance and Expression of Viral Genomes. *PLoS Pathog.* **13,** (2017).

141. Sanz, L. A. *et al.* Prevalent, Dynamic, and Conserved R-Loop Structures Associate with Specific Epigenomic Signatures in Mammals. *Mol. Cell* **63,** 167–178 (2016).

142. Lawler, J. L., Mukherjee, P. & Coen, D. M. Herpes Simplex Virus 1 DNA Polymerase RNase H Activity Acts in a 3’-to-5’ Direction and Is Dependent on the 3’-to-5’ Exonuclease Active Site. *J. Virol.* **92,** JVI.01813-17 (2018).

143. Gó Mez-Gonzá Lez, B. N. *et al.* Genome-wide function of THO/TREX in active genes

prevents R-loop-dependent replication obstacles. *EMBO J.* **30,** 3106–3119 (2011).

144. Lo Piano, A., Martínez-Jiménez, M. I., Zecchi, L. & Ayora, S. Recombination-dependent concatemeric viral DNA replication. *Virus Res.* **160,** 1–14 (2011).

145. Pindel, A. & Sadler, A. The Role of Protein Kinase R in the Interferon Response. *J. Interf. Cytokine Res.* **31,** 59–70 (2011).

146. Li, Y. *et al.* ICP34.5 protein of herpes simplex virus facilitates the initiation of protein translation by bridging eukaryotic initiation factor 2 alpha (eIF2-alpha) and protein phosphatase 1. *J. Biol. Chem.* **286,** 24785–24792 (2011).

147. Zheng, C. & Su, C. Herpes simplex virus 1 infection dampens the immediate early antiviral innate immunity signaling from peroxisomes by tegument protein VP16. *Virol. J.* **14,** 1–8 (2017).

148. Smith, M. C., Goddard, E. T., Perusina Lanfranca, M. & Davido, D. J. hTERT Extends the Life of Human Fibroblasts without Compromising Type I Interferon Signaling. *PLoS One* **8,** e58233 (2013).

149. Moumné, L., Campbell, K., Howland, D., Ouyang, Y. & Bates, G. P. Genetic knock-down of HDAC3 does not modify disease-related phenotypes in a mouse model of Huntington's disease. *PLoS One* **7,** e31080 (2012).

150. Abghqri, Z., Srulring, R. D., Nigida, S. M., Downer, D. N. & Nohmiost, A. J. Comparative Replication of HSV-1 in BALB / c and C57BL / 6 Mouse Embryo Fibroblasts In Vitro. *Invest Ophthalmol Vis Sci.* **27,** 909–914 (1986).

151. Halford, W. P., Balliet, J. W. & Gebhardt, B. M. Re-evaluating natural resistance to herpes simplex virus type 1. *J. Virol.* **78,** 10086–95 (2004).

152. Chen, L. *et al.* R-ChIP Using Inactive RNase H Reveals Dynamic Coupling of R-loops with Transcriptional Pausing at Gene Promoters. *Mol. Cell* **68,** 745–757.e5 (2017).

153. Hoelzer, K., Shackelton, L. A. & Parrish, C. R. Presence and role of cytosine methylation in DNA viruses of animals. *Nucleic Acids Res.* **36,** 2825–2837 (2008).

154. Valyi-Nagy, T., Deshmane, S., Dillner, A. & Fraser, N. W. Induction of cellular transcription factors in trigeminal ganglia of mice by corneal scarification, herpes simplex virus type 1 infection, and explantation of trigeminal ganglia. *J. Virol.* **65,** 4142–52 (1991).

155. Taddeo, B., Esclatine, A. & Roizman, B. The patterns of accumulation of cellular RNAs in cells infected with a wild-type and a mutant herpes simplex virus 1 lacking the virion host shutoff gene. *Proc. Natl. Acad. Sci. U. S. A.* **99,** 17031–17036 (2002).

156. Cai, X., Chiu, Y.-H. & Chen, Z. J. The cGAS-cGAMP-STING Pathway of Cytosolic DNA Sensing and Signaling. *Mol. Cell* **54,** 289–296 (2014).

157. Goubau, D., Deddouche, S. & Reis e Sousa, C. Cytosolic Sensing of Viruses. *Immunity* **38,** 855–869 (2013).

158. Melchjorsen, J., Matikainen, S. & Paludan, S. R. Activation and evasion of innate antiviral

immunity by herpes simplex virus. *Viruses* **1,** 737–759 (2009).

159. Mossman, K. L. *et al.* Herpes simplex virus triggers and then disarms a host antiviral response. *J. Virol.* **75,** 750–8 (2001).

160. Royer, D. J., Carr, M. M., Chucair-Elliott, A. J., Halford, W. P. & Carr, D. J. J. Impact of Type I Interferon on the Safety and Immunogenicity of an Experimental Live-Attenuated Herpes Simplex Virus 1 Vaccine in Mice. *J. Virol.* **91,** e02342-16 (2017).

161. Mao, H. & Rosenthal, K. S. Strain-dependent structural variants of herpes simplex virus type 1 ICP34.5 determine viral plaque size, efficiency of glycoprotein processing, and viral release and neuroinvasive disease potential. *J. Virol.* **77,** 3409–17 (2003).

162. Su, C., Zhan, G. & Zheng, C. Evasion of host antiviral innate immunity by HSV-1, an update. *Virology Journal* **13,** (2016).

163. Bishop, S. A. & Hill, T. J. Herpes simplex virus infection and damage in the central nervous system: immunomodulation with adjuvant, cyclophosphamide and cyclosporin A. *Arch. Virol.* **116,** 57–68 (1991).

164. Lundberg, P. *et al.* The immune response to herpes simplex virus type 1 infection in susceptible mice is a major cause of central nervous system pathology resulting in fatal encephalitis. *J. Virol.* **82,** 7078–88 (2008).

165. Kawada, J. *et al.* Evaluation of Systemic Inflammatory Responses in Neonates with Herpes Simplex Virus Infection. *J. Infect. Dis.* **190,** 494–498 (2004).

166. Julien, J.-P. & Kriz, J. Transgenic mouse models of amyotrophic lateral sclerosis. *Biochim. Biophys. Acta - Mol. Basis Dis.* **1762,** 1013–1024 (2006).

Appendices

Appendix 1: Supplementary Data

It was relevant to determine if the affect of SETX on viral gene expression was independent of DNA replication, but also if it was indirect by means of the antiviral response. IRF3/9 MEF were used for this purpose as previously described. SETX siRNA KD was >80% for upwards of 24 hours during infection, but no significant differences were noted between treatment conditions (*Figure 3.2.4a-d).* Like previous work with IRF3/9 MEF, phenotypes previously demonstrated in SETX MEF and HFF cells treated with siRNA were not recapitulated in the IRF3/9 $^{+/+}$ MEF. Additionally, there were not significant differences across genotypes or treatment conditions. This result further emphasized the inability of IRF3/9 MEFs to act as an antiviral independent model for SETX and HSV-1 infection.

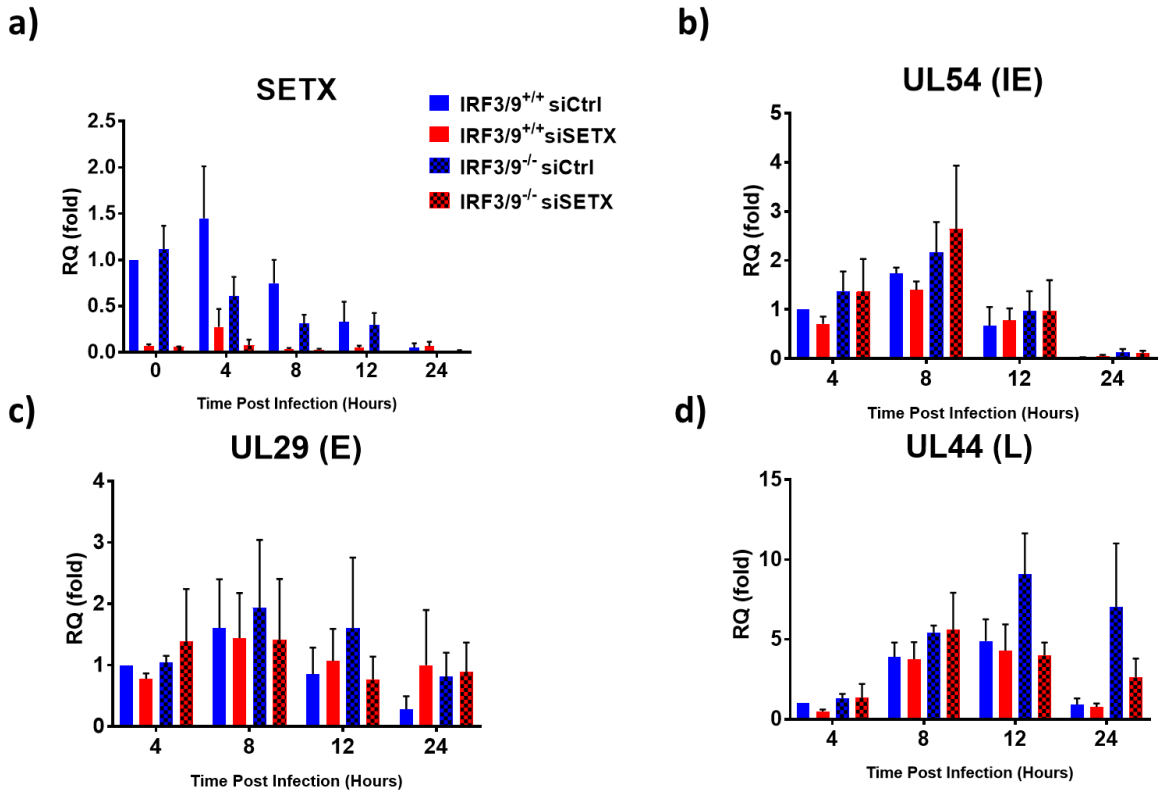

Figure S1.1. **SETX impact on HSV-1 gene expression not applicable to IRF3/9 MEF.** (a-d) IRF3/9 MEF were treated with siSETX or siCtrl prior to infection with HSV-1 KOS at MOI = 5. Cells were collected at the indicated times and expression of (a) SETX, (b) *UL54*, (c) *UL29* and (d) *UL44* were quantified by qRT-PCR relative to 18sRNA. Data represents the mean and standard error of 3 independent experiments. Data was shown to be insignificant by 2-way ANOVA for comparisons between siCtrl and siSETX conditions.

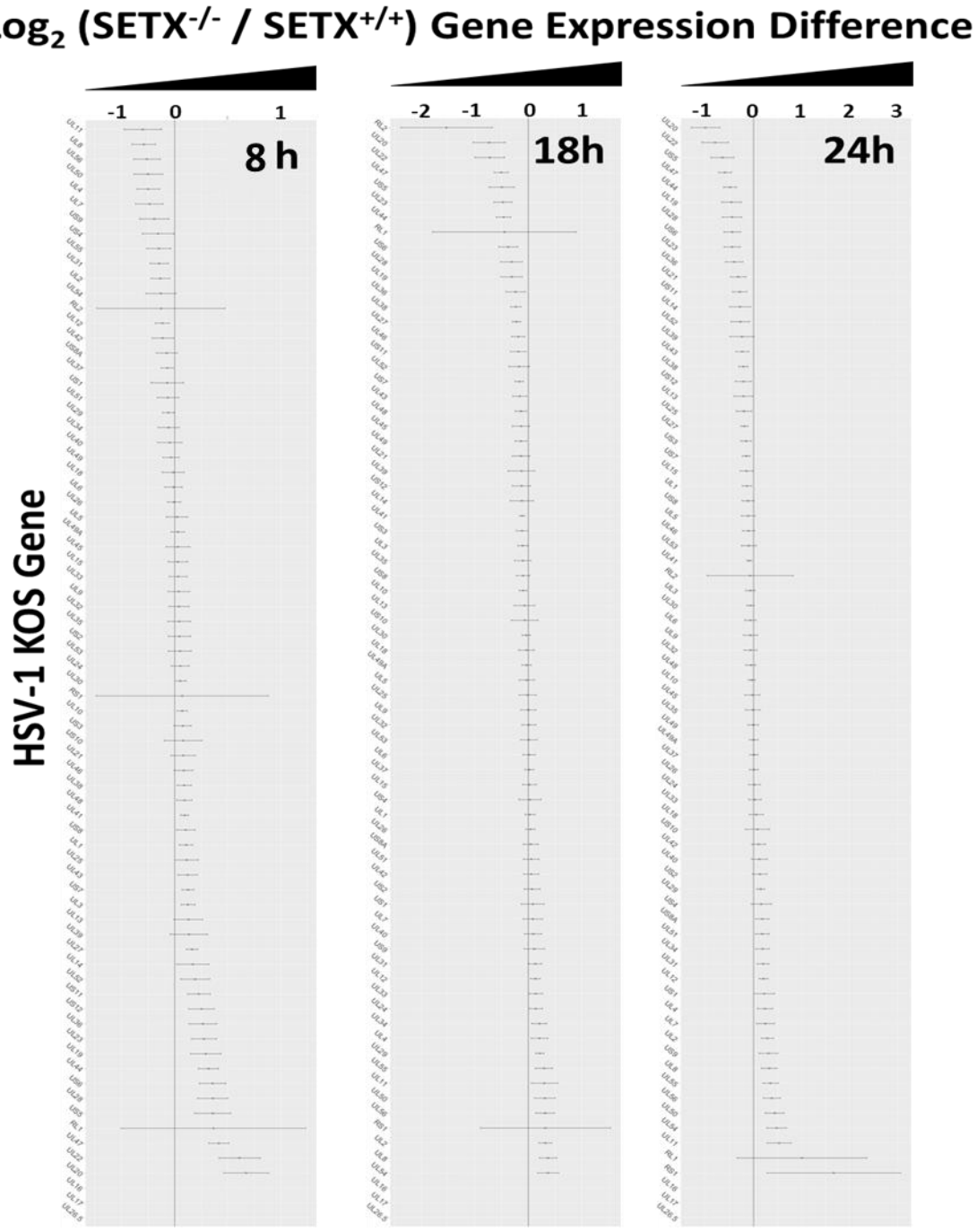

Figure S1.2. **Differential expression of HSV-1 genes during infection of SETX$^{+/+}$ and SETX$^{-/-}$ MEF.** Differential expression of viral genes from RNA sequencing SETX$^{+/+}$ and SETX $^{-/-}$ MEF infected with HSV-1 KOS (MOI = 5.0) across select timepoints. RNA was sequenced using Illumina HiSeq single read (50bp), via HISAT2, and then transcripts were aligned using Stringtie[108,109]. DESeq2 was used to test for differential expression against a Log (0) fold change null hypothesis and assigning a p-value via Wald test, adjusting for multiple testing through Benjamini and Hochberg procedure, and standard error of mean denoted with bars[110].

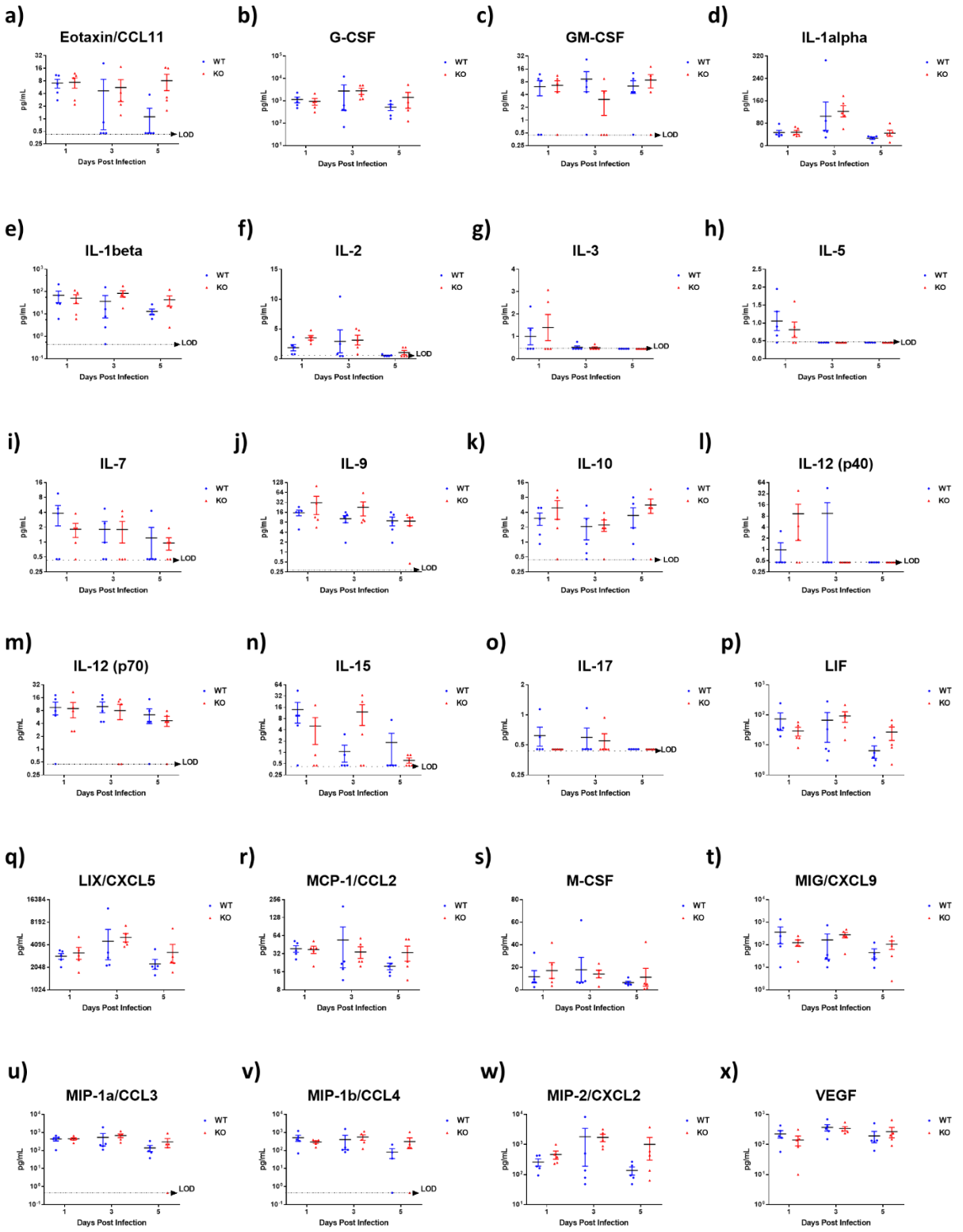

***Figure S1.3* Additional analytes of HSV-1 infected SETX mouse vaginal washes from MD-31 discovery assay.** (a-x) SETX $^{(+/+,\ -/-)}$ were infected intravaginally for one hour with 10^5 PFU of

HSV-1 17+ four days following treatment with 2.5mg of Depo-Provera. Vaginal washes were performed on days 1, 3, 5 and Eve Technologies MD-31 discovery assay was performed; cytokine and chemokine profiles were quantified. (a-i) Displays concentrations of cytokine/chemokines detected for n = 5 mice per group. All data was analyzed with two-way ANOVA and found to be non-significant for times measured.

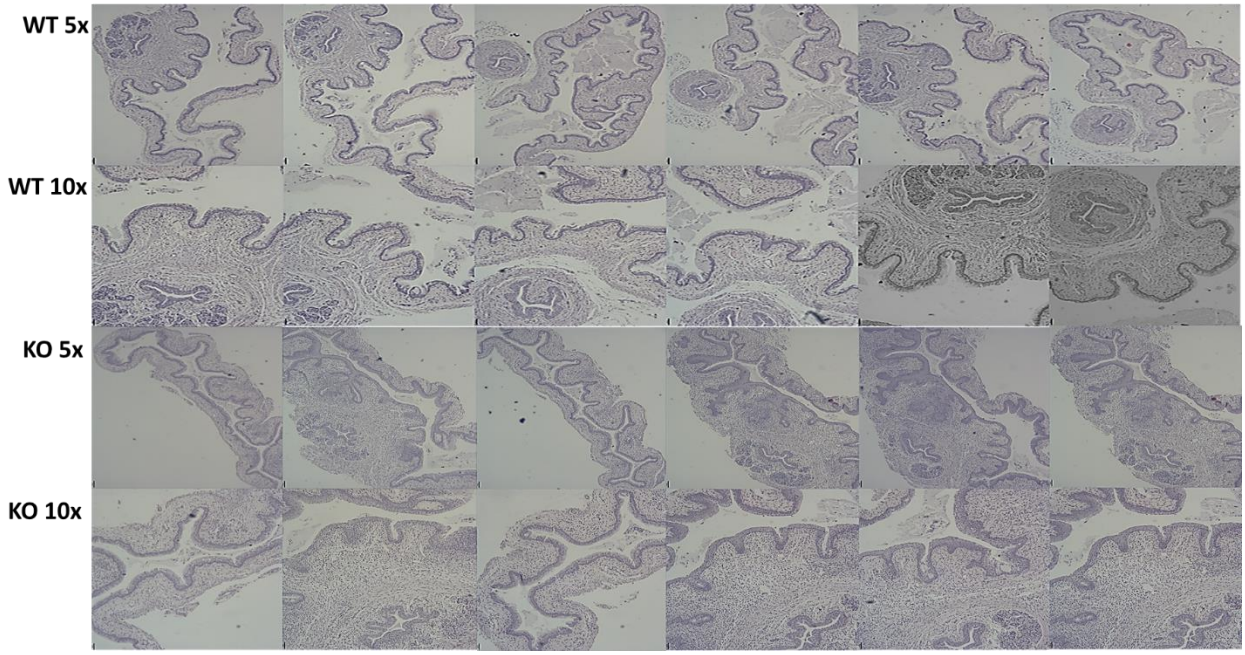

Figure S1.4 **Vaginal tract histology of HSV-1 infected SETX mouse.** SETX WT, KO $^{(+/+, -/-)}$ mice were infected intravaginally for one hour with 10^5 PFU of HSV-1 17+ four days following treatment with 2.5mg of Depo-Provera. Animals were euthanized at day 5 post infection, vaginal tracts were removed, sectioned along transverse plane, mounted and H&E stained. Images represents n = 1 per genotype at 5X and 10X magnifications.

Vaginal histology has been performed for one $SETX^{+/+}$ and $SETX^{-/-}$ mouse at day 5 during intravaginal HSV-1 infection (10^5 PFU) (*Figure S1.4)*. Experiment is on going and inconclusive so far.

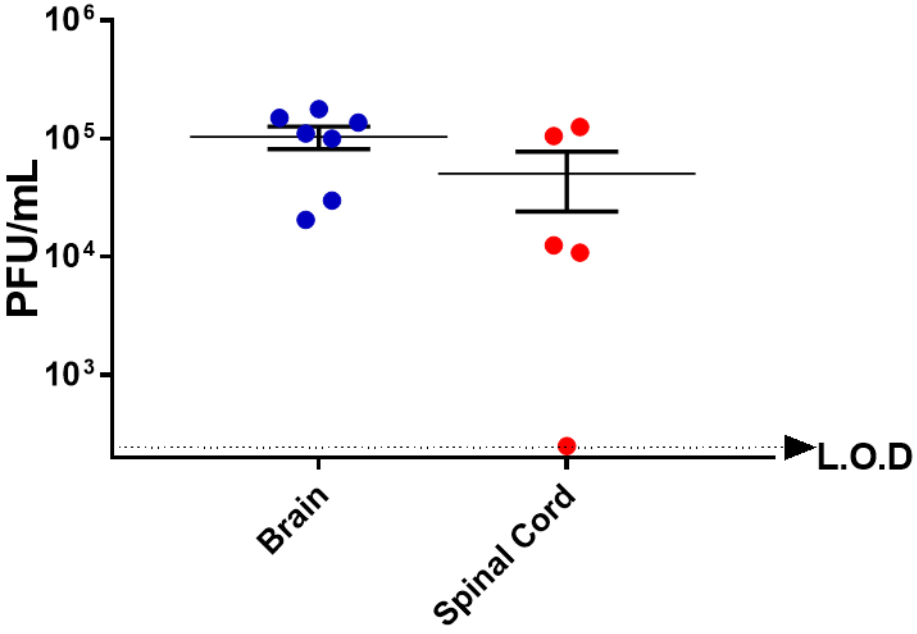

Figure S1.5. **HSV-1 invasion of CNS in animal display neuropathology.** SETX $^{(-/-)}$ were infected intravaginally for one hour with 10^5 PFU of HSV-1 17+ four days following treatment with 2.5mg of Depo-Provera. Animal was monitored and euthanized upon hind-limb paralysis. Brain and spinal cords were removed and homogenized. Homogenates were individually titred. Data represents n = 1 animals showing hind-limb paralysis.

Brain and spinal cord titres were performed for one SETX$^{-/-}$ mouse at endpoint during intravaginal HSV-1 infection (10^5 PFU) which displayed hind-limb paralysis. Results are inconclusive so far as no other sampling has been performed (*Figure S1.5)*.

Appendix 2: IAV Infection of SOD1^{G93A} Mice

SETX is among a myriad of genes that have been identified for their role in the development of ALS; perhaps the most studied is that of superoxide dismutase 1 (SOD1)[21,23,166]. Transgenic mouse models of ALS exist in which C57BL/6 mice express a copy of human SOD1 with a glycine-alanine mutation at amino acid 93 (G93A) mutation (SOD1$^{G93A)}$. The transgene results in an ALS-like phenotype (*Table 2.13.1*) in which mice develop hind limb paralysis [166]. With the recent development of IAV infection resulting in chronic inflammation of neural tissues[104], the potential influences of IAV infection on SOD1^{G93A} disease development became a significant potential. To date, no study had examined the influence of viral infection on SOD1^{G93A} disease onset and progression. The infection of SOD1^{G93A} was a side project, related to my interest in the intersection between viral infections and neurodegenerative diseases.

Wt and Tg SOD1^{G93A} mice were infected at 60 days of age with 0, 300 (0.1 LD50) or 3000 (1.0 LD50) PFU of IAV PR8 intranasally and monitored daily during infection (until 14 days post infection (*Figure S2.1a-b).* Day 60 was chosen as it is prior to phenotypical manifestations of any ALS-like phenotype[166]. Weight loss of animals was correlated to dosage, with 1.0 LD50 infected mice losing more weight than 0.1 LD50 animals (*Figure S2.1a).* Surviving mice *(Figure S2.1b)* were tested weekly through the inverted wire-mesh grip test (*Figure S2.1c*) which is a measure of hind limb strength, and by rotarod (*Figure S2.1d)* which is a measure of motor coordination. Previously infected Tg SOD1^{G93} mice exhibited more rapid disease progression relative to control animals and reached endpoint approximately 2 weeks earlier (*Figure S2.1b).* There were fewer differences between uninfected and infected transgenic mice in terms of hind limb strength and motor coordination, but it appeared infected transgenic mice lost hind limb strength and motor coordination slightly earlier than uninfected controls (*Figure S2.1c-d).*

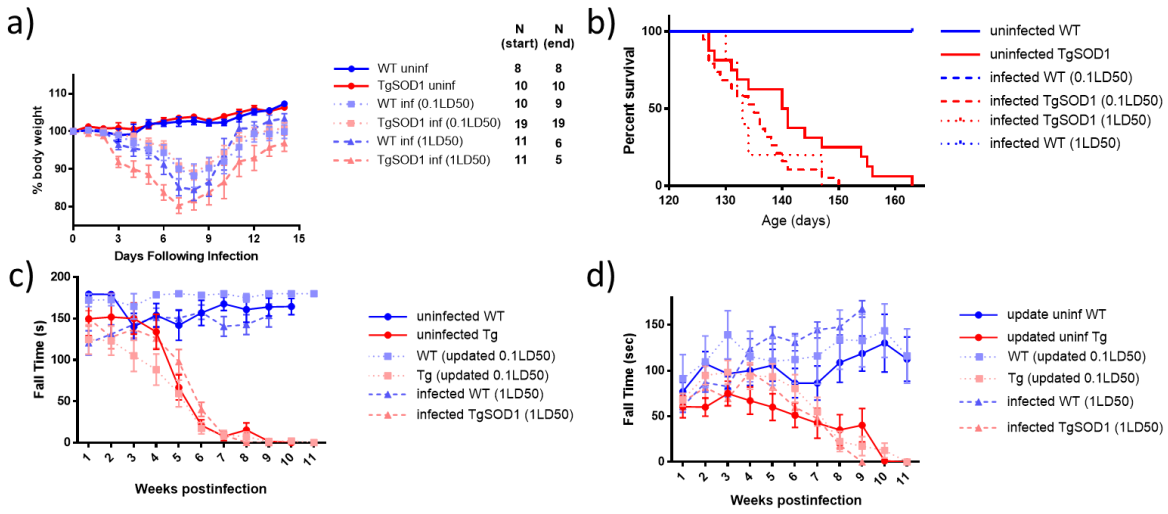

Figure S2.1. **Influenza infection of SOD-1 G93A mice exacerbates ALS-like phenotype.** Wild-type (WT) and SOD1-G93A (Tg) mice were infected with 0.1 LD50 (300PFU) or 1.0 LD50 (3000 PFU) of IAV (PR8) at the age of 60 days. (a) Weight loss was followed over the course of 14 days to monitor recovery of infection. (b) Endpoint survival of mice was assessed following recovery of infection using ALS clinical scoring where mice were euthanized upon inability to right after 30 s, a measure of ALS-like paralysis. (c) Inverted wire-mesh grip test was performed as a measure of hind limb grip strength (d) Mouse coordination was assessed through rotarod testing and mean fall time was recorded for three technical replicates.

The results demonstrated here provides strong evidence for a link between viral infection and neurodegenerative diseases. The addition of common viral infections such as IAV, or HSV-1, as either potential contributors or instigators of ALS on-set, and development would be a significant development within the neurodegenerative disease field. Infections of $SOD1^{G93A}$ using the HSV-1 infection model may yield additional information as unlike the PR8 IAV used for these experiments, HSV-1 is neurotropic and capable of producing disease symptoms of hind-limb paralysis not dissimilar to the phenotype that transgenic mice develop spontaneously.